

INVESTIGATION OF FRICTION IN SHEET METAL FORMING

A DOCTOR OF PHILOSOPHY THESIS

in

Modelling and Design of Engineering Systems (MODES)

(Main Field of Study: Manufacturing Engineering)

Atılım University

by

HAKAN KALKAN

JULY 2017

INVESTIGATION OF FRICTION IN SHEET METAL FORMING

A THESIS SUBMITTED TO

THE GRADUATE SCHOOL OF NATURAL AND APPLIED SCIENCES

OF

ATILIM UNIVERSITY

BY

HAKAN KALKAN

**IN PARTIAL FULFILLMENT OF THE REQUIREMENTS FOR THE
DEGREE OF**

DOCTOR OF PHILOSOPHY

IN

MODELING AND DESIGN OF ENGINEERING SYSTEMS (MODES)

(MAIN FIELD OF STUDY: MANUFACTURING ENGINEERING)

JULY 2017

Approval of the Graduate School of Natural and Applied Sciences, Atılım University.

Prof. Dr. Ali KARA

Director

I certify that this thesis satisfies all the requirements as a thesis for the degree of Doctor of Philosophy.

Prof. Dr. Abdülkadir ERDEN

Head of Department

This is to certify that we have read the thesis “Investigation of friction in sheet metal forming” submitted by “Hakan KALKAN” and that in our opinion it is fully adequate, in scope and quality, as a thesis for the degree of Doctor of Philosophy.

Prof. Dr. Bilgin KAFTANOĞLU

Supervisor

Examining Committee Members

Prof. Dr. Bilgin KAFTANOĞLU

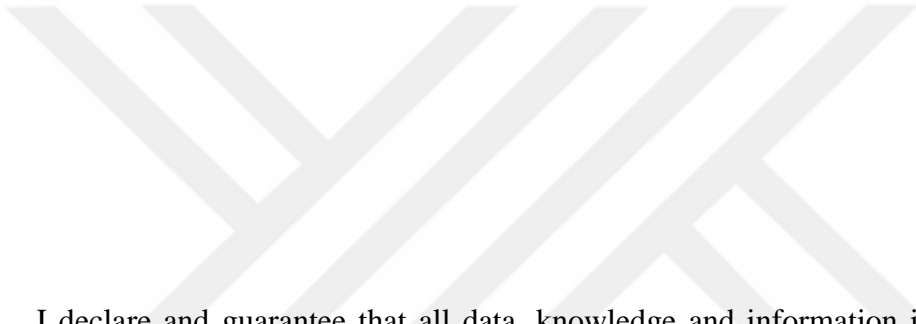
Prof. Dr. Metin AKKÖK

Prof. Dr. Birol KILKIŞ

Assoc. Prof. Dr. A. Hakan ARGEŞO

Asst. Prof. Dr. Erkan KONCA

Date: 12/07/2017



I declare and guarantee that all data, knowledge and information in this document has been obtained, processed and presented in accordance with academic rules and ethical conduct. Based on these rules and conduct, I have fully cited and referenced all material and results that are not original to this work.

Name, Last name: Hakan KALKAN

Signature:

ABSTRACT

INVESTIGATION OF FRICTION IN SHEET METAL FORMING

Kalkan, Hakan

PhD in Modelling and Design of Engineering Systems (MODES)

Supervisor: Prof. Dr. Bilgin KAFTANOĞLU

July 2017, 104 pages

Investigation of friction is carried out in the radial drawing region between the die and blank holder and also in the stretching zone over the punch in deep drawing. Two methods are developed to calculate the coefficient of friction in each zone using the experimentally determined data such as punch force diagrams and strain distributions obtained by an optical scanning system. The current methods differ from the existing techniques which are obtained in simulative tests. The proposed methods can be applied at room temperature and at elevated temperatures. In deep drawing tests, EN 10268 steel is used with dry and graphite lubrication and hot deep drawing tests are performed at 300 °C. Deep drawing tests are performed at different lubrication and temperature conditions. Blank holder load is another parameter which changes the punch loads. 9 different stretch forming tests are performed to determine the coefficient of friction in this zone. Three different materials are used with dry and paraffin lubricated conditions. Comparisons of friction coefficients are made with those obtained by other techniques.

Keywords: Friction, Deep drawing, Tribology

ÖZ

SAC ŞEKİLLENDİRME İŞLEMİNDE SÜRTÜNMENİN İNCELENMESİ

Kalkan, Hakan

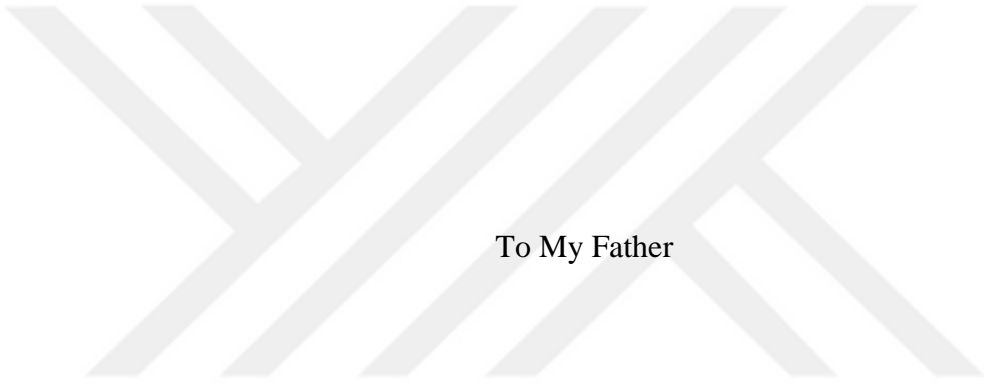
Doktora, Mühendislik Sistemlerinin Modellenmesi ve Tasarımı

Tez Yöneticisi: Prof. Dr. Bilgin KAFTANOĞLU

Temmuz 2017, 104 sayfa

Derin çekme işleminde sürtünme, baskı plakası-sac metal-kalıp yüzeyleri arasındaki radial çekme bölgesi ve zımba-sac metal arasında gerdirme bölgesinde gerçekleşmektedir. Bu bölgelerde oluşan sürtünme katsayısı, zımba kuvveti değerleri ve optik tarayıcıdan elde edilen genleme dağılımları kullanılarak iki yöntemle hesaplanmıştır. Bu hesaplama yöntemleri hem oda sıcaklığında hem de yüksek sıcaklıklarda kullanılabilir. Derin çekme testleri kuru ve grafit yağlayıcı koşullarda EN 10268 malzeme ile gerçekleştirilmiştir. Testler oda sıcaklığında ve 300 °C de zımba kuvvetini etkileyen farklı baskı kuvvetlerinde tekrarlanmıştır. Gerdirme bölgesi için ise 3 farklı çelik malzeme ile kuru ve parafin yağlayıcı koşullarda testler gerçekleştirilmiştir. Elde edilen sürtünme katsayısı değerleri diğer yöntemlerden elde edilen sonuçlar ile karşılaştırılmıştır.

Anahtar kelimeler: Sürtünme, Derin Çekme, Triboloji



To My Father

ACKNOWLEDGMENTS

I express my sincere appreciation to my supervisor Prof. Dr. Bilgin KAFTANOĞLU for his guidance and insight throughout the research. I wish to thank to the members of thesis committee: Prof. Dr. Metin AKKÖK, Prof. Dr. Birol Kılış, Assoc. Prof. Dr. A. Hakan ARGESO, Asst. Prof. Dr. Erkan Konca and Asst. Prof. Dr. Şehram Dizeci.

I would like to thank to head of Atılım University Manufacturing Engineering departement Prof. Dr. S. Engin Kılıç for his support and suggestions. I also would like to thank to all members of Manufacturing Engineering department and Metal Forming Center of Excellence.

I would like to thank my colleagues Resc. Eng. İsmail Gürbüz, M. Emin Tamer and Erdem Kayhan for their great support and valuable contribution.

Finally, I would like to thank to my parents, wife Meral and lovely daughter Ece always being with me during this study.

TABLE OF CONTENTS

ABSTRACT.....	iii
ÖZ.....	iv
DEDICATION.....	v
ACKNOWLEDGMENTS.....	vi
TABLE OF CONTENTS.....	vii
LIST OF TABLES.....	ix
LIST OF FIGURES.....	x
LIST OF NOTATIONS.....	xiii
CHAPTERS.....	1
1-INTRODUCTION.....	1
1.1 FRICTION IN SHEET METAL FORMING.....	1
1.2 AIM AND SCOPE OF THE THESIS.....	3
1.3 CONTENT OF THIS STUDY.....	4
2-LITERATURE SURVEY.....	5
2.1 DEEP DRAWING AND STRETCH FORMING.....	5
2.2 FRICTION MODELS USED IN METAL FORMING.....	8
2.3 LUBRICATION MECHANISMS IN METAL FORMING.....	10
2.4 MEASUREMENTS OF FRICTION IN SHEET METAL FORMING.....	12
2.5 PREVIOUS STUDIES OF FRICTION IN SHEET METAL FORMING.....	14
3-OBJECT OF PRESENT INVESTIGATION.....	19
4-MODELLING OF FRICTION IN DEEP DRAWING.....	21
4.1 DETERMINATION OF COEFFICIENT OF FRICTION IN RADIAL DRAWING ZONE.....	21
4.2 DETERMINATION OF COEFFICIENT OF FRICTION IN STRETCH FORMING ZONE.....	24
4.2.1 Investigation of the existing technique to calculate the coefficient of friction in stretch forming [2].....	25

4.2.2 Development of new equation to calculate the coefficient of friction in stretch forming.....	28
5-EXPERIMENTAL DETERMINATION OF FRICTION IN SHEET METAL FORMING.....	32
5.1 MATERIAL CHARACTERIZATION TESTS.....	33
5.1.1 Tensile test.....	33
5.1.2 Hydraulic bulge test.....	36
5.1.3 Flow curves of the test materials.....	38
5.2 SURFACE ROUGHNESS OF DIE AND WORKPIECE.....	40
5.3 DEEP DRAWING TESTS.....	40
5.3.1 Test Apparatus.....	41
5.3.1.1 Mechanical Press.....	41
5.3.1.2 Blank Holder.....	42
5.3.1.3 Heating System.....	42
5.3.1.4 Punch and load cell.....	43
5.3.1.5 Die Components.....	44
5.3.1.6 Measurements devices.....	44
5.3.2 Deep Drawing Test Evaluation.....	48
5.4 STRETCH FORMING TESTS.....	51
5.4.1 Test Apparatus.....	51
5.4.2 Stretch Forming Test Evaluation.....	53
6- RESULTS AND DISCUSSION.....	59
6.1 RESULTS OBTAINED FROM DEEP DRAWING TESTS.....	59
6.2 RESULTS OBTAINED FROM STRETCH FORMING TESTS.....	63
6.3 RESULTS OBTAINED FROM OTHER SOURCES.....	73
6.4 DISCUSSION OF RESULTS.....	74
7- CONCLUSION AND SUGGESTIONS FOR FUTURE WORK.....	75
REFERENCES.....	77
APPENDIXES.....	81

LIST OF TABLES

TABLE

Table 5.1: Chemical Compositions of the steels used in the experiments.....	33
Table 5.2: Mechanical Properties of EN 10346/ HX380LAD+Z, EN 10346/ HX220BD+Z and EN 10346/ DX54D+Z [35].....	35
Table 5.3: Deep drawing test parameters.....	49
Table 5.4: Calculation of the interfacial pressure.....	56
Table 5.5: Comparisons of the results of Eq. 4.42 and Eq. 4.72.....	58
Table 6.1 Deep drawing Test 1.....	59
Table 6.2 Deep drawing Test 2.....	60
Table 6.3 Deep drawing Test 3.....	60
Table 6.4 Deep drawing Test 4.....	61
Table 6.5 Deep drawing Test 5.....	61
Table 6.6 Deep drawing Test 6.....	62
Table 6.7 Deep drawing Test 7.....	62
Table 6.8 Deep drawing Test 8.....	63
Table 6.9: COF results for the deep drawing tests.....	63
Table 6.10: Stretch forming Test 1.....	64
Table 6.11 Stretch forming Test 2.....	65
Table 6.12 Stretch forming Test 3.....	66
Table 6.13 Stretch forming Test 4.....	67
Table 6.14 Stretch forming Test 5.....	68
Table 6.15 Stretch forming Test 6.....	69
Table 6.16 Stretch forming Test 7.....	70
Table 6.17 Stretch forming Test 8.....	71
Table 6.18 Stretch forming Test 9.....	72
Table 6.19: COF results for the stretch forming tests.....	73
Table 6.20: Results Obtained From Other Sources.....	73

LIST OF FIGURES

FIGURES

Figure 2.1: Schematic illustration of deep drawing and stretch forming operation. 1-Die, 2-workpiece, 3-blank holder, 4-punch and 5:draw beads [4].....	5
Figure 2.2: Stretch Forming [5].....	6
Figure 2.3: Possible failures as a result of poor control of friction and wear during axisymmetric deep drawing [4].....	8
Figure 2.4: Relationship between contact pressure and frictional stress [5].....	9
Figure 2.5: Stribeck curve showing onset of various lubrication mechanisms [5]....	11
Figure 2.6: Various tests to determine the coefficient of friction [5].....	12
Figure 2.7: Schematic view of the twist compression test [5].....	13
Figure 2.8: Deformed strip sample in Strip draw test [9].....	13
Figure 4.1: Main features of deep drawing.....	21
Figure 4.2: Forces acting on a segment of a round specimen [3].....	22
Figure 4.3: Stresses on element of shell wall [2].....	23
Figure 5.1: Typical tensile test specimen [19].....	34
Figure 5.2: The geometry of the tensile test specimen according to ASTM [20]....	35
Figure 5.3: Zwick Roell Z300 Tension/Compression Test Device	35
Figure 5.4: General view of Hydraulic Bulge Test setup.....	36
Figure 5.5: Schematic view of Hydraulic Bulge Test.....	37
Figure 5.6: HBT test specimen and stochastic pattern on the sheet material [20]....	38
Figure 5.7: Flow curve of the EN 10346/ HX380LAD+Z material.....	39
Figure 5.8: Flow curve of the EN 10346/ HX220BD+Z material.....	39
Figure 5.9: Flow curve of the EN 10346/ DX54D+Z material.....	40
Figure 5.10: C type mechanical press.....	41
Figure 5.11: Blank holder configuration [22].....	42
Figure 5.12: Induction heating system.....	43
Figure 5.13: Ram set.....	43
Figure 5.14: General view of the die assembly.....	44

Figure 5.15: Pressure transducer attached on hydraulic cylinder.....	44
Figure 5.16: Displacement transducer mounted on press and technical specifications of displacement transducer.....	45
Figure 5.17: Load cell and technical specifications of load cell.....	46
Figure 5.18: Data acquisition system and technical specifications.....	47
Figure 5.19: Software Package used for data processing.....	47
Figure 5.20: Punch loads at different blank holder loads for EN 10268 steel.....	48
Figure 5.21: Punch load-displacement graph at 26075 N and 13410 N BHL.....	50
Figure 5.22: Zwich BUP 600 Test Device and general view of the half sheet specimen.....	52
Figure 5.23: General view of the hemispherical punch.....	52
Figure 5.24: General view of the stochastic painting.....	53
Figure 5.25: Recorded image and strain distributions obtained from GOM Aramis optical measurement system.....	53
Figure 5.26: Workpiece geometry between Stage 120-Stage130.....	54
Figure 5.27: Strain distributions between Stage 120-Stage130.....	54
Figure 5.28: Strain distributions between Stage 120-Stage130.....	55
Figure 5.29: Interfacial pressure between stage 120 and 130.....	57
Figure 5.30: Coefficient of friction values using new derived equation (Eq. 4.72)..	57
Figure 5.31: Coefficient of friction values using Eq. 4.42.....	58
Figure 6.1: Punch loads for deep drawing Test 1.....	59
Figure 6.2: Punch loads for deep drawing Test 2.....	60
Figure 6.3: Punch loads for deep drawing Test 3.....	60
Figure 6.4: Punch loads for deep drawing Test 4.....	61
Figure 6.5: Punch loads for deep drawing Test 5.....	61
Figure 6.6: Punch loads for deep drawing Test 6.....	62
Figure 6.7: Punch loads for deep drawing Test 7.....	62
Figure 6.8: Punch loads for deep drawing Test 8.....	63
Figure 6.9: COF values using Eq. 4.42 for Test 1.....	64
Figure 6.10: COF values using new derived equation Eq. 4.72 for Test 1.....	64
Figure 6.11: COF values using Eq. 4.42 for Test 2.....	65
Figure 6.12: COF values using new derived equation Eq. 4.72 for Test 2.....	65
Figure 6.13: COF values using Eq. 4.42 for Test 3.....	66
Figure 6.14: COF values using new derived equation Eq. 4.72 for Test 3.....	66

Figure 6.15: COF values using Eq. 4.42 for Test 4.....	67
Figure 6.16: COF values using new derived equation Eq. 4.72 for Test 4.....	67
Figure 6.17: COF values using Eq. 4.42 for Test 5.....	68
Figure 6.18: COF values using new derived equation Eq. 4.72 for Test 5.....	68
Figure 6.19: COF values using Eq. 4.42 for Test 6.....	69
Figure 6.20: COF values using new derived equation Eq. 4.72 for Test 6.....	69
Figure 6.21: COF values using Eq. 4.42 for Test 7.....	70
Figure 6.22: COF values using new derived equation Eq. 4.72 for Test 7.....	70
Figure 6.23: COF values using Eq. 4.42 for Test 8.....	71
Figure 6.24: COF values using new derived equation Eq. 4.72 for Test 8.....	71
Figure 6.25: COF values using Eq. 4.42 for Test 9.....	72
Figure 6.26: COF values using new derived equation Eq. 4.72 for Test 9.....	72
Figure A.1: Test 1 Strain distributions-displacement	82
Figure A.2: Test 1 Strain distributions-angle, θ	83
Figure A.3: Test 1 Pressure distributions	83
Figure A.4: Test 2 Strain distributions-displacement	84
Figure A.5: Test 1 Strain distributions-angle, θ	84
Figure A.6: Test 2 Pressure distributions	85
Figure A.7: Test 3 Strain distributions-displacement	85
Figure A.8: Test 3 Strain distributions-angle, θ	86
Figure A.9: Test 3 Pressure distributions	86
Figure A.10: Test 4 Strain distributions-displacement.....	87
Figure A.11: Test 4 Strain distributions-angle, θ	87
Figure A.12: Test 4 Pressure distributions.....	88
Figure A.13: Test 5 Strain distributions-displacement.....	88
Figure A.14: Test 5 Strain distributions-angle, θ	89
Figure A.15: Test 5 Pressure distributions.....	89
Figure A.16: Test 6 Strain distributions-displacement.....	90
Figure A.17: Test 6 Strain distributions-angle, θ	90
Figure A.18: Test 6 Pressure distributions.....	91
Figure A.19: Test 7 Strain distributions-displacement.....	91
Figure A.20: Test 7 Strain distributions-angle, θ	92
Figure A.21: Test 7 Pressure distributions.....	92
Figure A.22: Test 8 Strain distributions-displacement.....	93

Figure A.23: Test 8 Strain distributions-angle, θ	93
Figure A.24: Test 8 Pressure distributions.....	94
Figure A.25: Test 9 Strain distributions-displacement.....	94
Figure A.26: Test 9 Strain distributions-angle, θ	95
Figure A.27: Test 9 Pressure distributions.....	95



LIST OF NOTATIONS

ABBREVIATIONS

BHF	Blank holder force
BUT	Bending under tension
COF	Coefficient of friction
DBT	Draw bead test
DR	Drawing ratio
FE	Finite element
FEM	Finite element method
HBT	Hydraulic bulge test
LDH	Limiting dome height test
LDR	Limiting drawing ratio
SDT	Strip draw test
TCT	Twist compression test
UTS	Ultimate tensile strength
YS	Yield strength

SYMBOLS

μ	Coefficient of friction
τ_f	Frictional shear stress
p	Normal pressure
k	Shear strength of the workpiece material

m	Shear factor
$\bar{\sigma}$	Flow stress of the workpiece material
A_r	Ratio of real contact area
A_a	Apparent contact area
α	Real contact contact area ratio
f'	Modified friction factor
m_r	Modified shear factor
τ_a	Average shear stress at contacting asperity peaks
τ_b	Average shear stress at the lubricant pockets
η	Lubricant viscosity
v	Sliding velocity
T	applied torque
r	mean radius of the tool
P	pressure applied on the tool
A	area of contact between tool and sample
R_a	Surface roughness
ε_θ	Logarithmic circumferential strain
R_m	Mean radius of deformed circle
R_0	Initial radius of circle
ε_t	Logarithmic through-thickness strain
t_m	Mean thickness after deformation
t_0	Original thickness
P	punch load
H	blank holder load
δP	punch load change

δH	blank holder load change
h	bulge depth
α	angle of embrance of the die
ρ'_d	die radius
ρ'_1	punch radius
F_1	friction force on upper surface
F_2	friction force on lower surface
p	Interfacial pressure between punch and sheet metal
k	Stress ratio = $\frac{\sigma_3}{\sigma_1}$
x	Stress ratio = $\frac{\sigma_2}{\sigma_1}$
R	Parameter of plastic anisotropy = $d\varepsilon_\omega^*/d\varepsilon_t^*$
r	Current radius to mean shell wall
r_0	Original radius to mean shell wall
ε_1	True plastic strains in meridional direction
ε_2	True plastic strains in circumferential direction
ε_3	True plastic strains in thickness directions
σ_1	Meridional stresses
σ_2	Circumferential stresses
σ_3	Thickness stresses
θ	Angle, that normal to an element of shell wall makes with the vertical
ρ_1	Meridional radius of curvature to mean shell wall
D	die diameter
ρ'_d	Die radius
ρ'_1	Radius of punch

σ_y	Yield strength
$\Delta L\%$	Percent elongation
$RA\%$	Reduction in cross sectional area
E	Young's modulus
ν	Poisson's ratio
A	Current cross section area of the specimen
σ_{eng}	Engineering stress
ε_{eng}	Engineering strain
F	Load
A_0	Initial cross sectional area
Δl	Longitudinal extension increment
l_0	Initial gage length
σ	True stress
ε	True strain
r_c	Die cavity radius,
t_0	Initial sheet thickness
σ_ϕ	Principle stress on the sheet surface
σ_θ	Principle stress on the sheet surface
R_ϕ	Corresponding radii of the curved surface at the dome apex
R_θ	Corresponding radii of the curved surface at the dome apex
P	Hydraulic bulge pressure,
t	Thickness at the dome apex
σ_{eqv}	Equivalent stress
ε_{eff}	Effective strain
F_c	Clamp force

P	Hydraulic bulge pressure
h_d	Dome height
ρ	Radius of curvature
r_f	Fillet radius of upper die
r_c	Radius of die cavity



CHAPTER 1

INTRODUCTION

1.1 FRICTION IN SHEET METAL FORMING

Friction is an important process parameter which controls the flow of material in the tool and the final quality of produced parts. It is important to know the magnitude of friction for a number of reasons. Estimation of load, energy requirements, tool wear of a deformation process can only be made with the knowledge of friction. In order to accurately predict the final shape or to design a deformation process to produce a given shape and find the loads applied to the workpiece, a thorough knowledge of friction is necessary.

The development of the finite element method for analysis of plastic deformation processes has provided a powerful tool for process simulation and optimization, which is a great value especially in the case of designing tools for sheet metal forming operations. To obtain reliable predictions of flow, strains and stresses, it is vital to have a reliable friction model. An accurate forming analysis can be done if the material behavior and friction conditions are modeled accurately. For material models, significant improvements have been made over the recent decades but the majority of the simulations still use approximations for friction coefficients.

Development of FE simulations reached a stage where the results can be used directly in the operations. Reducing time, cost and increasing the quality of the product are the aim of the simulations [1]. Time reduction is important for the early evaluation of producibility, reduction in the development times, reduction of the tryout times and quick response to needed modifications. Cost reduction provides lower product costs, reduction of the die costs, downsizing the press and increase of reliability. Increasing the product quality is another reason for the simulations. By

using the proper simulations optimal selection of the workpiece and production of more complicated parts can be achieved.

Geometry, material properties and coefficient of friction are the input parameters in FE simulations. The coefficient of friction is generally assumed constant in metal forming simulations. However, in the real processes, the frictional behavior depends on the sheet and tool material, contact pressure, sliding speed, lubrication and temperature on the sliding surface. This indicates the importance of correct determination of the coefficient of friction.

If the inputs are modeled correctly, punch force and blank holder force as a function of punch stroke, temperature distribution, pressure distribution on the tooling, stresses and strain distributions along the workpiece can be obtained.

There is a limited amount of research about investigation of friction in sheet metal forming. Previous studies could not fully explain the friction conditions. This thesis is aimed to investigate the friction in sheet metal forming by a new friction test method. Combination of material and friction modeling can be used in Finite Element Simulations. If the friction is modeled correctly Finite Element Simulations will give more accurate results. This result will be useful to decrease the cost and manufacturing time.

Successful sheet metal forming requires the knowledge on friction at the tool/material interface. Thus, it is necessary to have reliable methods to evaluate various stamping lubricants and determine the coefficient of friction quantitatively for use in Finite Element simulations. Thus, part, die and process design can be conducted and the cost and lead times of process development can be reduced.

Friction effects the forming loads and stresses transferred to the dies and this effect can be reduced by use of appropriate lubricants. The lubricant also affects the surface quality of the formed workpieces. If there is not enough lubrication between the punch and die interfaces, the product may have undesirable surface quality. Friction affects the wear of the dies. If proper lubrication can be applied between the die and the workpiece, wear of the dies can be reduced. Lubrication is in interaction with the surface quality and can be optimized to improve formability.

Contact between sheet metal and tool is important. To characterize this contact the surface quality is observed and its roughness is characterized both for sheet and tool materials.

The objectives of this study are to develop a method that can be used by sheet metal forming industry, for evaluating and determining lubricants and their coefficient of friction and develop dies that are used for sheet metal forming various materials to produce good quality parts with minimum waste and scrap.

In this thesis, the coefficient of friction in the deep drawing has been investigated. Additionally, lubrication effects on friction have been investigated. Lubrication is one of the important parameters that can improve part quality in sheet metal forming. Only the low friction is not sufficient to select lubricant. Tool and workpiece material, tool-workpiece interface, deformation zone and environment are the parameters which will affect the lubricant selection. So, the effects of different lubrications are investigated in this study.

In forming operations, it is very difficult to enter the interface between the workpiece and the die. This is the reason why friction in metal forming is not fully understood. On the other hand friction shear stress transferred through the interface is much smaller than the normal stress component transferred through the same interface. This difference causes the difficulty to measure the friction [2].

In this study interfacial pressure between the punch and the workpiece is calculated by using the plasticity equations. These new equations can be applied to the real deep drawing process. Coefficient of friction calculations at elevated temperatures are done by using different punch loads. So effect of the high temperature on coefficient of friction is are investigated.

Although friction is such an important factor in sheet metal forming operations in many forming applications actual friction conditions are not sufficiently known. In spite of much research on that important topic, there is a still lack of knowledge and need for continued research.

1.2 AIM AND SCOPE OF THE THESIS

The aim of this study is to improve the efficiency of sheet metal forming processes by using new methods to evaluate friction by using the experimental data such as strain distributions and punch load curves in the deep drawing process. Effects of lubrication and temperature can also be investigated using the proposed techniques.

Previous research about the investigation of friction in sheet metal forming provided the basis of the current study but the calculation of friction coefficient due to

nonlinear extrapolation and the manual measurement of strains resulted in higher errors [2]. It was also limited to room temperature.

In the past studies, strip draw and deep draw tests were commonly used to evaluate the stamping lubricants. Many studies have been focused on explaining friction mechanisms under different loading conditions in forming operations using experimental, analytical and numerical methods [3]. Although some basic friction characterization is obtained at present, friction mechanism still is not properly understood in depth, since it is a highly complex process. The main contribution of this study is to develop new techniques to calculate the friction coefficient to get more accurate results for the FE simulations. This will reduce the cost and the operation time in sheet-metal forming.

1.3 CONTENT OF THIS STUDY

This thesis consists seven main chapters. In the first chapter, brief information is given about the friction in sheet metal forming and aim of the thesis is explained. In the second chapter sheet metal forming operations are discussed, and effect of friction in sheet metal forming operations is given. Also previous studies about calculation of friction in sheet metal forming are discussed. In the third chapter object of present investigation is discussed. Theoretical studies about calculation of friction are given in the fourth chapter. In sheet metal forming operations friction occurs at two different regions, “stretch forming zone” and “radial drawing zone”. Some experiments were done to calculate the friction in these two zones. All these experimental parameters are explained in the fifth chapter. Results of the experiments and discussion are given in the sixth chapter. Conclusions obtained from the results and the suggestions for the future work are given in the last chapter.

CHAPTER 2

LITERATURE SURVEY

2.1 DEEP DRAWING AND STRETCH FORMING

Deep drawing is the sheet metal forming process which is most commonly used in forming industry. Punch, die and blank holder are the main parts of the operation. Workpiece is placed between the die and the blankholder. Blankholder force prevents the wrinkling in the flange region.

Cylindrical, conical and box shaped parts can be produced by using flat sheets. In deep drawing operations it is possible to produce final shaped workpieces using minimal operations minimal scraps.

Deep drawing process is mostly used in automotive and aircraft industry. It is a common process in sheet metal forming due to production of different shaped parts and different dimension ranges from very small to several meters. On the other hand rapid press cycle is the other advantage of this process. Complex axisymmetric and non-axisymmetric geometries can be produced with a few operations.

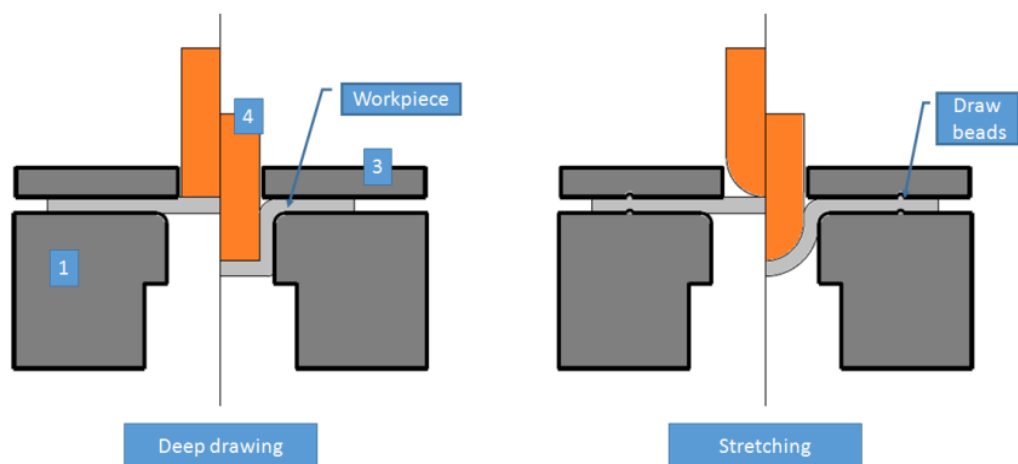


Figure 2.1: Schematic illustration of deep drawing and stretch forming operation. Common features: 1-Die, 2-workpiece, 3-blank holder, 4-punch and 5:draw beads [4].

Figure 2.1 shows the set up of the two commonly applied sheet metal forming processes deep drawing and stretch forming. From the Figure 2.1, it is clear that the main parts of the operation are the punch, die and blankholder.

Deep drawing is one of the most widely used sheet metal forming operations to produce cup shaped components at a high production rate. This process is suitable for mass production.

Pots, pans, containers, sinks, beverage cans, automotive panels and aircraft panels are the typical products of this operations.

Required equipment to carry out this process is the hydraulic press, mechanical press or transfer press. Carbon and alloy steels, aluminum alloys, titanium alloys and high temperature alloys can be formed with this process.

Stretch forming is a sheet metal forming operations which is very similar to deep drawing. The difference from the deep drawing is the material is clamped tightly between the binder and die. Lock beads restrict the deformation area. In Figure 2.2, schematic view of the stretch forming operation can be seen.

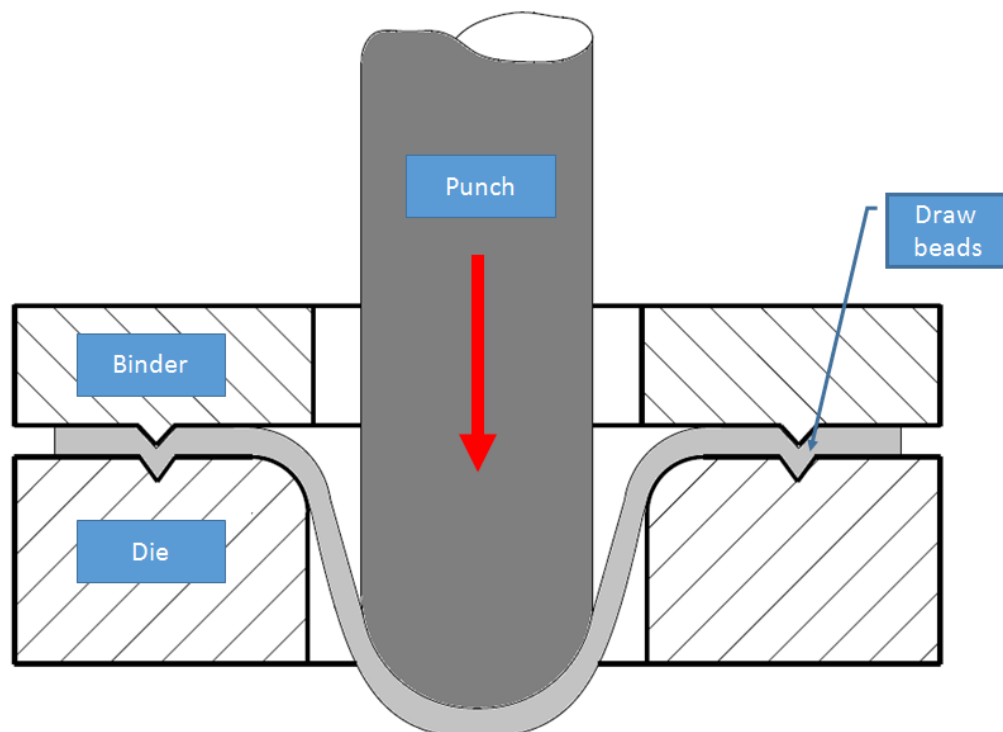


Figure 2.2: Stretch Forming [5].

In deep drawing operations, punch forces the material in to die. High compressive stresses act on the workpiece. If blankholder force is not suitable, there will be defects named as wrinkling. Wrinkling is the most common defect in deep drawing operations. It can damage the dies and produced parts.

There are many important variables in deep drawing operations. One is material and friction factors, coefficient of friction between punch-workpiece-die, normal anisotropy, limiting drawing ratio, and strain hardening coefficient. Other variables are tooling and equipment factors, which are punch corner radius, die corner radius, clearance, blankholder pressure and speed of the punch.

Drawability of the material used in the deep drawing of round cups can be measured by drawing ratio.

The drawing ratio of deep drawing operation:

$$DR = \frac{\text{Blank diameter, } d_0}{\text{Inner cup diameter, } d_1}$$

The limiting drawing ratio:

$$LDR = \frac{\text{Maximum blank diameter, (without fracture)}}{\text{Inner cup diameter}}$$

LDR can be increased by decreasing blank holder-sheet friction, decreasing sheet-die friction and increasing sheet-punch friction. Increasing relative ratio of blank thickness to diameter, increasing ratio of punch corner radius to punch diameter, decreasing relative punch diameter, using a material with high strain hardening exponent, increasing normal anisotropy and decreasing planar anisotropy are the other parameters which increase the limiting drawing ratio.

Among these parameters, friction is the most critical parameter to increase the formability.

If the lubrication in sheet metal forming is not sufficient, there will be high friction between the contacting bodies. This situation limits the material flow and formed products may be fractured. Examples of fractured parts can be seen in Figure 2.3. To prevent such defects lubricant conditions should be determined correctly. Wear is another parameter which has a direct negative influence on the products dimensions. Galling, that can occur during forming of metal also damages the tools and scratched products may occur.






Failure type		Friction	WEAR			
		poor lubrication	die clearance to narrow due to galling	worn draw bead	die clearance to large	die radius to large
Crack cylindrical part		■	■			
Sec. wrinkle pucker		■		■	■	■
Crack near bottom		■	■			
Drawing marks		■	■			
Asymmetrical flange		■				

Figure 2.3: Possible failures as a result of poor control of friction and wear during axisymmetric deep drawing [3].

2.2 FRICTION MODELS USED IN METAL FORMING

Coulomb, Tresca and Modified shear friction models are the models used in metal forming. In sheet metal forming operations Coulomb's friction model Eq.1.1 and shear friction model Eq. 1.2 are commonly used to describe frictional conditions [4].

$$\tau_f = \mu p \quad 1.1$$

where μ is the coefficient of friction (COF), p is the normal pressure, and τ_f is the frictional shear stress.

Coulomb's friction model is valid for low contact pressure [4]. But, in many forming processes interfacial pressure p , can reach a multiple of the yield strength of the material. In this case, frictional shear stress τ_f may exceed the k , shear strength of the workpiece material. So, the linear relationship between τ_f and p will not be valid at high contact pressure levels because of the coefficient of friction becomes meaningless when μp exceeds τ_f .

Metal forming operations like rolling, wire drawing and sheet metal forming can be given as examples of low contact pressure. On the other hand in closed die forging and extrusion operations contact pressure will commonly rise much higher than the flow stress of the workpiece.

Under high contact pressure, the Coulomb friction model may fail to describe the actual friction conditions. To avoid the limitations of Coulomb's model, the shear friction model Eq. 1.2 was proposed by Orowan [6].

$$\tau_f = f\bar{\sigma} = m\frac{\bar{\sigma}}{\sqrt{3}} = mk \quad 1.2$$

where f is the friction factor, m is the shear factor, $0 \leq m \leq 1$, k is the shear strength, $\bar{\sigma}$ is the flow stress of the workpiece material.

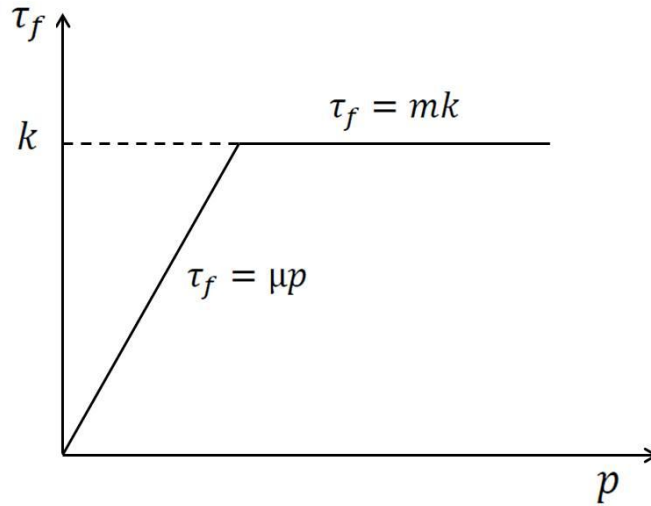


Figure 2.4: Relationship between contact pressure and frictional stress [5]

According to the shear friction model frictional shear stress τ_f , is proportional to the normal pressure similar to the Coulomb's model at low pressure values. However, it equals to the shear strength, k at high interfacial pressure p . The relationship between contact pressure and frictional stress can be seen in Figure 2.4.

Surface roughness causes discrete contact spots when two flat surfaces are placed in contact. The total area of these discrete contact spots creates the real contact area, A_r , and A_a is the apparent contact area. The ratio of real contact area, A_r , to the apparent contact area A_a , is known as the real contact contact area ratio, α . To consider the effect of real contact area, α on friction Wanheim and Bay proposed a general friction model [6].

$$\tau_f = f'\alpha k = m_r\frac{\bar{\sigma}}{\sqrt{3}} \quad 1.3$$

where f' is the modified friction factor, m_r is the modified shear factor which is a function of real contact area, $\bar{\sigma}$ is the flow stress, and α is the real contact area ratio

A_r/A_a . In this model the frictional shear stress τ_f is a function of real contact area, α .

According to the Wanheim and Bay's model lubrication effect did not taken into account. To take lubricant effect into account, a complex friction model was proposed by Bowden and Tabor [8]. In this model boundary and mixed film lubrication regimes at the tool-workpiece interface was developed.

Frictional shear stress can be calculated by the following equation;

$$\tau_f = \alpha\tau_a + (1 - \alpha)\tau_b \quad 1.4$$

Where α is the real contact area ratio, τ_a is the average shear stress at contacting asperity peaks, and τ_b is the average shear stress at the lubricant pockets. This model formulates the real contact area ratio, α , related to τ_a and the lubricant behavior related to τ_b that is influenced by viscosity, pressure, sliding speed and film thickness.

Although this model includes more detailed considerations to formulate the lubricant behavior, it is a difficult model to apply to practical metal forming problems.

2.3 LUBRICATION MECHANISMS IN METAL FORMING

In sheet metal forming, lubrication is an important parameter which affects friction conditions. Different lubrication mechanisms can be applied to the sheet metal forming processes. The dry condition, Boundary lubrication, Mixed-film lubrication and Hydrodynamic lubrication conditions are the lubrication conditions used in these operations.

Streibeck curve which illustrates the various types of lubrication mechanisms can be seen in Figure 2.5. In this curve η is the lubricant viscosity, v is the sliding velocity and p is the normal pressure [4].

In dry condition mechanism, there is no lubrication between the surfaces, so friction is high in this condition. If the frictional conditions do not significantly influence part quality, these conditions can be used. So, it is suitable only a few operations in metal forming such as hot rolling of plates and nonlubricated extrusion of aluminum alloys.

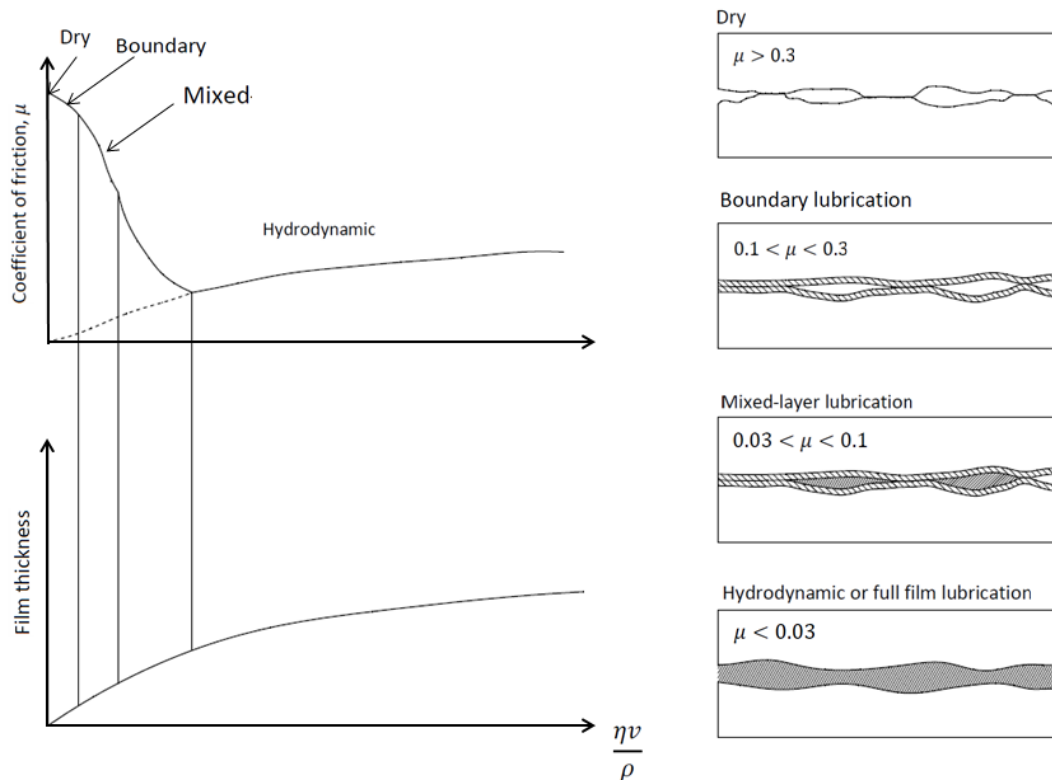


Figure 2.5: Stribeck curve showing onset of various lubrication mechanisms [5].

Boundary lubrication is the most widely used lubrication mechanism in metal forming operations. In these condition single or multimolecular films of lubricants provide the surface contact.

Mixed-layer lubrication is the other mostly used mechanism in sheet metal forming [5]. In this case micropeaks and the microvalleys of the metal surfaces are filled with the lubrication.

Hydrodynamic lubrication mechanism is useful in wire drawing or rolling processes where the workpiece moves with high speed into the dies. This is a favored mechanism due to large velocities at the material-tool interface creates hydrodynamic conditions. Hydrodynamic lubrication mechanism provides low friction conditions. Because there is no longer direct contact between the surface asperities of the two bodies.

Lubricant selection in this mechanism depends on some parameters. Methods of lubricant application, types of additives, corrosion control, cleanliness and removal methods and compatibility with other lubricants should be considered to select suitable lubricants.

2.4 MEASUREMENTS OF FRICTION IN SHEET METAL FORMING

Strip drawing test (SDT), draw bead test (DBT), limiting dome height test (LDH) and twist compression (TCT) tests are used to measure coefficient of friction and evaluate the lubrication performance.

Frictional conditions between the punch and sheet metal effects the location of fracture in LDH test. When the metal strip pulled through a roller element, thickness of the metal strip significantly reduces. This test is useful to test stamping lubricants. All these tests are useful to evaluate the performance of the lubricant at different locations of the die. It can be seen from Figure 2.6 that, deformed workpiece is under different states of stress and strain.

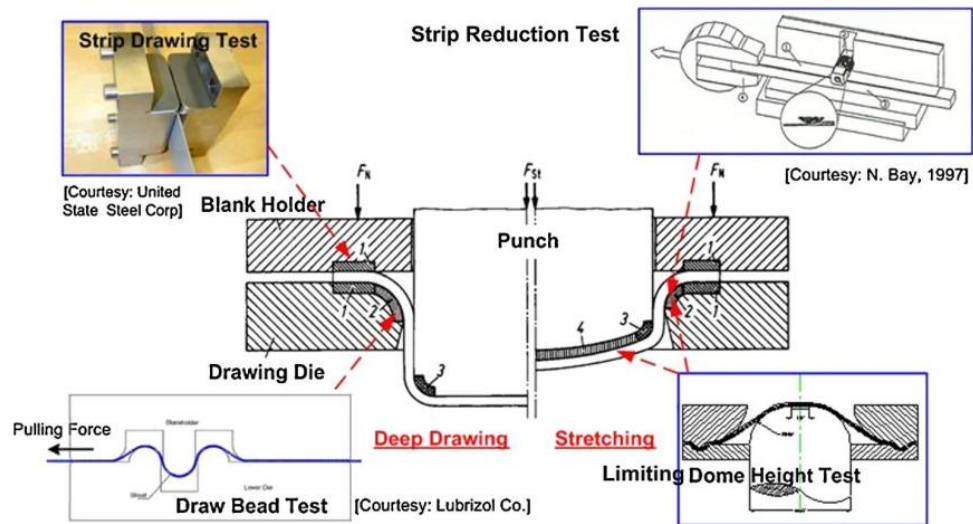


Figure 2.6: Various tests to determine the coefficient of friction [5].

The twist compression test seen in Figure 2.7 is widely used to determine the coefficient of friction for stamping lubricants for different tool coatings. In this test torque and pressure are measured when rotating tool is pressed to a fixed metal specimen. The coefficient of friction between the tool and the specimen can be calculated by the following equation.

$$\mu = \frac{T}{rPA} \quad 2.1$$

where μ is the coefficient of friction, T is the applied torque, r is the mean radius of the tool, P is the pressure applied on the tool and A is the area of contact between tool and sample.

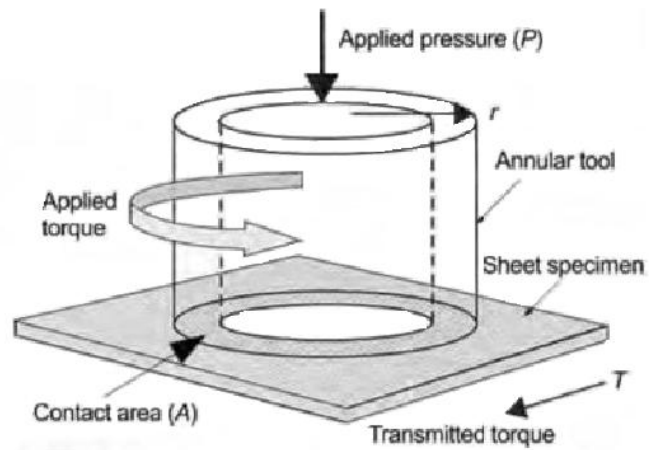


Figure 2.7: Schematic view of the twist compression test [5].

The strip drawing test is suitable to test high strength steels. Effect of different die radii, materials and lubricants are taken into account in this test. Schematic view of strip draw test can be seen in Figure 2.8.

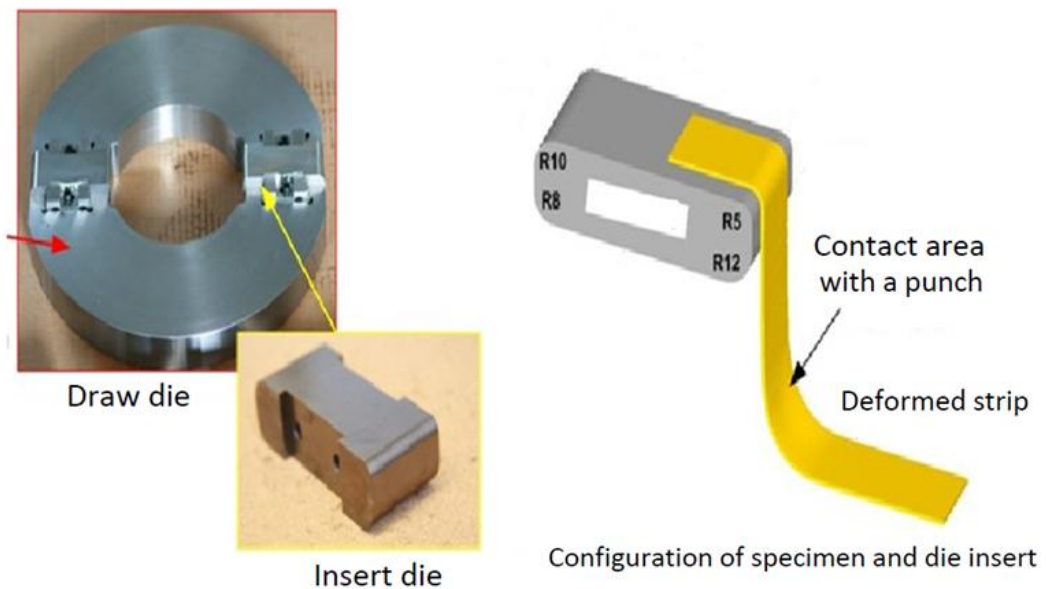


Figure 2.8: Deformed strip sample in Strip draw test [9].

Strip elongation and punch forces are the evaluation criteria to evaluate the performance of lubricants. Good lubrication will reduce the coefficient of friction and this will decrease the punch force and strip elongation.

The stresses and strains that exist at various locations in the workpiece may be different. We may obtain different values for the coefficient of friction while applying different tests with the same sheet material and lubricant. Because stresses and strains at various locations may be different in the workpiece. Furthermore, laboratory tests have limitations on emulating process conditions that exist in real sheet metal forming operations.

2.5 PREVIOUS STUDIES OF FRICTION IN SHEET METAL FORMING

Previous research about the investigation of friction in sheet metal forming provided the basis of the current study but the calculation of friction coefficient due to nonlinear extrapolation and the manual measurement of strains resulted in higher errors [2]. It was also limited to room temperature. Radial drawing and stretch forming regions of deep drawing were developed to calculate the coefficient of friction. In this study, it was found especially for the grease lubricants that the coefficient of friction decreased with increasing deformation. The coefficient of friction values for the radial drawing region were comparable to values which were found by other researchers using bending under tension. Values for the stretch forming region was found higher than the coefficient of friction values obtained from radial drawing region. It was also noticed that values for coefficient of friction decrease with the continued deformation.

In the past studies, strip draw and deep draw tests were commonly used to evaluate the stamping lubricants. Blank holder surface was polished to a surface roughness $R_a = 0,25 - 0,35 \mu m$. The dies used in this study had a surface roughness $R_a = 0,2 \mu m$. The criteria used for evaluation was maximum blank holder force and strip length in strip draw test and flange length in deep drawing test. Coefficient of friction was determined for different lubrication conditions and blank holder forces by comparing the results of FE simulations with experimental data. In such research, water-based lubricants performed better than petroleum-based lubricants and also coefficient of friction reduced with the increase in blankholder force with all other conditions remaining unchanged [10]. Many studies have been focused on explaining friction mechanisms under different loading conditions in forming operations using experimental, analytical and numerical methods. Although some basic friction

characterization is obtained at present, friction mechanism still is not properly understood in depth since it is a highly complex process.

The coefficient of friction under lubricated conditions at elevated temperature was also found. The coefficient of friction in hot stamping was measured using tribometer. Simulative experiments were carried out using steel sheet under dry conditions. It was shown that the use of lubricants was effective for decreasing the stamping load and die wear in hot stamping [11]. Coefficient of friction data obtained in strip drawing test was used in another study to show the importance of the lubrication on process parameters. Lubricant viscosity, drawing speed, die angle, stress-strain hardening characteristics of workpiece material and friction conditions in the workpiece tool interface were investigated [12]. The limits of lubrication was also investigated by using strip reduction test. In the experimental tests the threshold drawing lengths for film breakdown have been determined for different combinations of reduction and tool preheat temperature. Threshold drawing lengths before galling have been found for three different reductions and tool preheat temperatures showing good agreement with experimental results in. The analysis explained that the scatter observed in experimentally determined limits of lubrication indicated the influence of reduction and tool preheat temperature on the development of the maximum tool surface temperature with drawing length [13].

The drawability and frictional characteristics of pure molybdenum sheet at elevated temperature were investigated, and inverse comparison method was used to evaluate the frictional conditions [14]. Effect of die radius surface roughness of the tools, drawing speed, and blank holder force and lubrication type on coefficient of friction between flange and radius regions of the tools and sheet metal was investigated [15]. Surface parameters also affect the coefficient of friction. Deformation of sheet metal during forming was investigated and surface parameters were derived from three-dimensional surface measurements. The changes of topography during deformation process are decisively determined by the stress condition in the material plane and by the slip speed [16]. Correlation between the surface topography of dies and friction with sheet were investigated by using the bending under tension test. Linear regression coefficients between the friction and texture characterization parameters were tested. None of the height, spacing material volume, void or segmentation parameters showed good correlations. Developed area surface gradient, relative area

and complexity showed strong correlations [17]. Friction forces were modelled by introducing a relation between the surface parameters [18].

Variable friction model based on the regime of the lubrication has been integrated to a finite element program to analyze the sheet metal forming processes. The developed model was verified by comparing the numerically obtained axial and circumferential strains with the experimental results. It was found that the axial and circumferential strains are considerably affected by the value of the coefficient of friction around the punch and die profiles [19].

Load scanning type tester and draw bead type device used an experimental study to investigate the tribological characteristics of sheet metal forming. As a result, it was concluded that experimental techniques load scanning always produce lower friction values. This difference could be due to the highest contact pressure on the load scanning test. On the other hand roughness of the die material has a significant effect on the coefficient of friction [20].

To investigate the pressure dependence of the coefficient of friction in sheet metal forming, camera and video system was used with a transparent die. In the medium range, the coefficient of friction decreased with increasing pressure by closed lubricant pools in which the hydrostatic pressure is generated according to the hydrostatic-boundary lubrication model. The coefficient of friction decreases also in the higher pressure with increasing normal pressure and the lubrication regime is characterized by oil permeation into the real contact area according to the boundary hydrostatic and micro-plasto-hydrodynamic lubrication model [21].

Effect of plastic strain on surface roughness and coefficient of friction investigated using tension bending test. Smooth surface aluminum sheets were used as a workpiece. It was concluded that the surface roughness of the inner surface of specimen increased with increasing average contact pressure due to the surface roughening of the specimen at the lower pressure, but it decreased with increasing average contact pressure due to the flattening of surface asperities at the higher pressure [22].

Blank holder force and blank shape effect on the final part quality were also investigated. During the experiments it was found that the oval blank shape worst formability from a fracture point of view, among the three blank shapes as oval, oblong and rectangle. Control of a blank holder force as function of time improves the formability and quality of final part. However, BHF control in time is not enough

by it self. Since the deformation characteristics are not uniform around the periphery of the rectangle, the blank holder force has to be controlled as a function location. Metal flow can be controlled by using drawbeads on the sides of the rectangle. However, blank holding pressure may still be necessary to eliminate the wrinkles completely [23]. Controlled FEM simulation can be applied to determine the history of the blank holding force-BHF in deep drawing of aluminum sheet. In this method feedback control of the forming machine is possible by evaluating the data provided by the simulated results and movement of the machine is then changed automatically to suitable ones. As a result of this method desirable forming path or history of the working condition can be traced [24].

To investigate the effect of die shoulder friction studies were conducted with a transducer for determining the tension in a sheet metal strip. Although both an increase in sheet thickness and a decrease in the die shoulder radius resulted in an increase in strip tension, the study showed the friction coefficient trajectories of the tests to be largely unaffected by the die shoulder radii, sheet thickness and drawbead penetration speed used in this study [25].

Some simulative tests were performed to investigate friction in sheet metal forming. It was noticed that according to the bending under tension - BUT test punch speed and pin radius on sheet metal forming can be investigated. From the results of this it was concluded that the coefficient of friction values are reasonable for both dry and lubricated conditions [26]. To evaluate the average frictional coefficient at the interface between a sheet metal specimen and a tooling pin, an experimental equipment was derived. In this way several materials were tested and the influence of the surface finish of the tooling pin, of the tooling pin diameter, contact pressure and lubricants were investigated [27]. For the quick calculation of coefficient of friction in sheet metal forming strain distribution on the strip on a cylindrical surface was used. The Capstan equation is used to evaluate the coefficient of friction acting between the sheet strip and cylindrical surface. This method is rough but quick to evaluate coefficient of friction in sheet metal forming [28].

A friction model that can be used in large FE simulations was developed which includes flattening mechanisms to determine the real area of contact at a microscopic level. The developed friction model was validated by means of FE simulations at a micro-scale. Comparison between the analytical and the FE simulation is obtained in case of crushing a rough surface by a normal load. It was also found that work

hardening effects do not play a significant role in the case of pure normal loading. The model also implemented in a FE code and applied to a full-scale sheet metal forming simulations. Results of the simulations were reasonable values for the coefficient of friction in case of normal loading [29].

An inverse analysis that combines the FEM and optimization algorithm was developed to determine flow stress and interface friction simultaneously. The results indicated that with this method it was possible to predict the flow stress and friction with acceptable accuracy [30].

Results from such simulative tests were used in finite element analysis as input. Such simulations are important tools for sheet metal forming industry and importance of the friction data were emphasized [31]. Based on recent advances in friction modelling a pressure slip rate and temperature dependent friction model suited for numerically stable multi-dimensional regression analysis was presented and implemented in Abaqus [32]. Tribological size effects on friction was investigated with a test method strip drawing with deflection. This method can be used for a very small process dimension. The friction functions can also be integrated in the FEM simulation which makes it possible to simulate a sheet metal forming process with consideration of tribological size effects [33].

CHAPTER 3

OBJECT OF PRESENT INVESTIGATION

In sheet metal forming industry use of finite element simulations allow to decrease manufacturing costs and time. Geometry, material models and friction models are the main inputs of the FE simulations. Commercial CAD software enables to design die, workpiece and blank holder geometry accurately. On the other hand material characterization tests like tensile test or bulge tests allows to obtain flow curve of the materials at the room temperature and high temperature. However it was discussed in the previous section, there is a limited research about determination of friction in sheet metal forming.

For the stretch forming zone this study aims to calculate the coefficient of friction dependent on the interfacial pressure between the punch and workpiece. Previous study about this topic assumes that the coefficient of friction is independent on interfacial pressure. However, in real process pressure effects the coefficient of friction. Determination of the dependency of the coefficient of friction on the interfacial pressure will enable to obtain more accurate results. This development is the one of the most important improvement of this study. In this way for the FE simulations friction models will be modelled more accurately. This will cause to get accurate results from the simulations.

On the other hand for deep drawing operations radial drawing zone is also investigated in this study. High temperature real deep drawing tests are performed at different blank holder loads to obtain different punch loads.

Graphite and paraffin lubrications are also used to investigate the effect of lubrication. Beside lubricants surface roughnesses of the die and workpiece were also measured to observe the effect on coefficient of friction.

As a result of this study interfacial pressure dependent coefficient of friction calculations are obtained for stretch forming zone. Elevated and room temperature real deep drawing tests are also improved to get accurate results from coefficient of friction calculations in sheet metal forming.

If the accuracy of the inputs of FE simulations increase, the results will be more reliable. So, this study may contribute to get better performance from FE simulations to decrease manufacturing costs and process time.



CHAPTER 4

MODELLING OF FRICTION IN DEEP DRAWING

Main features of deep drawing operation can be seen in Figure 4.1. It can be seen from the figure that radial drawing zone and stretch forming zones are the zones where friction occurs. These two zone will be analyzed separately to obtain the coefficient of friction.

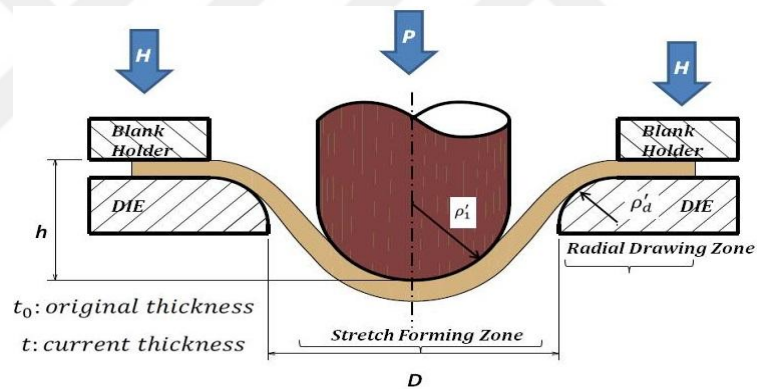


Figure 4.1: Main features of deep drawing.

4.1 DETERMINATION OF COEFFICIENT OF FRICTION IN RADIAL DRAWING ZONE

In radial drawing zone there is friction between sheet metal, die and blankholder. For radial drawing region an expression can be derived to calculate the coefficient of friction by using the equilibrium equations [3].

Circumferential strains can be calculated from the mean deformed radii and original radii of the scribed circles using following equations:

$$\varepsilon_{\theta} = \ln \frac{R_m}{R_0} \quad 4.1$$

where ε_θ =logarithmic circumferential strain

R_m =mean radius of deformed circle

R_0 =initial radius of circle

For the thickness strains;

$$\varepsilon_t = \ln \frac{t_m}{t_0}$$

4.2

where ε_t =logarithmic through-thickness strain

t_m =mean thickness after deformation

t_0 =original thickness

The forces acting on a segment of a round specimen subtended by an angle $\delta\theta$ are as illustrated in the top of the Figure 4.2. The plan view shows the distribution of forces acting on a segment of the flat flange. The circumferential stresses induced by plastic deformation of the flange are denoted by σ_θ and these can be assumed to be unaffected by friction, to a first-order approximation, for any given value of α .

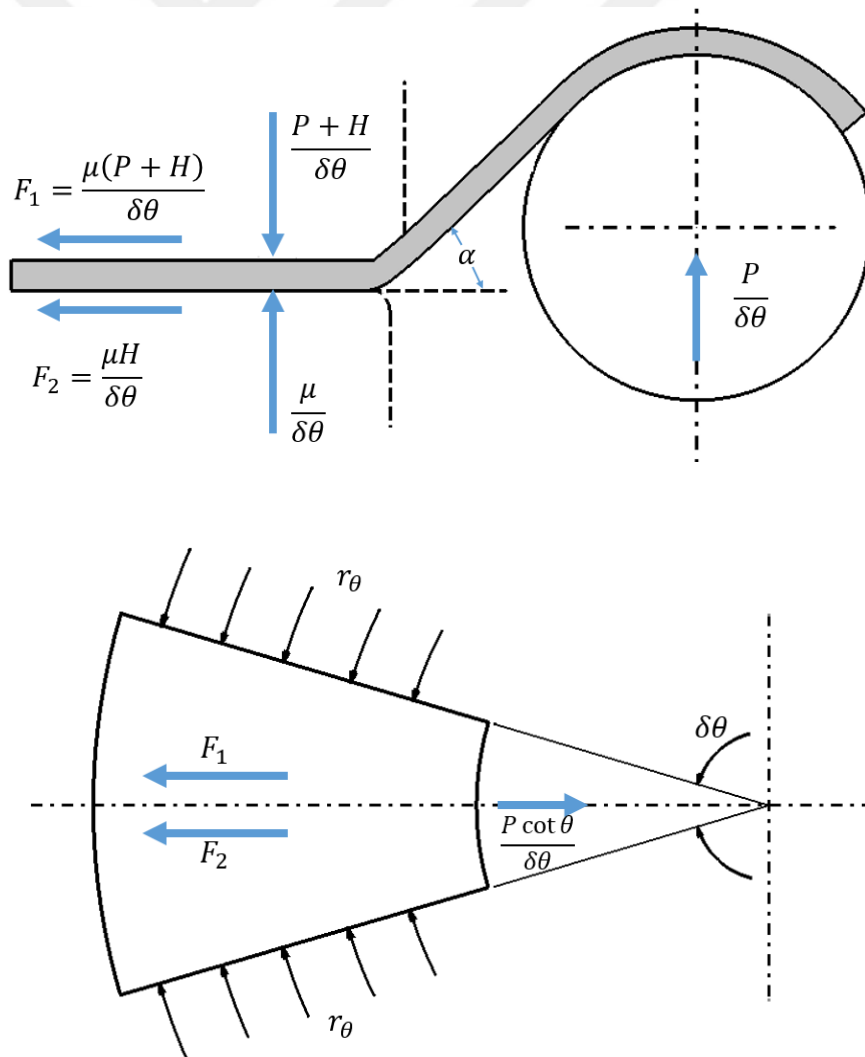


Figure 4.2: Forces acting on a segment of a round specimen [3].

In Figure 4.2 and Figure 4.3;

P : punch load

H : blank holder load

μ : coefficient of friction

h : bulge depth

α : angle of embrace of the die

ρ'_d : die radius

ρ'_1 : punch radius

$F_1 = \frac{\mu(P+H)}{\delta\theta}$ = friction force on upper surface

$F_2 = \frac{\mu H}{\delta\theta}$ = friction force on lower surface

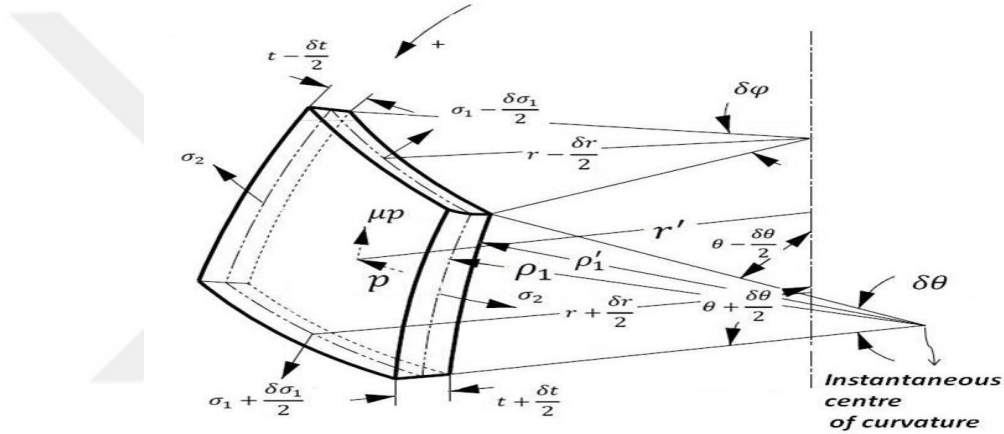


Figure 4.3: Stresses on element of shell wall [2].

In the absence of friction F_1 and F_2 would be absent, and equilibrium of horizontal forces would require that the horizontal component of $\frac{P}{\delta\theta}$, namely $\frac{P \cot \theta}{\delta\theta}$, should balance the circumferential stresses in the flange. This value of punch load may be denoted by P_0 . If it is assumed that the circumferential stresses σ_θ are not affected by the increase of shear stresses on the surface, then horizontal equilibrium requires that,

$$\frac{P \cot \alpha}{\delta\theta} = \frac{P_0 \cot \alpha}{\delta\theta} + F_1 + F_2$$

$$P \cot \alpha = P_0 \cot \alpha + \mu(P + 2H) \quad 4.3$$

Differentiating this equation keeping P_0 and α constant,

$$\mu = \frac{\delta P \cot \alpha}{\delta P + 2\delta H} \quad 4.4$$

The variation of $\cot \alpha$ with depth of penetration h can be determined on the assumption that the thickness of the sheet material remains constant and equal to its original thickness t_0 , from consideration of the geometry of the bulge, which leads to the equation where the symbols refer to the dimensions indicated in Figure 4.2.

$$h = \left(\frac{D}{2} + \rho'_d\right) \tan \alpha - (\rho'_1 + \rho'_d + t_0)(\sec \alpha - 1) \quad 4.5$$

Thus, the value of μ can be estimated for the same value of h from two tests carried out under identical conditions, with the exception that the blank holder load is altered by an amount δH , which lead to a change in P of δP . It may be pointed out here that the effect of punch load on friction appears to have been neglected in the theories of Chung and Swift and Fukui [3]. Since the punch load is normally much higher than the blank holding load, neglect of this likely to lead to significant errors if it is desired to include the effect of friction in the analysis.

The method suggested here for estimating the coefficient of friction during pressing or drawing has the advantage that is being measured in the actual process and not in simulative process. It is theoretically also possible to predict any variation of μ during the operation, due for example to the effect of punch load on friction. The main disadvantage is that the result is dependent on taking the difference between large, nearly equal, quantities and is therefore subject to some error. The error in neglecting the effect of increase in frictional stresses on the circumferential stresses in the flange is also not known; this error will clearly be eliminated by plotting μ versus δH and extrapolating back to zero δH .

This technique can be used at room temperature or at high temperatures provided that the appropriate data is obtained. Applying this equation at high temperatures is the new improvement of this study.

4.2 DETERMINATION OF COEFFICIENT OF FRICTION IN STRETCH FORMING ZONE:

Coefficient of friction in stretch forming zone can be calculated by using the equilibrium equations. According to the existing technique, coefficient of friction is independent of the interfacial pressure between the punch and workpiece. However, new developed equation takes the interfacial pressure into account.

In the next sections investigation of the existing technique and development of the new equation will be discussed.

4.2.1 Investigation of the existing technique to calculate the coefficient of friction in stretch forming [2].

$$\frac{d(\sigma_1 t)}{d\theta} + 2(\sigma_1 t) \cot \theta = p\rho(\cot \theta + \mu) \quad 4.6$$

$\frac{d(\sigma_1 t)}{d\theta} = (\sigma_1 t)'$ the derivation of the equation can be shown below

$$(\sigma_1 t)' + 2\sigma_1 t \cot \theta = p\rho(\cot \theta + \mu) \quad 4.7$$

$$\underbrace{(\sigma_1 t)'}_{y'} + \underbrace{\sigma_1 t}_{y} \underbrace{2 \cot \theta}_{P(x)} = \underbrace{p\rho(\cot \theta + \mu)}_{Q(x)} \quad 4.8$$

Eq. 4.8 is a first order linear ordinary differential equation. To solve this equation each term is multiplied by $e^{\int 2 \cot \theta d\theta}$.

$$e^{\int P(\theta)d\theta} = e^{\int 2 \cot \theta d\theta} = e^{\ln \sin \theta + c} \quad 4.9$$

$$a^x = e^{x \ln a} \rightarrow e^{2 \ln |\sin \theta|} = \text{Sin}^2 \theta \quad 4.10$$

$$(y)' + 2y \cot \theta = p\rho(\cot \theta + \mu) \quad 4.11$$

$$y = \sigma_1 t \quad 4.12$$

$$y' \text{Sin}^2 \theta + 2y \cot \theta \text{Sin}^2 \theta = p\rho(\cot \theta + \mu) \text{Sin}^2 \theta \quad 4.13$$

$$y' \text{Sin}^2 \theta + 2y \frac{\cos \theta}{\sin \theta} \sin \theta \sin \theta = p\rho \left(\frac{\cos \theta}{\sin \theta} + \mu \right) \sin \theta \sin \theta \quad 4.14$$

$$y' \text{Sin}^2 \theta + 2y \sin \theta \cos \theta = p\rho \sin \theta \cos \theta + p\rho \text{Sin}^2 \theta \mu \quad 4.15$$

$$y' \text{Sin}^2 \theta + 2y \sin 2\theta = p\rho \sin \theta \cos \theta + p\rho \text{Sin}^2 \theta \mu \quad 4.16$$

$$y' \text{Sin}^2 \theta + \sin 2\theta y = p\rho \sin \theta \cos \theta \quad 4.17$$

$$\underbrace{y'}_{v'} \underbrace{\text{Sin}^2 \theta}_u + \underbrace{\sin 2\theta}_{u'} \underbrace{y}_{v} = \underbrace{p\rho \sin \theta \cos \theta + p\rho \mu \text{Sin}^2 \theta}_{(uv)'} \quad 4.18$$

$$(uv)' = p\rho \sin \theta \cos \theta + p\rho \mu \text{Sin}^2 \theta \quad 4.17$$

$$(\sigma_1 t \sin^2 \theta)' = p\rho \sin \theta \cos \theta + p\rho\mu \sin^2 \theta \quad 4.18$$

$$\sigma_1 t \sin^2 \theta = \int (p\rho \sin \theta \cos \theta) d\theta + \int (p\rho\mu \sin^2 \theta) d\theta \quad 4.19$$

$$\sigma_1 t \sin^2 \theta = p\rho \int (\sin \theta \cos \theta) d\theta + p\rho\mu \int (\sin^2 \theta) d\theta \quad 4.20$$

Integration of trigonometric functions:

$$\int (\sin cx \cos cx) dx = \frac{1}{2c} \sin^2 cx$$

$$\int (\sin x \cos x) dx = \frac{1}{2} \sin^2 x$$

$$\int (\sin^2 cx) dx = \frac{x}{2} - \frac{1}{4c} \sin 2cx$$

$$\int (\sin^2 x) dx = \frac{x}{2} - \frac{1}{4} \sin 2x$$

$$\sigma_1 t \sin^2 \theta = p\rho \int (\sin \theta \cos \theta) d\theta + p\rho\mu \int (\sin^2 \theta) d\theta \quad 4.21$$

$$\sigma_1 t \sin^2 \theta = p\rho \left(\frac{1}{2} \sin^2 \theta \right) + p\rho\mu \left(\frac{\theta}{2} - \frac{\sin 2\theta}{4} \right) \quad 4.22$$

$$\frac{\sigma_1 t \sin^2 \theta}{t \sin^2 \theta} = \frac{p\rho}{t \sin^2 \theta} \left(\frac{\sin^2 \theta}{2} \right) + \frac{p\rho\mu}{t \sin^2 \theta} \left(\frac{\theta}{2} - \frac{\sin 2\theta}{4} \right) \quad 4.23$$

$$\sigma_1 = \frac{p\rho}{2t} + \frac{p\rho\mu}{2t} \left(\frac{\theta}{\sin^2 \theta} - \frac{2 \sin \theta \cos \theta}{2 \sin \theta \sin \theta} \right) \quad 4.24$$

$$\sigma_1 = \frac{p\rho}{2t} + \frac{p\rho\mu}{2t} \left(\frac{\theta}{\sin^2 \theta} - \frac{\cos \theta}{\sin \theta} \right) \quad 4.25$$

$$\sigma_1 = \frac{p\rho}{2t} \left[1 + \mu \left(\frac{\theta}{\sin^2 \theta} - \frac{\cos \theta}{\sin \theta} \right) \right] \quad 4.26$$

$$\sigma_1 = \frac{p\rho}{2t} \left[1 + \frac{\mu}{\sin \theta} \left(\frac{\theta}{\sin \theta} - \cos \theta \right) \right] \quad 4.27$$

$$\sigma_1 = \frac{p\rho}{2t} \underbrace{\left[1 + \frac{\mu}{\sin \theta} \left(\frac{\theta}{\sin \theta} - \cos \theta \right) \right]}_A = \frac{p\rho}{2t} A \quad 4.28$$

$$\sigma_2 = \frac{p\rho}{t} - \sigma_1 \quad 4.29$$

$$\frac{\sigma_2}{\sigma_1} = x = \frac{\frac{p\rho}{t} - \frac{p\rho A}{2t}}{\frac{p\rho A}{2t}} = \frac{\frac{p\rho}{t} \left[\frac{1-A}{2} \right]}{\frac{p\rho}{t} \left[\frac{A}{2} \right]} = \frac{1-\frac{A}{2}}{\frac{A}{2}} = \frac{\frac{2-A}{2}}{\frac{A}{2}} = \frac{2-A}{A} = \frac{2}{A} - 1 \quad 4.30$$

$$x = \frac{2}{\left[1 + \frac{\mu}{\sin \theta} \left(\frac{\theta}{\sin \theta} - \cos \theta \right) \right]} - 1 \quad 4.31$$

$$x + 1 = \frac{2}{\left[1 + \frac{\mu}{\sin \theta} \left(\frac{\theta}{\sin \theta} - \cos \theta \right) \right]} \quad 4.32$$

$$(x + 1) \left[1 + \frac{\mu}{\sin \theta} \left(\frac{\theta}{\sin \theta} - \cos \theta \right) \right] = 2 \quad 4.33$$

$$(x + 1) + \frac{(x+1)\mu}{\sin \theta} \left(\frac{\theta}{\sin \theta} - \cos \theta \right) = 2 \quad 4.34$$

$$\frac{(x+1)\mu}{\sin \theta} \left(\frac{\theta}{\sin \theta} - \cos \theta \right) = 2 \quad 4.35$$

$$(x + 1) + \frac{(x+1)\mu}{\sin \theta} \left(\frac{\theta}{\sin \theta} - \cos \theta \right) = 2 \quad 4.36$$

$$\frac{(x+1)\mu}{\sin \theta} \left(\frac{\theta}{\sin \theta} - \cos \theta \right) = 2 - x - 1 = 1 - x \quad 4.37$$

$$\frac{\mu}{\sin \theta} \left(\frac{\theta}{\sin \theta} - \cos \theta \right) = \frac{1-x}{1+x} \quad 4.38$$

$$\mu \left(\frac{\theta}{\sin \theta} - \cos \theta \right) = \frac{(1-x) \sin \theta}{(1+x)} \quad 4.39$$

$$\mu \left(\frac{\theta - \sin \theta \cos \theta}{\sin \theta} \right) = \frac{(1-x) \sin \theta}{(1+x)} \quad 4.40$$

$$\mu = \frac{(1-x) \sin \theta}{(1+x)} \frac{\sin \theta}{(\theta - \sin \theta \cos \theta)} \quad 4.41$$

$$\mu = \frac{(1-x) \sin^2 \theta}{(1+x)(\theta - \sin \theta \cos \theta)} \quad 4.42$$

4.2.2 Development of new equation to calculate the coefficient of friction in stretch forming.

In the stretch forming zone, coefficient of friction can also be calculated by using the equilibrium and the plasticity equations. Figure 4.2 shows the stresses acting on an element of shell wall.

where:

h : bulge depth

p : interfacial pressure between punch and sheet metal

k : stress ratio = $\frac{\sigma_3}{\sigma_1}$

x : stress ratio = $\frac{\sigma_2}{\sigma_1}$

R : parameter of plastic anisotropy = $d\varepsilon_\omega^*/d\varepsilon_t^*$

r : current radius to mean shell wall

r_0 : original radius to mean shell wall

$\varepsilon_1, \varepsilon_2, \varepsilon_3$: true plastic strains in meridional, circumferential and thickness directions

$\sigma_1, \sigma_2, \sigma_3$: Meridional, circumferential and thickness stresses

θ : Angle, that normal to an element of shell wall makes with the vertical

μ : Coefficient of friction

ρ_1 : Meridional radius of curvature to mean shell wall

Equilibrium equation in axial direction is [2]:

$$\frac{1}{r} \frac{d}{dr} (\sigma_1 t r) + \left[p \rho_1' \frac{r'}{r} (\tan \theta - \mu) - \sigma_1 t \tan \theta - \sigma_2 \frac{\rho_1 t}{r \cos \theta} \right] \frac{d\theta}{dr} = 0 \quad 4.43$$

In the thickness direction [2]:

$$\frac{1}{r} \frac{d}{dr} (\sigma_1 t r) + \left[\sigma_1 t \cot \theta - p \rho_1' \frac{r'}{r} (\cot \theta + \mu) \right] \frac{d\theta}{dr} = 0 \quad 4.44$$

Subtracting Eq. 4.43 from Eq. 4.44:

$$p = \frac{t}{\rho r} (\sigma_1 r + \sigma_2 \rho_1 \sin \theta) \quad 4.45$$

From Eq. 4.45, it is clear that the interfacial pressure is a function of θ . In addition to θ, σ_1 and σ_2 stresses must be known to calculate the pressure, but it is not possible to

measure the stresses during deformation. These two stresses can be calculated approximately, by using strain distributions and the flow curve of the material.

Then effective strain can be calculated with the following equation:

$$\bar{\varepsilon} = \sqrt{\frac{2}{3}(\varepsilon_1^2 + \varepsilon_2^2 + \varepsilon_3^2)} \quad 4.46$$

$$\text{Assuming; } \frac{\sigma_3}{\sigma_1} \cong 0 \quad 4.47$$

Effective stress will be equal to:

$$\bar{\sigma} = \sqrt{\{\sigma_1^2 - \sigma_1\sigma_2 + \sigma_2^2\}} \quad 4.48$$

Relation between the σ_1 and σ_2 values can be obtained from the strain measurements.

$$\frac{d\varepsilon_1}{d\varepsilon_2} = \frac{\frac{2}{3}d\lambda\left[\sigma_1 - \frac{1}{2}(\sigma_2 + \sigma_3)\right]}{\frac{2}{3}d\lambda\left[\sigma_2 - \frac{1}{2}(\sigma_1 + \sigma_3)\right]} = r_\varepsilon \quad 4.49$$

$$\frac{\sigma_2}{\sigma_1} = \frac{2r_\varepsilon + 1}{2 + r_\varepsilon} \quad 4.50$$

Interfacial pressure can be calculated by the following equation;

$$p = \sigma_1 t \left[\frac{1}{\rho} + \frac{x \sin \theta}{r} \right] \quad 4.51$$

Recalling the Eq. 4.43 and Eq. 4.44 in thickness and axial directions,

For a hemispherical punch

$$r = \rho_1 \sin \theta \quad \text{and} \quad dr = \rho_1 \cos \theta d\theta \quad 4.52$$

and for thin shells

$$r \sim r' \quad \text{and} \quad \rho_1 = \rho'_1 \quad 4.53$$

Substituting Eq. 4.52 and Eq. 4.53 in Eq. 4.44:

$$\frac{d(\sigma_1)}{d\theta} + 2(\sigma_1 t) \cot \theta = p\rho(\cot \theta + \mu) \quad 4.54$$

Eq. 4.54 is a first order linear differential equation. To solve this equation, each term is multiplied by $e^{\int 2 \cot \theta d\theta}$.

$$(\sigma_1 t)' (\sin \theta)^2 + 2(\sigma_1 t) \cot \theta (\sin \theta)^2 = p\rho(\cot \theta + \mu) (\sin \theta)^2 \quad 4.55$$

$$(\sigma_1 t)'(\sin \theta)^2 + 2(\sigma_1 t) \frac{\cos \theta}{\sin \theta} (\sin \theta)^2 = p\rho \left(\frac{\cos \theta}{\sin \theta} + \mu \right) (\sin \theta)^2 \quad 4.56$$

$$(\sigma_1 t)'(\sin \theta)^2 + 2(\sigma_1 t) \sin \theta \cos \theta = p\rho \sin \theta \cos \theta + p\rho\mu(\sin \theta)^2 \quad 4.57$$

$$(\sigma_1 t)'(\sin \theta)^2 + (\sigma_1 t) \sin 2\theta = p\rho \sin \theta \cos \theta + p\rho\mu(\sin \theta)^2 \quad 4.58$$

$$v'u + u'v = (uv)'$$

$$(uv)' = p\rho \sin \theta \cos \theta + p\rho\mu(\sin \theta)^2$$

$$\text{here } u = (\sin \theta)^2$$

$$\text{so, } v = (\sigma_1 t)$$

$$(\sigma_1 t(\sin \theta)^2)' = p\rho \sin \theta \cos \theta + p\rho\mu(\sin \theta)^2 \quad 4.59$$

$$\sigma_1 t(\sin \theta)^2 = \int p\rho \sin \theta \cos \theta d\theta + \int p\rho\mu(\sin \theta)^2 d\theta \quad 4.60$$

$$\sigma_1 t(\sin \theta)^2 = \rho \int p \sin \theta \cos \theta d\theta + \rho\mu \int p(\sin \theta)^2 d\theta \quad 4.61$$

Existing theory derived in the previous study [2] is independent of interfacial pressure. In this study pressure is approximately calculated by using the plasticity equations. Using interfacial pressure value with the equilibrium equations, new equation for determination coefficient of friction can be derived. Following steps shows how the new equation derived

By using Eq. 4.51, interfacial pressure can be expressed as;

$$p = a\theta^2 + b\theta + c \quad 4.62$$

Pressure distribution fitted to a second order polynomial curve can be in Figure 5.29.

$$\int p \sin \theta \cos \theta d\theta = \frac{1}{8} [(-4c(\cos \theta)^2) + (a - 2b\theta - 2a\theta^2) \cos(2\theta) + b + 2a\theta \sin 2\theta] \quad 4.63$$

$$\int p(\sin \theta)^2 d\theta = \frac{[2\theta(6c+3b\theta+2a\theta^2)-3(b+2a\theta)\cos(2\theta)-3(-a+2c+2b\theta+2a\theta^2)\sin(2\theta)]}{24} \quad 4.64$$

$$\sigma_1 t(\sin \theta)^2 = \rho(A + \mu B) \quad 4.65$$

$$\sigma_1 = \frac{\rho}{t(\sin \theta)^2} (A + \mu B) \quad 4.66$$

$$\sigma_2 = \frac{p\rho}{t} - \sigma_1 \quad 4.67$$

$$\sigma_2 = \frac{p\rho}{t} - \frac{\rho}{t(\sin \theta)^2} (A + \mu B) \quad 4.68$$

$$\sigma_1 t (\sin \theta)^2 = \rho A + \rho \mu B \quad 4.69$$

$$\sigma_2 = \frac{\rho}{t} \left[p - \frac{1}{t(\sin \theta)^2} (A + \mu B) \right] \quad 4.70$$

$$\frac{\sigma_2}{\sigma_1} = \frac{p - \frac{1}{(\sin \theta)^2} (A + \mu B)}{\frac{1}{(\sin \theta)^2} (A + \mu B)} = x \quad 4.71$$

To calculate the coefficient of friction in stretch forming following equation can be used.

$$\mu = \frac{p - \frac{A}{(\sin \theta)^2} (x+1)}{\frac{B}{(\sin \theta)^2} (x+1)} \quad 4.72$$

where;

$$A(\theta) = \frac{1}{8} [(-4c(\cos \theta)^2) + (a - 2b\theta - 2a\theta^2) \cos(2\theta) + (b + 2a\theta) \sin(2\theta)]$$

$$B(\theta) = \frac{1}{24} [2\theta(6c + 3b\theta + 2a\theta^2) - 3(b + 2a\theta) \cos(2\theta) - 3(-a + 2c + 2b\theta + 2a\theta^2) \sin(2\theta)]$$

CHAPTER 5

EXPERIMENTAL DETERMINATION OF FRICTION IN SHEET METAL FORMING

As discussed before radial drawing zone and stretch forming zone are the zones where the friction occurs in sheet metal forming operations.

In this study to find the coefficient of friction between the die, workpiece and blank holder real scale deep drawing test are performed by using the hemispherical punch. EN 10268 steel is as workpiece material. Two tests are carried out under identical conditions only changing the blank holder load. Change in the blank holder load δH will lead to a change in punch load as, δP . Deep drawing experiments are also done at high temperatures. Due to high temperature graphite lubricant is used to determine the effect of lubricant on coefficient of friction.

Stretch forming tests are also done to find the coefficient of friction between the punch and workpiece. Hemispherical punch is used to form the EN 10346/ DX54D+Z, EN 10346/ HX380LAD+Z and EN 10346/ HX220BD+Z materials. Strain distributions obtained at two different stage of the test by using the optical measurements. New developed equation is used to find the coefficient of friction dependent on the interfacial pressure. For the corresponding values effective stresses and effective strains must be known to find the coefficient of friction by using the new developed equation. So material characterization is also given for the materials which were used in stretch forming tests. As a lubricant paraffin is used to determine effect of lubricant on the stretch forming zone.

Surface roughness is also another important parameter which effects the friction in sheet metal forming. For the radial drawing region surface roughness measurements are also done for the die and workpiece.

Detailed information about the test parameter and test apparatus will be discussed in the next sections.

5.1 MATERIAL CHARACTERIZATION

This thesis aims to find the coefficient of friction in sheet metal forming dependent on the interfacial pressure. It is very difficult to model the contacting body interfaces. However, interfacial pressure between the punch and sheet metal approximately calculated by using the plasticity equations. As discussed in the previous chapter, if we assume that $\frac{\sigma_3}{\sigma_1} \cong 0$, meridional and circumferential stresses can be calculated by using the effective stress equation in Eq. 4.48. So, to find the coefficient of friction between the punch and workpiece effective stresses and effective strains of the workpiece material must be known. EN 10346/ DX54D+Z, EN 10346/ HX380LAD+Z and EN 10346/ HX220BD+Z are the three different sheet material used in the stretch forming tests.

For the steel grades used in the experiments, chemical compositions are shown in Table 5.1 [34].

Table 5.1: Chemical Compositions of the steels used in the experiments.

Corresponding			C max.	Si max.	Mn max.	P max.	S max.	Al max.	V max.	Nb max.	Ti max.
Standard	Similar standard	Erdemir Steel Grade									
EN 10268	-	7140	0.14	0.50	1.60	0.03 0	0.02 5	0.015	-	0.09 0	0.15
EN 10346/ HX220BD+Z	52814/9.52 873	380 ⁽¹⁾⁽²⁾	0.007- 0.06	0.50	0.15- 0.70	0.05- 0.09	0.03	0.02- 0.07	-	-	-
EN 10346/ HX380LAD+ Z	52811/9.52 873	368 ⁽³⁾	0.12	0.50	1.50	0.03 0	0.03 0	0.015 (min)	0.1	0.10	
EN 10346/ DX54D+Z	52806/9.52 873	326	0.008	0.03	0.30	0.02	0.02 0	0.02 (min)		0.03 5	0.11

1) % Ni+%Cu+%Cr+%Mo≤0.5, 2) % C+% P≤0.16 3) % Nb+Ti+V≤0.22

In Atılım University Metal Forming Center of Excellence material characterization test are performed by the following methods [35].

5.1.1 Tensile Test

Tensile test is widely used method to obtain the mechanical properties of sheet materials. Mechanical properties such as, tensile strength (UTS), yield strength (σ_y), percent elongation ($\Delta L\%$), reduction in cross sectional area ($RA\%$), Young's

modulus (E) and Poisson's ratio (ν) can be found by the use of this test techniques. Tensile specimen is shown in Figure 5.1.

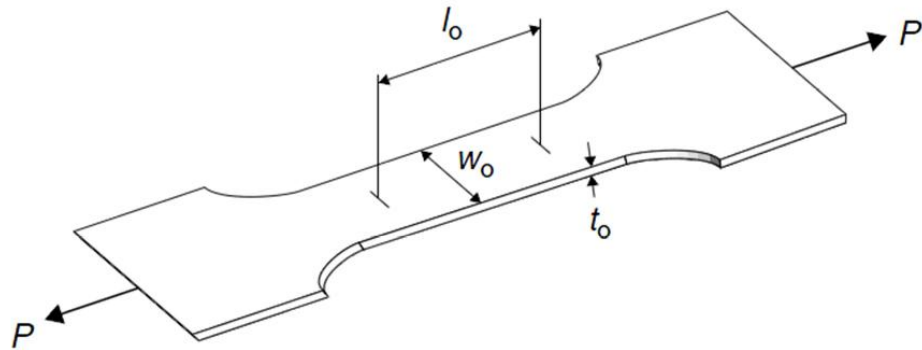


Figure 5.1: Typical tensile test specimen [35].

True stress can be calculated by the following equation:

$$\sigma = \frac{F}{A} \quad 5.1$$

A is the current cross section area of the specimen. During the tensile testing, current cross sectional area decreases with the applied load.

However, the volume of the gage section is constant.

$$A_0 l_0 = A l \quad 5.2$$

True stress can be defined as;

$$\sigma = \frac{F l}{A_0 l_0} \quad 5.3$$

True strain is;

$$d\varepsilon = \frac{dl}{l} \quad 5.4$$

$$\varepsilon = \int_{l_0}^l d\varepsilon = \int_{l_0}^l \frac{dl}{l} = \ln \frac{l}{l_0} \quad 5.5$$

where,

σ_{eng} : Engineering stress (MPa)

ε_{eng} : Engineering strain (mm/mm)

F : Load (N)

A_0 : Initial cross sectional area (mm^2)

Δl : Longitudinal extension increment (mm)

l_0 : Initial gage length (mm)

σ : True stress MPa

ε : True strain (mm/mm)

Three repeated tensile tests for different directions ($0^\circ, 45^\circ, 90^\circ$) are performed for EN 10346/ HX380LAD+Z, EN 10346/ HX220BD+Z and EN 10346/ DX54D+Z materials. The geometry of the tensile test specimen can be seen in Figure 5.2.

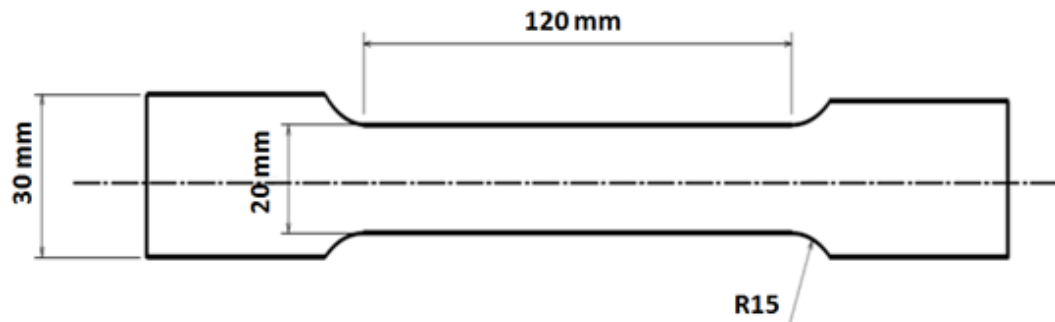


Figure 5.2: The geometry of the tensile test specimen according to ASTM [35].

Tensile test is performed ($10 \text{ mm}/\text{min}$) by applying constant extension rate using Zwick Roell Z300 tension and compression testing device shown Figure 5.3.



Figure 5.3: Zwick Roell Z300 Tension/Compression Test Device

Mechanical properties obtained by tension tests are given in Table 5.2.

Table 5.2: Mechanical Properties of EN 10346/ HX380LAD+Z, EN 10346/ HX220BD+Z and EN 10346/ DX54D+Z [35].

Sheet Materials	YS (MPa)	UTS	Poisson Ratio	R_0	R_{45}	R_{90}
EN 10346/ HX380LAD+Z	381	512	0.33	0.801	1.213	1.119
EN 10346/ HX220BD+Z	237	401	0.33	1.700	1.327	2.005
EN 10346/ DX54D+Z	156	351	0.33	2.071	1.527	2.507

5.1.2 Hydraulic Bulge Test

Hydraulic bulge test (HBT) leads to much higher strains compared to the tensile test because of the biaxial loading conditions. In deep drawing operation, maximum plastic strain may reach 70 %, therefore, extrapolation is necessary due to the limitation of the tensile test. In this test, instantaneous measurement of dome apex radius, sheet thickness and pressure are required.

Thickness strain is obtained by the volume constancy from measured in plane strains.

$$\varepsilon_{xx} + \varepsilon_{yy} + \varepsilon_{zz} = 0 \quad 5.6$$

$$\varepsilon_{xx} + \varepsilon_{yy} = -\varepsilon_{zz} \quad 5.7$$

$$\varepsilon_{eqv} = -\varepsilon_{zz} = \ln\left(\frac{t}{t_0}\right) \quad 5.8$$

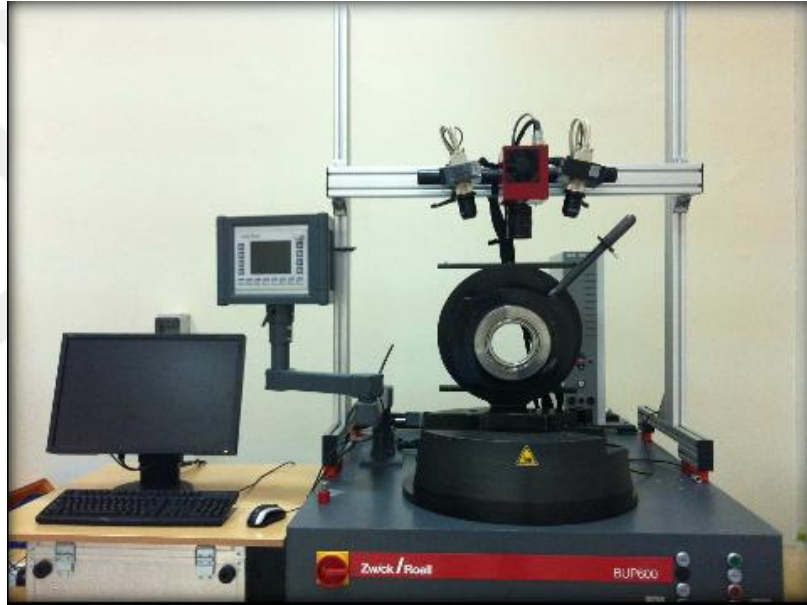


Figure 5.4: General view of Hydraulic Bulge Test setup.

The statement of problem can be considered as plane stress condition;

$$\varepsilon_{zz} = \varepsilon_{thickness} \neq 0 \quad 5.9$$

$$\sigma_{zz} = \sigma_{thickness} = 0 \quad 5.10$$

The membrane theory is used to determine the biaxial stress state. Therefore bending stress is neglected. Die cavity is selected according to membrane theory. However, there is no rule or standard for fillet radius.

$$\frac{r_c}{t_0} > 50$$

where;

r_c : Die cavity radius,

t_0 : Initial sheet thickness

Stresses and strain conditions on membrane theory define a relationship between membrane stresses for hydraulic bulge test in room temperatures [36].

Equilibrium equation is expressed by the following equation;

$$\frac{\sigma_\phi}{R_\phi} + \frac{\sigma_\theta}{R_\theta} = \frac{P}{t} \quad 5.11$$

where;

σ_ϕ and σ_θ are principle stress on the sheet surface,

R_ϕ and R_θ are the corresponding radii of the curved surface at the dome apex,

P is the hydraulic bulge pressure,

t is the sheet thickness at the dome apex.

If it is assumed that the bulge shape is spherical, two principle stress and radius and curvature are equal.

$$R_\phi = R_\theta = R \quad 5.12$$

$$\sigma_\phi = \sigma_\theta = \sigma_{eqv} \quad 5.13$$

Therefore;

$$\sigma_{eqv} = \frac{PR}{2t} \quad 5.14$$

σ_{eqv} (Equivalent stress) can be calculated by the von Misses Yield Criterion.

$$\sigma_{eqv} = \left[(\sigma_{xx} - \sigma_{yy})^2 + (\sigma_{yy} - \sigma_{zz})^2 + (\sigma_{zz} - \sigma_{xx})^2 + 6(\tau_{xy}^2 + \tau_{yz}^2 + \tau_{xz}^2) \right]^{\frac{1}{2}} \quad 5.15$$

Effective strain is equivalent to thickness strain;

$$\varepsilon_{eff} = -\varepsilon_t = \left(\frac{t_d}{t_0} \right) \quad 5.16$$

Schematic view of the hydraulic bulge test can be seen in the following figure.

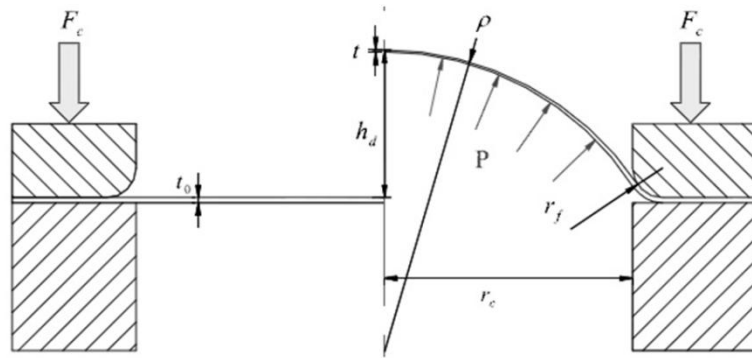


Figure 5.5: Schematic view of Hydraulic Bulge Test.

F_c : Clamp force

P : Hydraulic bulge pressure

h_d : Dome height

ρ : Radius of curvature

r_f : Fillet radius of upper die

r_c : Radius of die cavity

t_0 : Initial sheet thickness

t : Current sheet thickness

Hydraulic bulge tests are performed for 120 mm die opening. GOM Aramis optical measurement system used to measure the deformation which mounted on the Zwick BUP 600 testing device. It can be seen in Figure 5.4.

160 mm diameter -drawbeads are used to prevent material flow during the test. Deformation distribution recorded with the 20 frames per second by GOM Aramis. Hydraulic bulge test specimen and stochastic pattern on the sheet metal can be seen in Figure 5.6.

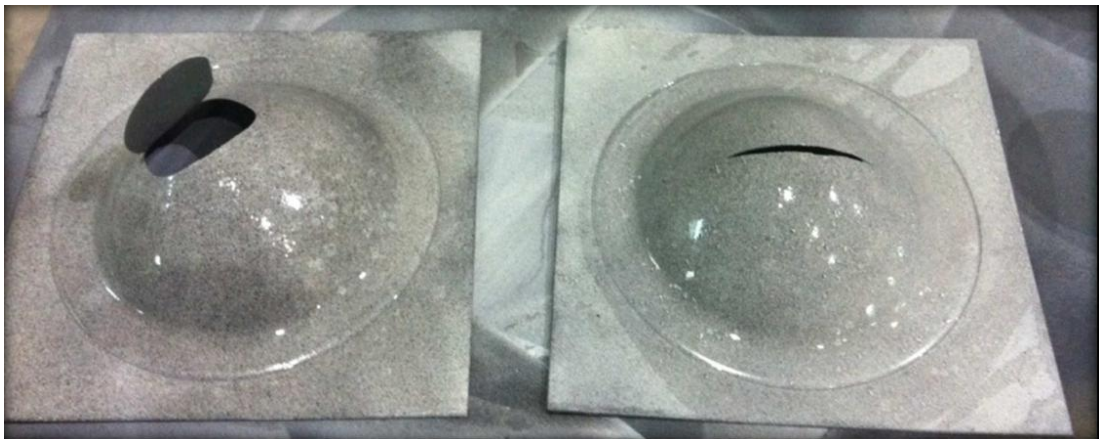


Figure 5.6: HBT test specimen and stochastic pattern on the sheet material [35].

5.1.3 Flow Curves of the Test Materials

Flow curves obtained from tensile test and hydraulic bulge test can be seen in Figure 5.7, 5.8 and 5.9. For the corresponding effective strain values effective stresses can be calculated. Then assuming $\frac{\sigma_3}{\sigma_1} \cong 0$, circumferential and meridional stresses σ_1 and σ_2 approximately be calculated. This will lead us to calculate the interfacial pressure between the punch and workpiece.

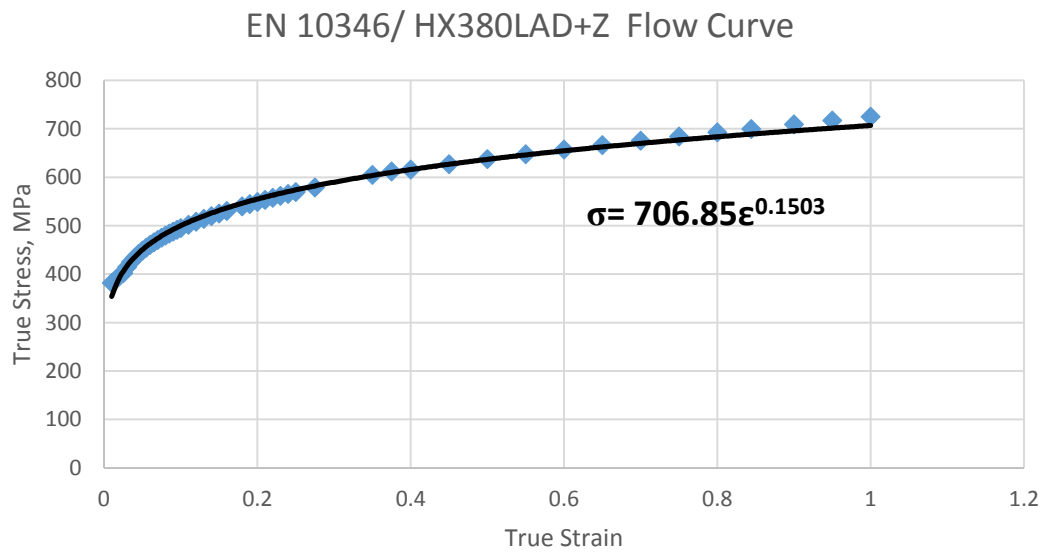


Figure 5.7: Flow curve of the EN 10346/ HX380LAD+Z material.

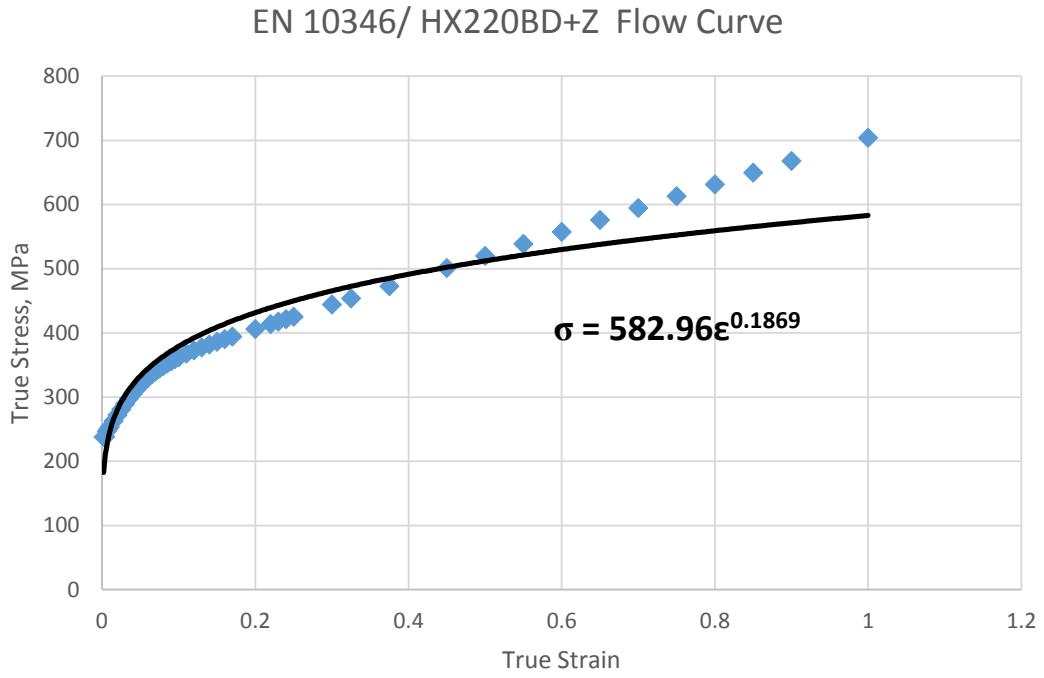


Figure 5.8: Flow curve of the EN 10346/ HX220BD+Z material.

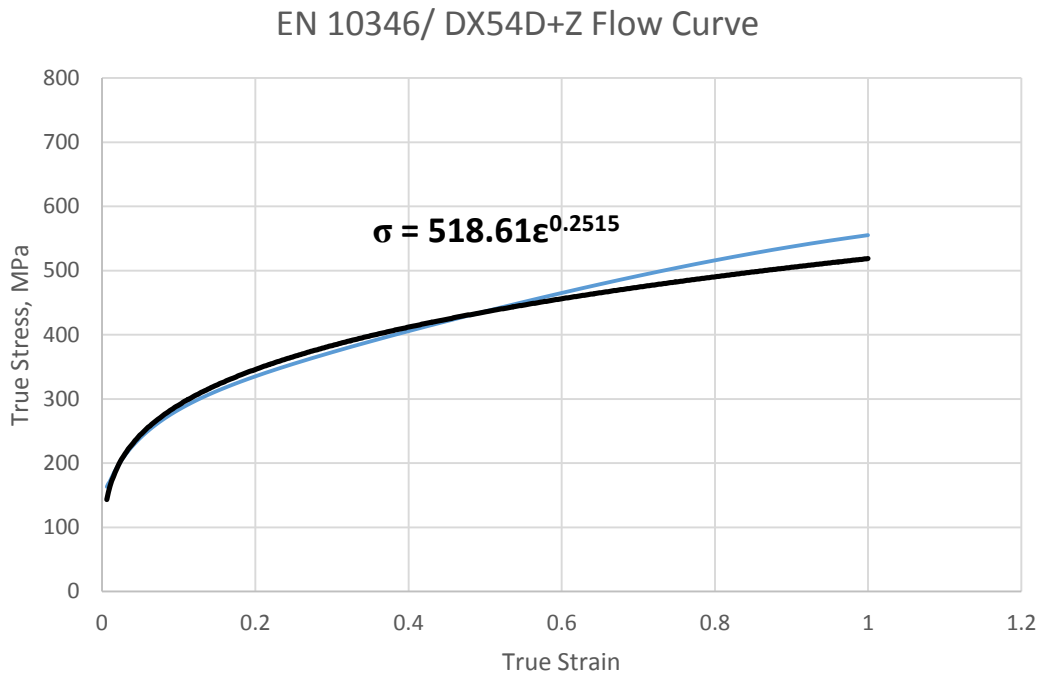


Figure 5.9: Flow curve of the EN 10346/ DX54D+Z material.

5.2 SURFACE ROUGHNESS OF DIE AND WORKPIECE

Surface roughness is an important parameter which characterizes the friction conditions. If the surface of tool or sheet is very smooth, contact area increases and there may not be enough space for lubricant. Thus, surface roughness effects also lubrication conditions.

In the radial drawing region, the surface roughness of the drawing die is found as $R_a = 0.20 \mu\text{m}$ and the surface roughness of the sheet metal is around $R_a = 1.82 \mu\text{m}$ as measured using an Alicona® system.

Measurements reports of the surface roughness values can also be seen in Appendixes.

5.3 DEEP DRAWING TESTS

Deep drawing tests are performed to find the coefficient of friction in the radial drawing zone. Dry and graphite lubricated conditions are investigated at room temperature and at 300 °C. Different blank holder loads are applied to same tests to obtain different punch loads under identical conditions.

In deep drawing tests C type 80 tons mechanical press is used with the hydraulic system which controls blank holder load. Deep drawing tests are also performed at high temperatures. Induction heating system is used to heat workpiece between the die and blank holder. Some measurement devices are used to obtain the test results. Load cell is used to measure the punch load, displacement gauge is used to measure the punch displacement and thermocouples are used to measure the temperature of the workpiece before drawing.

Test apparatus and heating system used in the experiments will be explained in the next section.

5.3.1 Test Apparatus

5.3.1.1 Mechanical Press

The mechanical press used in the deep drawing tests can be seen in Figure 5.10. It has 80 tons load capacity and 110 mm stroke. Hydraulic controlled blank holder system, induction heating system, load cell and displacement gauge are selected according to the press capacity.



Figure 5.10: C type mechanical press.

5.3.1.2 Blank Holder

Hydraulic controlled two identical cylinders are operated simultaneously. Cylinders are connected to the base plate in the blank holder configuration. Blank holder is powered by the hydraulic power control unit.

Bushings are used to provide blank holder movement on the same axis. Configuration of the blank holder can be seen in Figure 5.11.

THE BLANK HOLDER SET (Part No : 3)	
Part No	DESCRIPTION
3.1	THE BLANK HOLDER CONFIGURATION
3.2	THE HYDRAULIC CYLINDER SET
3.3	THE CONNECTOR PLATE (FIXING CYLINDERS TO TABLE OF PRESS)

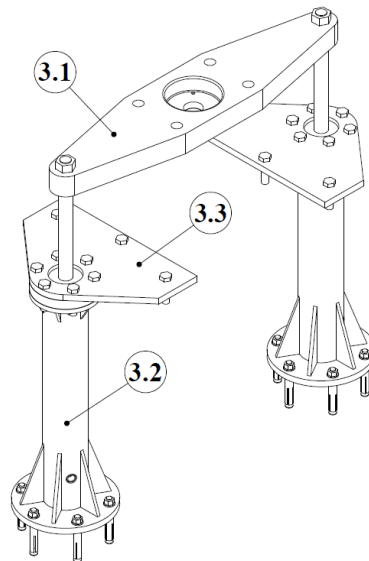


Figure 5.11: Blank holder configuration [37].

5.3.1.3 Heating System

Induction heating system is used to heat the workpiece between the die and blank holder. It is preferred due to possibility of the heating only the desired location. High power densities at induction heating provides high heat generation rate. This enables fast heating. Power and heating time control also enables to control heat rate and depth of heating. Beyond these advantages it is not very economical compared to the furnace heating.

Induction Heating having 50W power capacity with frequency ranging from 1,7 kHz to 12 kHz is used to heat the flange zone of blank, in this study.

Induction heating system can be seen in Figure 5.12.

Copper coil which is the part of heating system is fixed in die. The copper pipe, primary coil, is wrapped around the die ring in die. The copper pipe is insulated to prevent electrical short cut by covering it with soft mica sheet.



Figure 5.12: Induction heating system.

5.3.1.4 Punch and load cell

44 mm diameter hemispherical punch is used with a load cell in deep drawing tests. 100 tons load cell assembled between the ram and the punch to obtain the punch load during deep drawing operation.

THE RAM SET (Part No: 2)	
Part No	DESCRIPTION
2.1	THE RAM
2.2	THE LOAD CELL
2.3	THE PUNCH

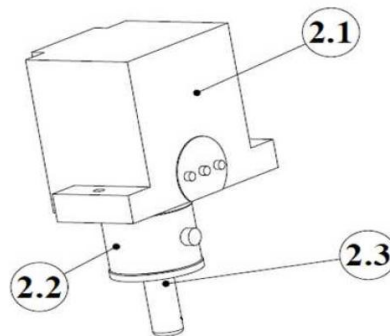


Figure 5.13: Ram set.

5.3.1.5 Die Components

Die base plate and the die heater configuration can be seen in Figure 5.14. Guide columns are used for centering. In some applications blank holder force has to be reduced. To reduce the blank holder force, four helical springs are used.

THE DIE ASSEMBLY (Part No : 4)	
Part No	DESCRIPTION
4.1	THE DIE BASE PLATE SET
4.2	THE DIE-HEATER CONFIGURATION

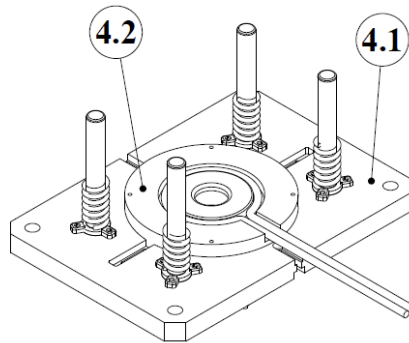


Figure 5.14: General view of the die assembly.

5.3.1.6 Measurement devices

Hydraulic Pressure Transducer: the hydraulic pressure transducer is mounted on the cylinder to control pressure on the blank holder. It senses the pressure in cylinder and send signal to hydraulic power unit to keep blank holder at a constant pressure value. In hydraulic system, there is also a pressure gauge, which can be controlled manually to adjust blank holding pressure.


View of the pressure transducer can be seen in Figure 5.15.



Figure 5.15: Pressure transducer attached on hydraulic cylinder.

Displacement Transducer: It is used to monitor the punch motion and connected to the data acquisition system to record the displacement data during deep drawing operation. Stroke of the punch is 110 mm, so 0-200 mm displacement potentiometer is suitable for this test.


Technical specifications and view of the displacement transducer can be seen in Figure 5.16.



Precision Potentiometric Output Ranges:0-3 to 0-30 inches [0-75 to 0-750 mm] 3K - 10K ohms, IP65	
Specification Summary	
GENERAL	
Full stroke ranges	0-3 to 0-30 inches [0-75 to 0-750 mm]
Output signal	Voltage divider (potentiometer)
Linearity	±0.04 to 0.1 % full stroke
Repeatability	Essentially infinite
Life expectancy	50 million cycles
Enclosure material	Aluminum
Sensor	Conductive plastic linear potentiometer
Operating speed	200 inches (5m) per second, max
ELECTRICAL	
Input resistance	5K to 10K ohms (±20%),
Recommended maximum input voltage	25-30 V (AC or DC)
Recommended operating wiper current	<1 µA
ENVIRONMENTAL	
Enclosure design	IP65
Operating temperature	-22 to 212 °F
Vibration	Up to 10 G's to 2000 Hz maximum

Figure 5.16: Displacement transducer mounted on press and technical specifications of displacement transducer.

Load cell: The centre-hole type compression load cell was used in the experiments to measure the punch load. Press capacity is 80 tons, so 100 tons capacity load cell is convenient. Centre-hole type load cells enable stable measurement under eccentric load conditions. In addition to this, it can make precise measurements in warm conditions.



Specifications		
Type	KCE-1MNA	KCE-1.5MNA
Capacity	1 MN	
Rated output	1.25 mV/V \pm 10%	
Nonlinearity	0.5 % RO	
Hysteresis	0.5 % RO	
Temperature effect on zero	0.1 % RO/ $^{\circ}$ C	
Temperature effect on span	0.05 % / $^{\circ}$ C	
Compansated temp. range	-10 ~ + 60 $^{\circ}$ C	
Temperature range	-20 ~ + 70 $^{\circ}$ C	
Over load	120 %	
Input/output resistance	350 ohm \pm 1 %	
Recommended exit voltage	Less than 10 V	
Zero balance	5 % RO	
Weight	8.5 kg	12.2 kg

Figure 5.17: Load cell and technical specifications of load cell.

Data acquisition system: The data acquisition system developed and produced by National Instrument (NI USB – 6259 M Series) are used to collect signals sent by the load cell connected to punch, the displacement transducer and two infrared temperature sensors placed on bottom of die. It has 16 differential or 32 single ended analog input channels, total 48 digital I/O channels, and a counter/timer. The signals are amplified and fed through an A/D converter. For data transfers, it is equipped with USB signal stream, programmed I/O. The other specifications of this board can be seen in Figure 5.18.

All measurement devices including data acquisition unit used in setup are powered by DC Batteries to reduce noise level in the measurements. So the quality of data/signal streaming is significantly increased.

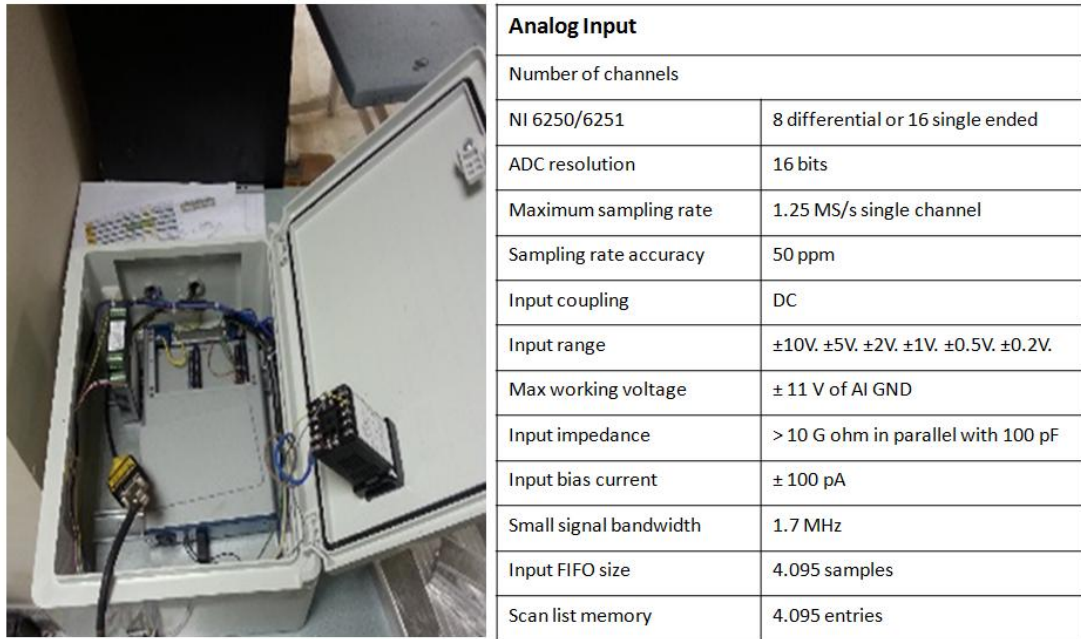


Figure 5.18: Data acquisition system and technical specifications.

Data processing software (Hera): Hera is the name of a commercial software developed by Nell Electronic Company in Turkey. It receives, records, monitors, processes data sent from data logger. It is an object oriented programming package, the proceeded data can be displayed in different modes of graphical form or tabulated form. The collected log files are compatible with the office softwares. An example of a workbench data collection screen can be seen in Figure 5.19.



Figure 5.19: Software Package used for data processing.

5.3.2 Deep Drawing Test Evaluation

In deep drawing tests, EN 10268 steel is used with dry and graphite lubrication. 1,5 mm thick sheet material and 42 mm diameter hemispherical punch are used.

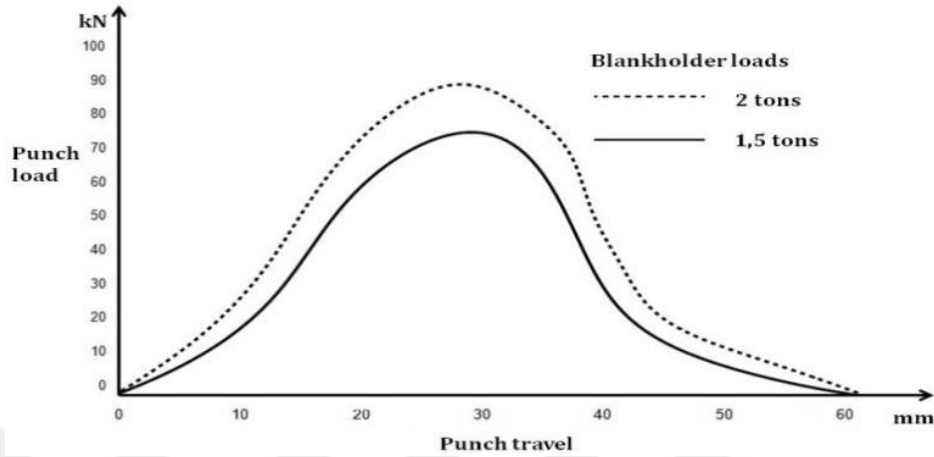


Figure 5.20: Punch loads at different blank holder loads for EN 10268 steel with dry lubrication.

Two identical test are performed at different blankholder loads and two different punch load curves are obtained as shown in Figure 5.20.

In Eq. 4.4 it was discussed before coefficient of friction for radial drawing zone can be calculated with the punch load change δP , blank holder load change δH , and the angle of embrace α .

$$\mu = \frac{\delta P \cot \alpha}{\delta P + 2\delta H} \quad 4.4$$

In this study calculations are done at four different embrace angles as 15° , 30° , 35° and 40° . To calculate the punch loads at these angles bulge depth h is necessary. Bulge depth equation is also discussed in Eq. 4.5.

$$h = \left(\frac{D}{2} + \rho'_d\right) \tan \alpha - (\rho'_1 + \rho'_d + t_0)(\sec \alpha - 1) \quad 4.5$$

Bulge depth of the deformed workpiece can be calculated as a function of embrace angle. D die diameter, ρ'_d die radius, ρ'_1 radius of punch and t_0 original thickness of the workpiece must be known to use Eq. 4.5.

Parameters used in the deep drawing test are given in Table 5.3.

Table 5.3: Deep drawing test parameters

α	D, mm	ρ'_d, mm	ρ'_1, mm	t_0, mm	h, mm
15°	45	6	21	1,2	6,63
30°	45	6	21	1,2	12,04
35°	45	6	21	1,2	13,66
40°	45	6	21	1,2	15,21

According to the parameters which can be seen in Table 5.3 punch loads can be calculated from punch load-displacement curve. It is clear from the table that, punch load at maximum angle can be calculated at 15,21 mm displacement. So, first 15-16 mm displacement will be satisfactory to calculate the punch loads at selected angles.

Deep drawing tests are also performed at high temperature as 300 °C.

Graphite based dry lubricant Oraphi Graphene 702 is used to determine the lubrication effect. Properties of the lubricant can be seen in Appendix C. It lowers the coefficient of friction, protects parts contact corrosion and prevents premature wear. Operating temperature of the lubricant is between -70°C to $+900^{\circ}\text{C}$. In this study hot deep drawing tests are performed at 300°C . So, Graphene 702 is suitable at room temperature and high temperature.

Deep drawing test are performed at different lubrication and temperature conditions. Blank holder load is another parameter which changes the punch loads. Blank holder force can be adjusted by the hydraulic power unit. Pressure in the hydraulic cylinders, weight of the blank holder and type of the springs are the parameters to calculate the blank holder load.

- A case study of calculating friction at radial drawing zone:

Material: EN 10268 (Erdemir 7140) Steel

Lubrication: Graphite

Temperature: Room

Blank holder load;

$$H = F_H + W_{BH} - F_S \quad 4.6$$

where;

H : Blank holder load

F_H : Hydraulic load

W_{BH} : Weight of the blank holder

F_S : Spring load

To have two different blank holder load, hydraulic power unit set 35 bar and 45 bar.

$F_{H1} = 24950 \text{ N}$ at 35 bar hydraulic pressure,

$F_{H2} = 37614 \text{ N}$ at 45 bar hydraulic pressure,

$W_{BH} = 95 \text{ kg} = 931,95 \text{ N}$

$F_S = 4 * 86,6 * 36 = 12470,4 \text{ N}$, 4 spring at 36 mm displacement with spring

constant $k = 86,6 \frac{\text{N}}{\text{mm}^2}$

$H_1 = 24950 + 931,95 - 12470,4 = 13410 \text{ N}$

$H_2 = 37614 + 931,95 - 12470,4 = 26075 \text{ N}$

$\delta H = H_2 - H_1 = 26075 - 13410 = 12665 \text{ N}$

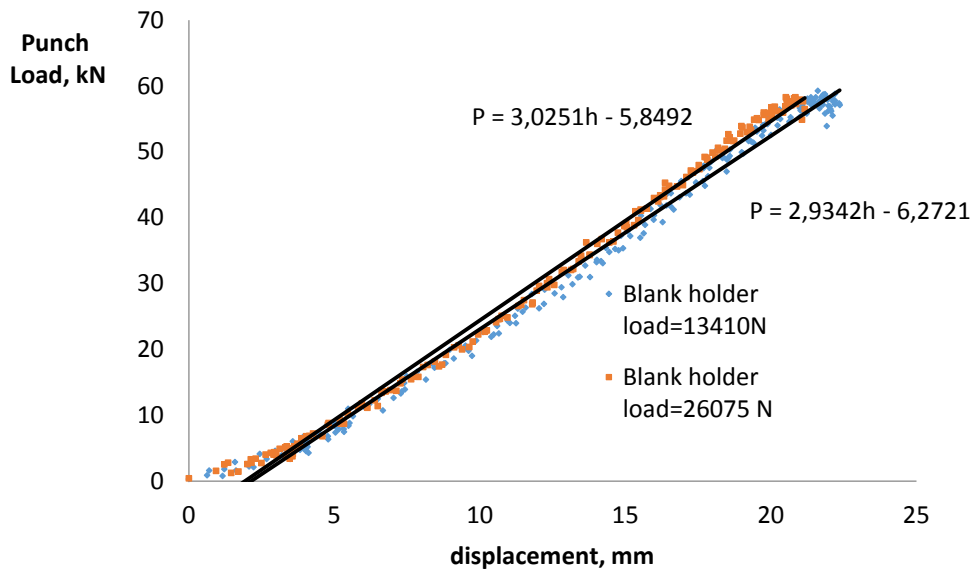


Figure 5.21: Punch load-displacement graph at 26075 N and 13410 N blank holder loads.

Punch loads at different blank holder loads can be calculated by the equations shown in Figure 5.21.

$$P_1 = 2,9497h - 6,54$$

$$P_{1-15^\circ} = 2,9497 * 6,63 - 6,54 = 13,016 \text{ kN} = 13016 \text{ N}$$

$$P_{1-30^\circ} = 2,9497 * 12,04 - 6,54 = 28,974 \text{ kN} = 28974 \text{ N}$$

$$P_{1-35^\circ} = 2,9497 * 13,06 - 6,54 = 32,048 \text{ kN} = 31983 \text{ N}$$

$$P_{1-40^\circ} = 2,9497 * 15,21 - 6,54 = 38,357 \text{ kN} = 38324 \text{ N}$$

$$P_2 = 3,0251h - 5,8492$$

$$P_{2-15^\circ} = 3,0251 * 6,63 - 5,8492 = 14,207 \text{ kN} = 14207 \text{ N}$$

$$P_{2-30^\circ} = 3,0251 * 12,04 - 5,8492 = 30,573 \text{ kN} = 30573 \text{ N}$$

$$P_{2-35^\circ} = 3,0251 * 13,06 - 5,8492 = 33,658 \text{ kN} = 33658 \text{ N}$$

$$P_{2-40^\circ} = 3,0251 * 15,21 - 5,8492 = 40,162 \text{ kN} = 40162 \text{ N}$$

$$\delta P_{15^\circ} = P_{2-15^\circ} - P_{1-15^\circ} = 14207 - 13016 = 1191 \text{ N}$$

$$\delta P_{30^\circ} = P_{2-30^\circ} - P_{1-30^\circ} = 30573 - 28974 = 1599 \text{ N}$$

$$\delta P_{35^\circ} = P_{2-35^\circ} - P_{1-35^\circ} = 33658 - 31983 = 1675 \text{ N}$$

$$\delta P_{40^\circ} = P_{2-40^\circ} - P_{1-40^\circ} = 40162 - 38324 = 1838 \text{ N}$$

$$\mu = \frac{\delta P \cot \alpha}{\delta P + 2\delta H}$$

$$\mu_{15} = \frac{\delta P_{15} \cot \alpha}{\delta P_{15} + 2\delta H} = \frac{1191 * \cot 15}{1191 + 2 * 12665} = 0,167$$

$$\mu_{30} = \frac{\delta P_{30} \cot \alpha}{\delta P_{30} + 2\delta H} = \frac{1599 * \cot 30}{1599 + 2 * 12665} = 0,102$$

$$\mu_{35} = \frac{\delta P_{35} \cot \alpha}{\delta P_{35} + 2\delta H} = \frac{1675 * \cot 35}{1675 + 2 * 12665} = 0,088$$

$$\mu_{40} = \frac{\delta P_{40} \cot \alpha}{\delta P_{40} + 2\delta H} = \frac{1838 * \cot 40}{1838 + 2 * 12665} = 0,080$$

5.4 STRETCH FORMING TESTS

9 different stretch forming tests are performed to calculate the coefficient of friction in this zone. Strain distributions at different stages are used to determine the incremental strains between two stages. Paraffin used as a lubricant to reduce the coefficient of friction. Test apparatus used in the experiments will be explained in the next section.

5.4.1 Test Apparatus

Zwick BUP 600 test device and optical measurement system of GOM Aramis simultaneously used in the experiments to obtain the strain distributions on the deformed workpiece. Recall that the same test device is used for hydraulic bulge test experiments which can be seen in Figure 5.22.

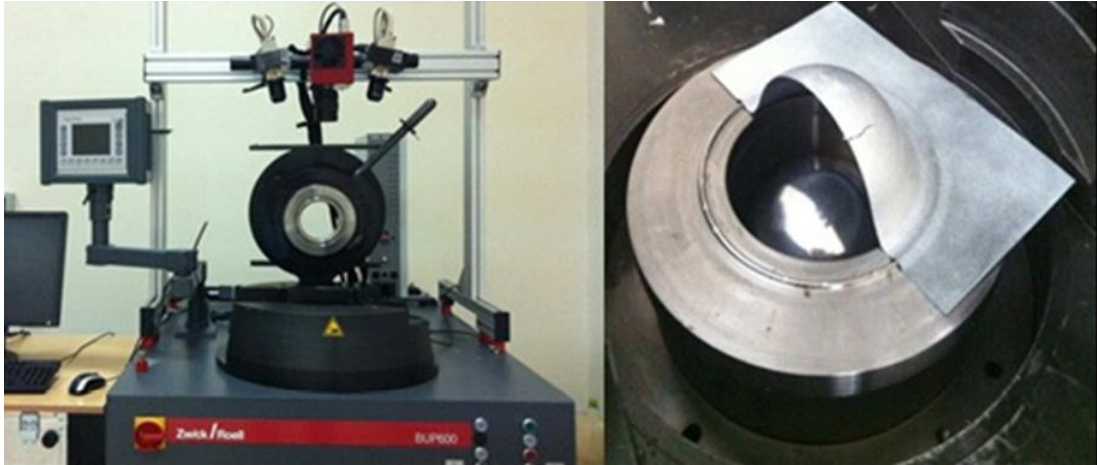


Figure 5.22: Zwick BUP 600 Test Device and general view of the half sheet specimen.

Blank holder and punch force capacity is 600 kN of this BUP 600 test device. Spherical punch geometry can be seen in Figure 5.23. Technical drawing of the spherical punch is also given Appendixes.



Figure 5.23: General view of the hemispherical punch.

Speed of the punch and blank holder force are adjustable parameters before the test. Blank holder force set to 240 kN and speed of the punch is 2.5 mm/s. The gauge section is stretched with the spherical punch. EN 10346/ HX380LAD+Z, EN 10346/ HX220BD+Z and EN 10346/ DX54D+Z are the workpiece materials. Die material is also GGG70L-heat treated die steel.

3D optical strain measurement system is used to measure the strain distributions on the workpiece during the process. The stochastic painting method is applied on the workpiece. General view of the painted workpiece can be seen in Figure 5.24. Deformation of the workpiece recorded by the GOM system at 10 frames per second. Recorded image and strain distributions can be seen in Figure 5.25.

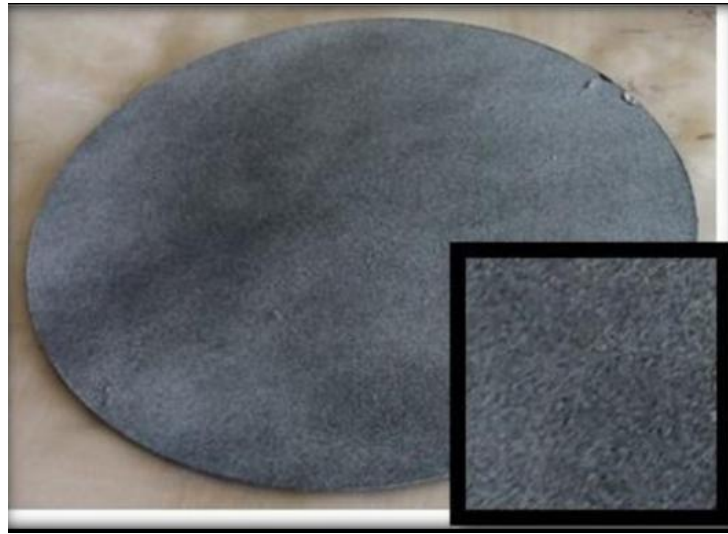


Figure 5.24: General view of the stochastic painting.

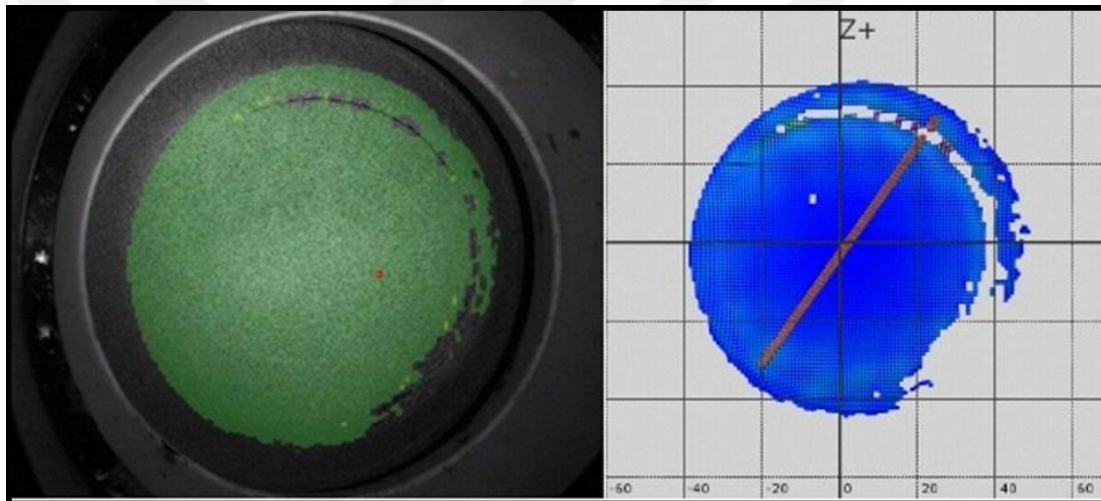


Figure 5.25: Recorded image and strain distributions obtained from GOM Aramis optical measurement system.

5.4.2 Stretch Forming Test Evaluation

In stretch forming zone, 9 different tests are carried out. Three different materials are used with dry and paraffin lubricated conditions. 1,2 mm thick, 250 mm square sheets are tested.

Zwick BUP 600 test device is used with the Gom Aramis optical scanning system simultaneously.

- A case study of calculating friction at stretch forming zone:

Material: EN 10346/ HX380LAD+Z Steel

Lubrication: Dry

Temperature: Room

Stages: 130-120

Geometry of workpieces can be seen in Figure 5.26 at different stages.

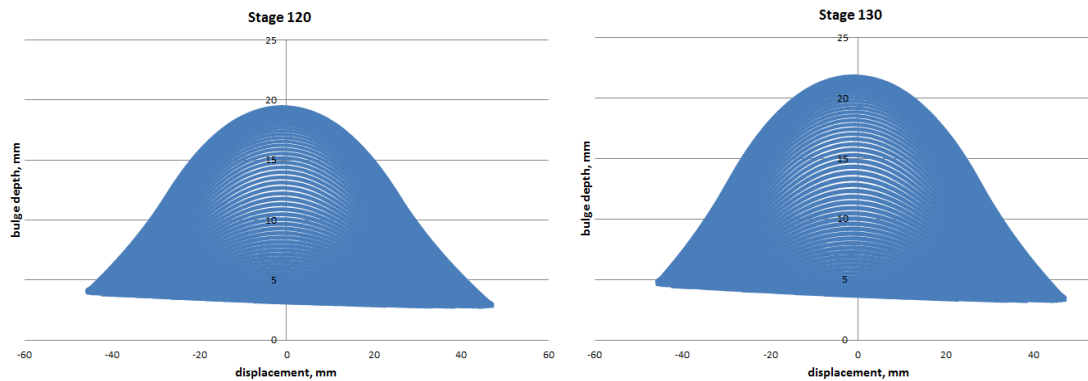


Figure 5.26: Workpiece geometry between Stage 120-Stage130.

According to the Figure 5.26, bulge depths are different between the stages 120 and 130. It means that the deformations are also different. By the use of the optical measurement system Gom Aramis strains can be measured along the deformation axis. Assuming the deformation is same on the half of the geometry, in the first 40 mm strain distributions can be seen in Figure 5.27.

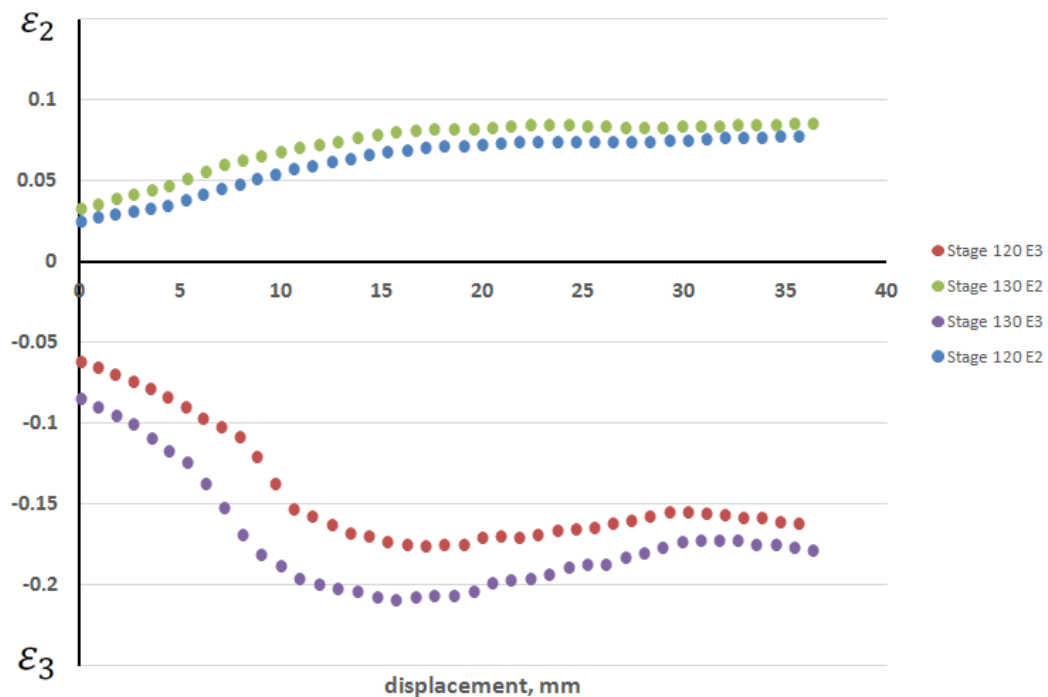


Figure 5.27: Strain distributions between Stage 120-Stage130.

In Figure 5.27 strain distributions-displacement graph can be seen. However, to calculate the coefficient of friction according to the Eq. 4.72 we need to obtain the strain distributions-vertical angle, θ graph. Geometry relations given in Figure 4.3

can be used to convert strain distributions-displacement graph to strain distributions-vertical angle, θ graph.

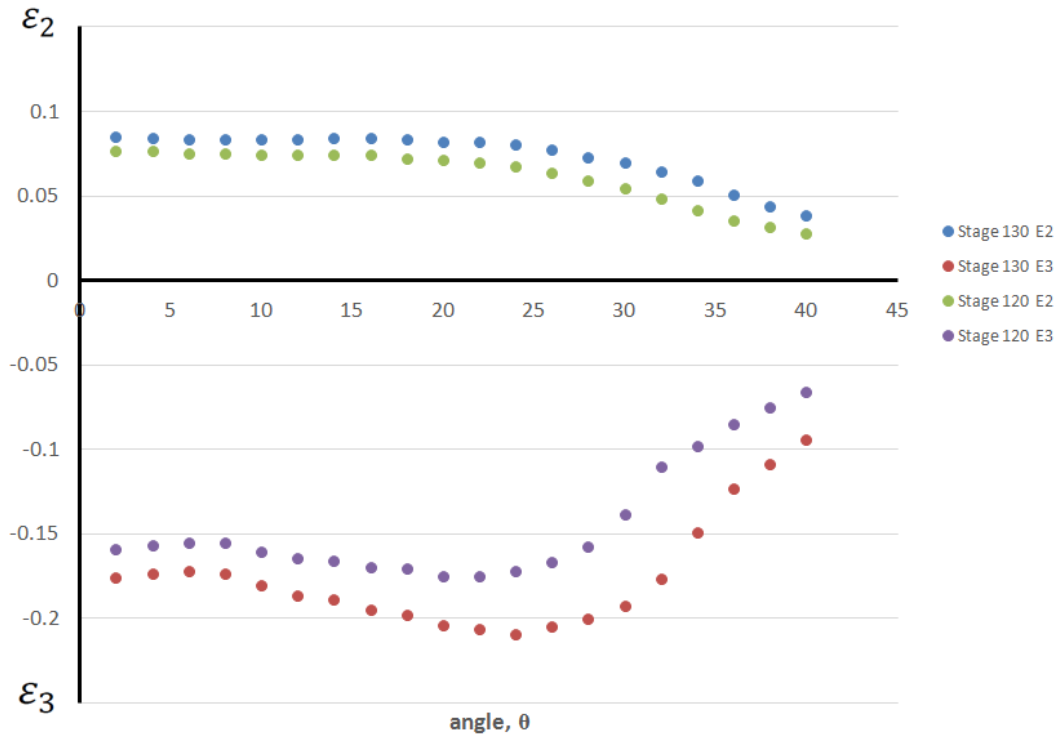


Figure 5.28: Strain distributions between Stage 120-Stage130.

Incremental strains can be calculated from Figure 5.28 to calculator ϵ ,

Recall Eq. 4.49.

$$\frac{d\epsilon_1}{d\epsilon_2} = \frac{\frac{2}{3}d\lambda\left[\sigma_1 - \frac{1}{2}(\sigma_2 + \sigma_3)\right]}{\frac{2}{3}d\lambda\left[\sigma_2 - \frac{1}{2}(\sigma_1 + \sigma_3)\right]} = r_\epsilon \quad 4.49$$

Using the material properties obtain from tensile and bulge tests $\sigma_2/\sigma_1 = x$ stress ratio can be calculated.

For the EN 10346/ DX54D+Z steel material relation between the equivalent strain and equivalent stress can be expresses from Figure 5.9;

$$\bar{\sigma} = 518,61\bar{\epsilon}^{0,215}$$

Equivalent strains can be calculated from Figure 5.28. For the corresponding values equivalent stresses can be found from the relation obtained from Figure 5.9.

Using Eq. 4.48 which is the equivalent stress equation and the Eq. 4.49 stress ratio equations;

$$\bar{\sigma} = \sqrt{\{\sigma_1^2 - \sigma_1\sigma_2 + \sigma_2^2\}} \quad 4.48$$

$$\sigma_1 = \frac{\bar{\sigma}}{\sqrt{1-x+x^2}}$$

σ_1 and σ_2 stresses can approximately calculated. If the stresses are known, interfacial pressure is also approximately calculated from the above equations.

$$p = \frac{t}{\rho r} (\sigma_1 r + \sigma_2 \rho_1 \sin\theta) \quad 4.45$$

$$p = \sigma_1 t \left[\frac{1}{\rho} + \frac{x \sin\theta}{r} \right] \quad 4.51$$

Table 5.3 shows the calculation steps and corresponding values of the interfacial pressure.

Table 5.4 Calculation of the interfacial pressure.

θ (degree)	θ (radians)	$\bar{\epsilon}$	$\bar{\sigma}$ (MPa)	σ_1 (MPa)	σ_2 (MPa)	Pressure (MPa)
40	0,69813	0,09534	312,891	333,575	286,981	17,0662
38	0,66322	0,10941	322,287	346,249	291,246	17,6402
36	0,62831	0,12417	331,174	353,080	303,730	18,1957
34	0,59341	0,15033	345,069	376,575	301,054	18,7941
32	0,55850	0,17924	358,369	402,205	285,373	19,1739
30	0,52359	0,19504	364,939	405,813	301,229	19,7021
28	0,48869	0,20289	368,048	402,978	318,389	20,1833
26	0,45378	0,20709	369,671	399,206	330,495	20,5936
24	0,41887	0,21150	371,349	404,118	326,223	20,9941
22	0,38397	0,20832	370,141	396,892	335,785	21,3768
20	0,34906	0,20593	369,224	397,091	332,954	21,7737
18	0,31415	0,19878	366,431	386,762	341,984	22,0811
16	0,27925	0,19592	365,292	384,434	342,536	22,4269
14	0,24434	0,18913	362,534	380,369	341,578	22,7390
12	0,20944	0,18719	361,729	379,009	341,530	23,0475
10	0,17453	0,18096	359,108	371,352	345,463	23,2222
8	0,13962	0,17404	356,110	367,032	344,078	23,4052
6	0,10472	0,17208	355,244	357,172	353,285	23,3879
4	0,06981	0,17397	356,076	363,805	347,808	23,6794
2	0,03490	0,17624	357,070	359,940	354,128	23,6647

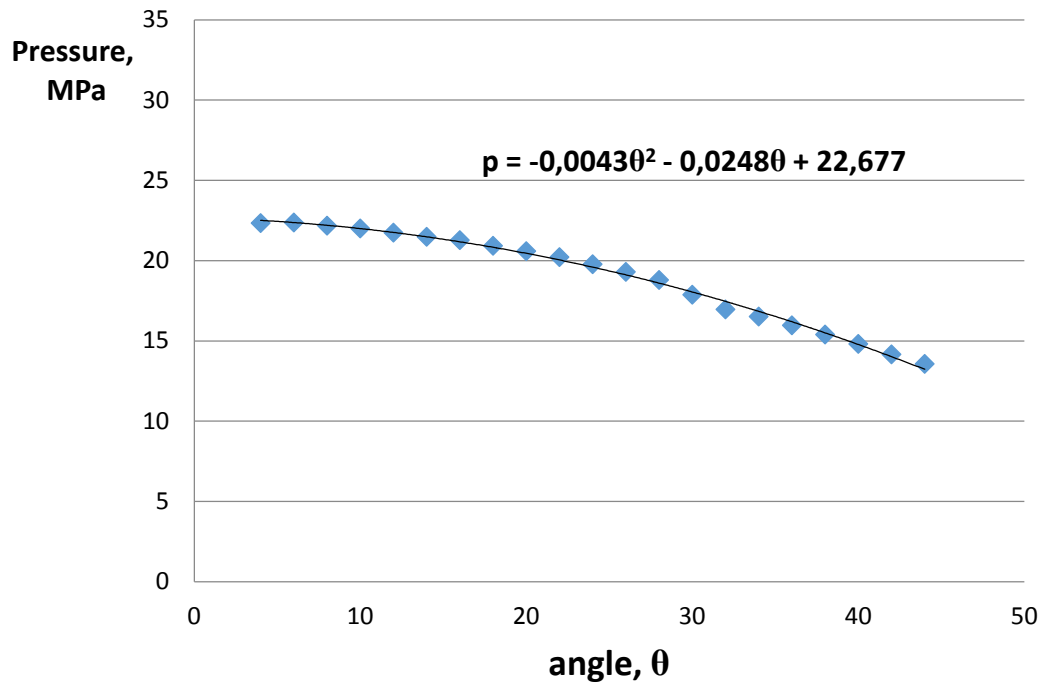


Figure 5.29: Interfacial pressure between stage 120 and 130

Calculated interfacial pressure graph fit to a second order polynomial curve. Constants of this curve, a, b and c can be used in the derived equations to find the coefficient of friction dependent on interfacial pressure.

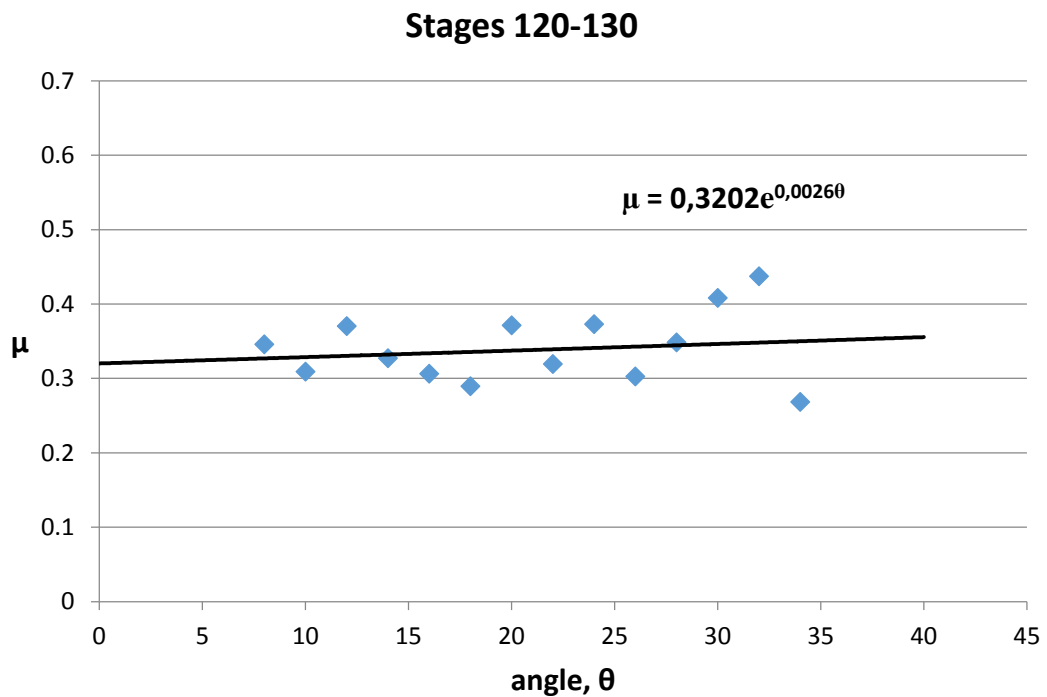


Figure 5.30: Coefficient of friction values using new derived equation (Eq. 4.72).

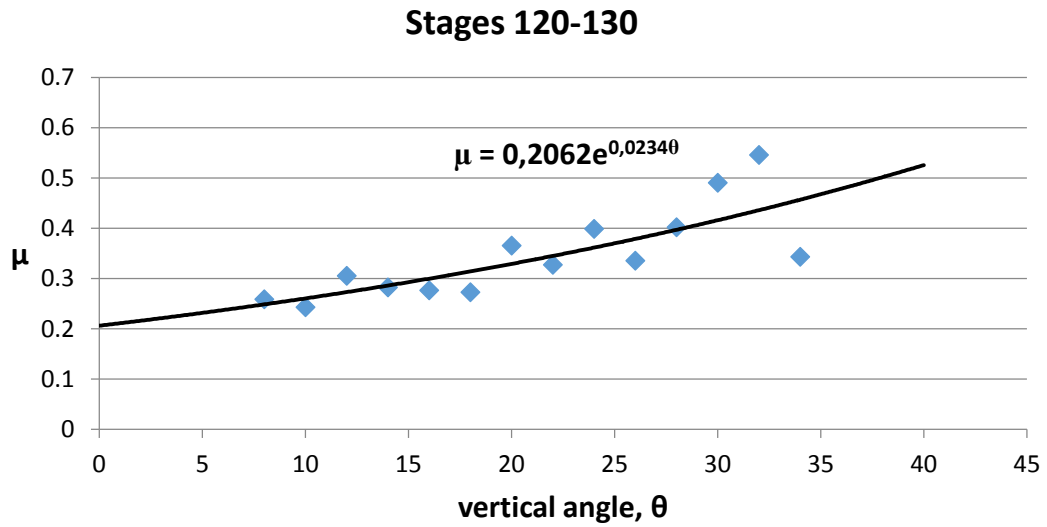


Figure 5.31: Coefficient of friction values using Eq. 4.42

Coefficient of friction values are calculated by using new derived equation and existing equation. Due to assumptions equations are not valid when $\theta = 0^\circ$, at the top of the punch. To find the coefficient of friction at the top, calculated values are fitted to an exponential curve. $\mu = 0,3202e^{0,0026\theta}$ is the first equation obtained from new derived equation. According to this equation $\mu = 0,320$ where $\theta = 0^\circ$. From the Figures 5.30 and 5.31 it is clear that the new method increased the accuracy of the result because of the curve interval is decreased. Maximum and minimum values of the interval can be seen in Table 5.5. By using the exponential curve fit, COF at the pole where $\theta = 0$ can be found. This technique allows to find COF value between the maximum and minimum value of COF. Exponential curve fitting is preferred due to range of results. Other methods like linear curve fitting is not suitable, because the results are found out of the COF distribution.

Table 5.5 Comparisons of the results of Eq. 4.42 and Eq. 4.72.

	Max value of COF	Min value of COF	Interval	Extrapolated COF
Eq. 4.72	0,43	0,26	0,16	0,32
Eq. 4.42	0,54	0,24	0,30	0,20

CHAPTER 6

RESULTS AND DISCUSSION

6.1 RESULTS OBTAINED FROM DEEP DRAWING TESTS

To find the coefficient of friction in radial drawing zone using Eq. 4.4, two identical deep drawing operations are carried. Blank holder load H is altered by an amount of δH which will lead to a change in punch load P of δP . Tests are performed under different conditions to investigate the effect of lubrication and temperature. Investigation the coefficient of friction under high temperature condition is an important improvement for this study.

High temperature tests are performed at room temperature and at 300 °C. Graphite lubricant is used to investigate the lubrication effect. 1,2 mm thick EN 10268 steel is used as a workpiece material. The diameter of the hemispherical punch is 42 mm.

Table 6.1 Deep drawing Test 1.

Material	Temperature	Lubrication	BH Loads
EN 10268	Room	Dry	22350-14900 N

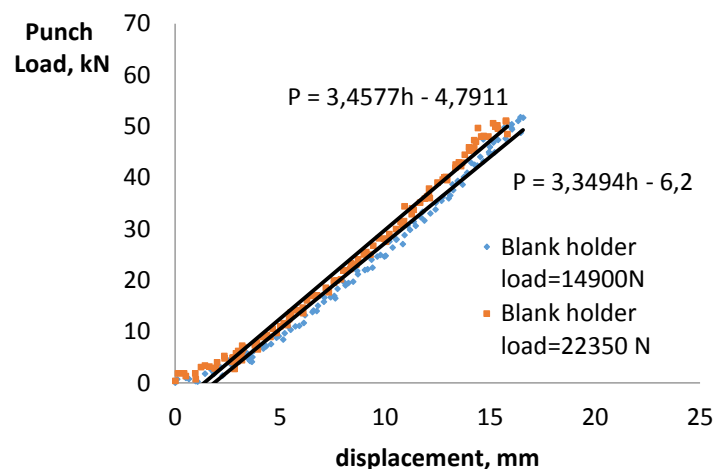


Figure 6.1: Punch loads for deep drawing Test 1.

Table 6.2 Deep drawing Test 2.

Material	Temperature	Lubrication	BH Loads
EN 10268	Room	Dry	29800-22350 N

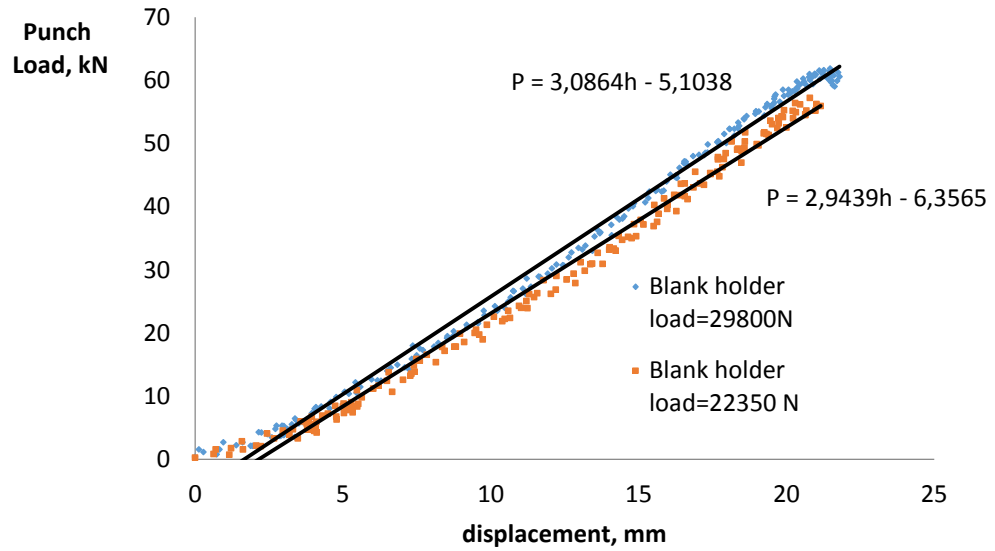


Figure 6.2: Punch loads for deep drawing Test 2.

Table 6.3 Deep drawing Test 3.

Material	Temperature	Lubrication	BH Loads
EN 10268	Room	Graphite	22350-14900 N

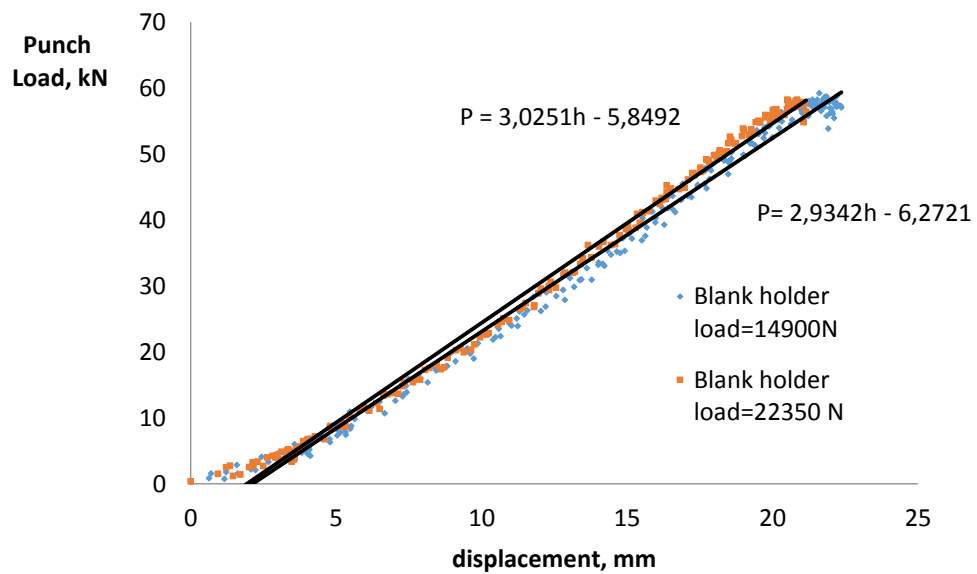


Figure 6.3: Punch loads for deep drawing Test 3.

Table 6.4 Deep drawing Test 4.

Material	Temperature	Lubrication	BH Loads
EN 10268	Room	Graphite	22350-14900 N

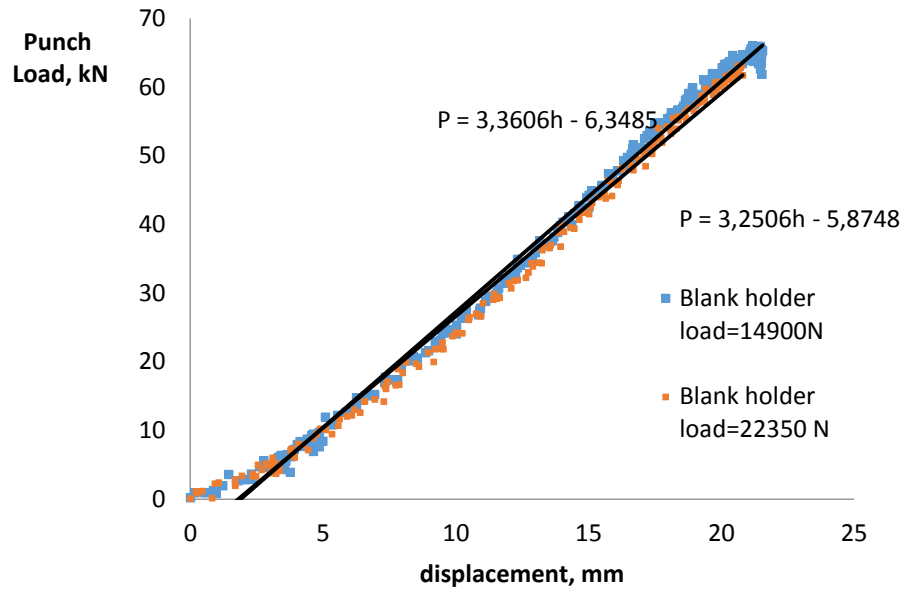


Figure 6.4: Punch loads for deep drawing Test 4.

Table 6.5 Deep drawing Test 5.

Material	Temperature	Lubrication	BH Loads
EN 10268	300 °C	Dry	22350-14900 N

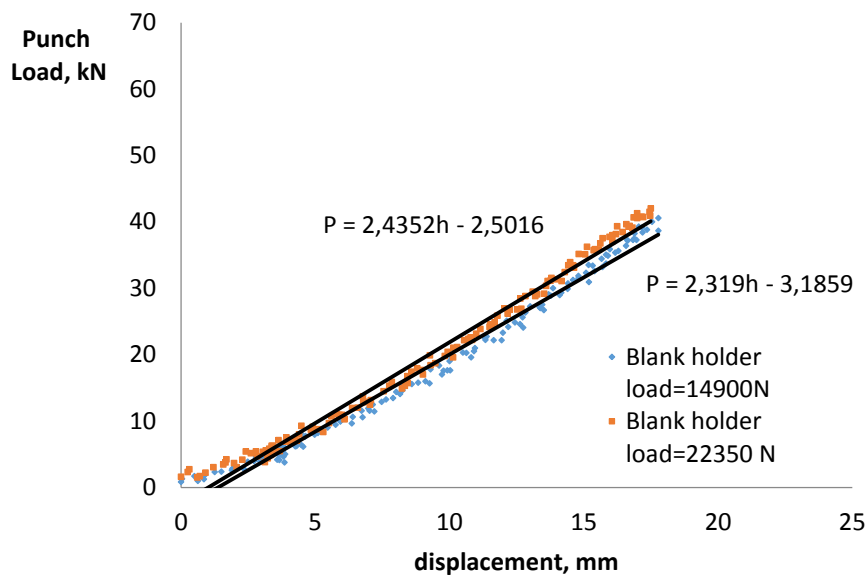


Figure 6.5: Punch loads for deep drawing Test 5

Table 6.6 Deep drawing Test 6.

Material	Temperature	Lubrication	BH Loads
EN 10268	300 °C	Dry	29800-22350 N

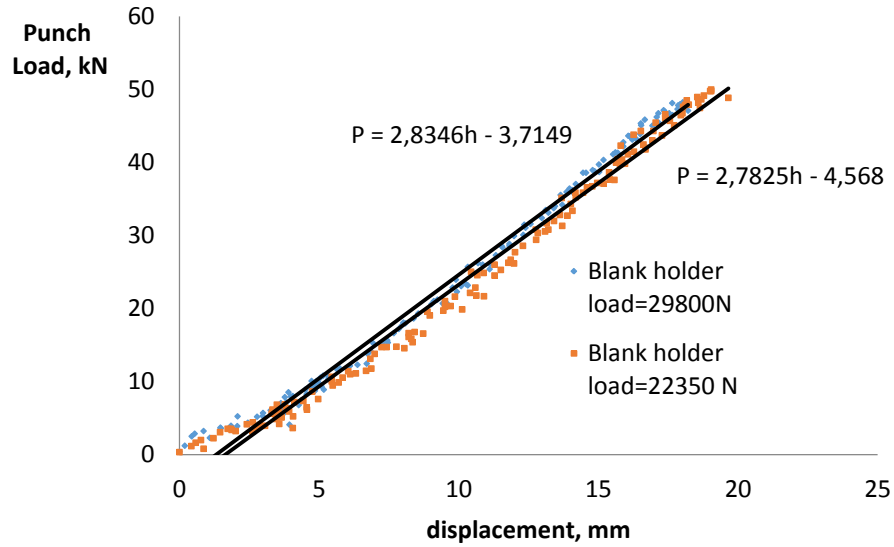


Figure 6.6: Punch loads for deep drawing Test 6.

Table 6.7 Deep drawing Test 7.

Material	Temperature	Lubrication	BH Loads
EN 10268	300 °C	Graphite	22350-14900 N

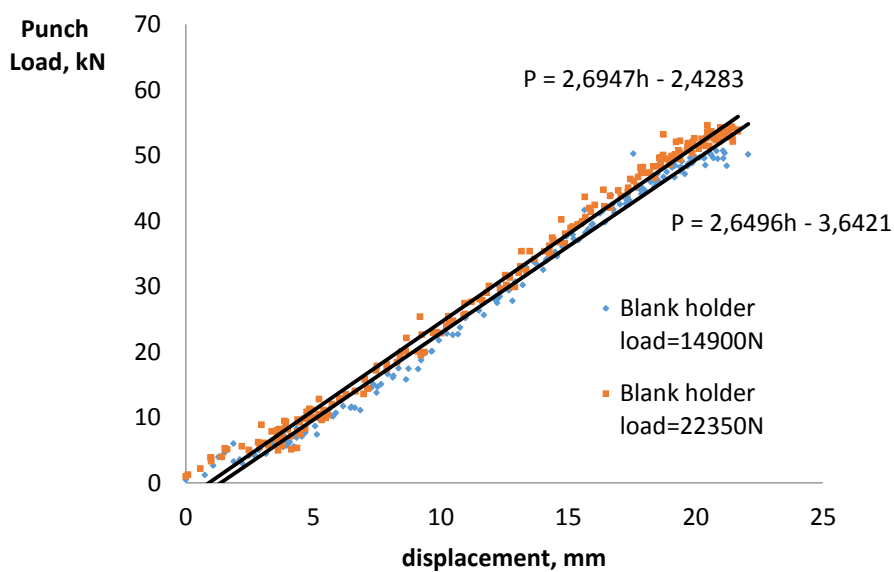


Figure 6.7: Punch loads for deep drawing Test 7.

Table 6.8 Deep drawing Test 8.

Material	Temperature	Lubrication	BH Loads
EN 10268	300 °C	Graphite	22350-14900 N

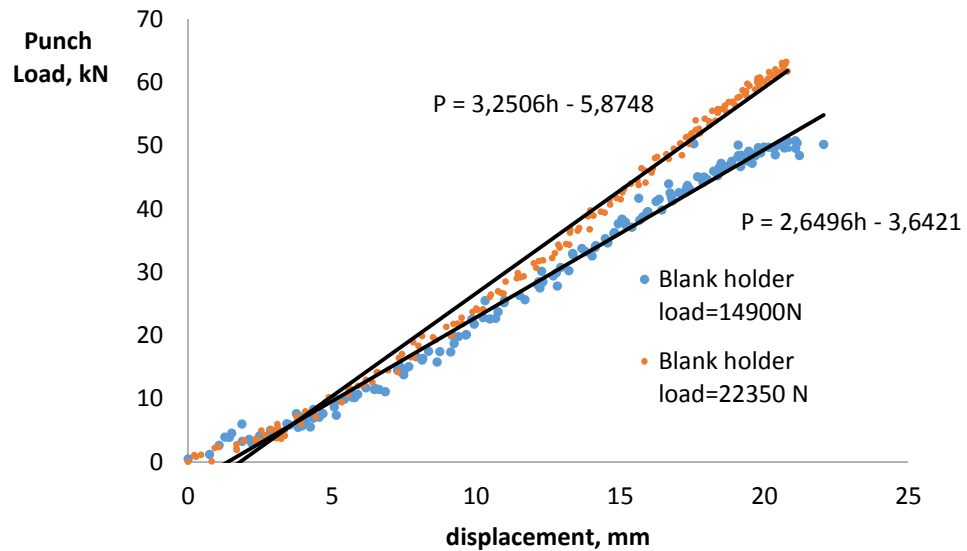


Figure 6.8: Punch loads for deep drawing Test 8.

Results obtained from the deep drawing tests can be seen in Table 6.9.

Table 6.9: Cof results for the deep drawing tests.

Material Grade	Lubricant	Angle	Blankholder Loads (N)	Coefficient of friction	
				Room temp.	300 °C
EN 10268	Dry	15	22350	0,38	0,30
		30		0,32	0,23
		35	14900	0,28	0,20
		40		0,24	0,20
EN 10268	Dry	15	29800	0,35	0,31
		30		0,33	0,35
		35	22350	0,32	0,29
		40		0,30	0,29
EN 10268	Graphite	15	22350	0,11	0,17
		30		0,09	0,13
		35	14900	0,08	0,14
		40		0,07	0,13
EN 10268	Graphite	15	29800	0,15	0,15
		30		0,10	0,20
		35	22350	0,13	0,15
		40		0,07	0,13

6.2 RESULTS OBTAINED FROM STRETCH FORMING TESTS

9 different stretch forming test results can be seen in Table 6.19. Coefficient of friction values are calculated by using strain distributions at two different stages. Bulge depths in Table 6.19 shows the two stages of the test.

Table 6.10: Stretch forming Test 1

Material	Temperature	Lubrication	Bulge depth
EN 10346/DX54D+Z	Room	Dry	19,08-21,50 mm

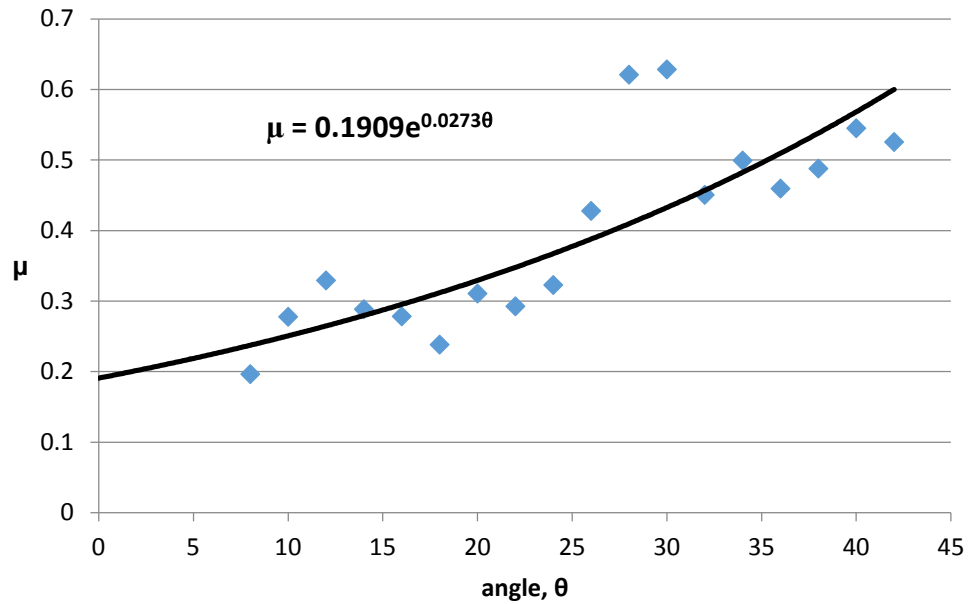


Figure 6.9: COF values using Eq. 4.42 for Test 1

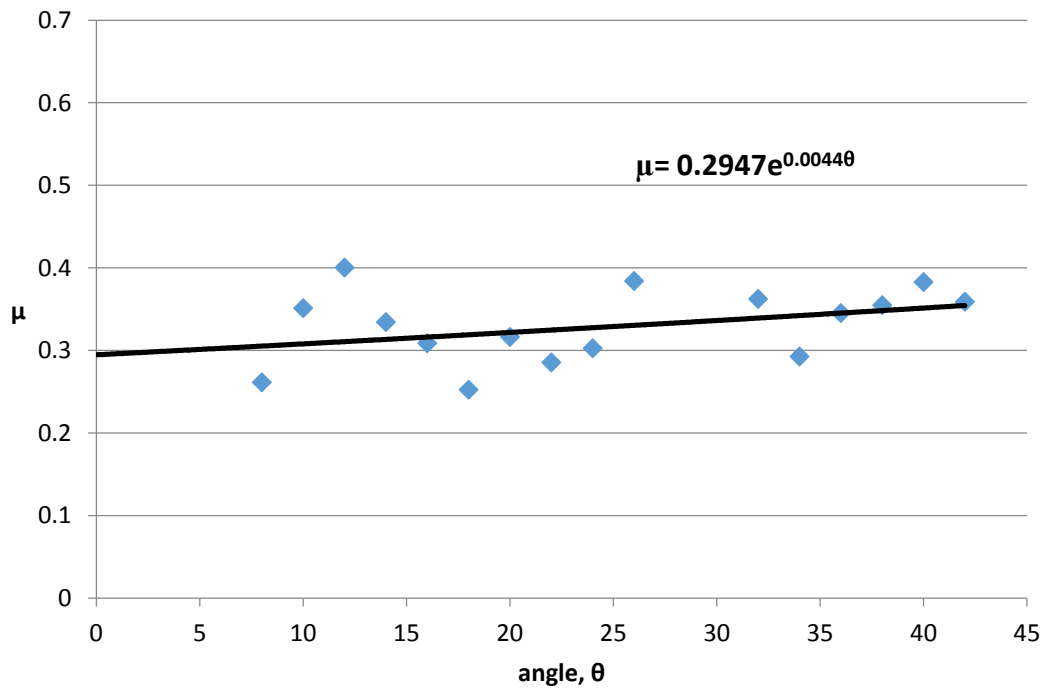


Figure 6.10: COF values using new derived equation Eq. 4.72 for Test 1.

Table 6.11 Stretch forming Test 2

Material	Temperature	Lubrication	Bulge depth
EN 10346/DX54D+Z	Room	Dry	25,13-29,69 mm

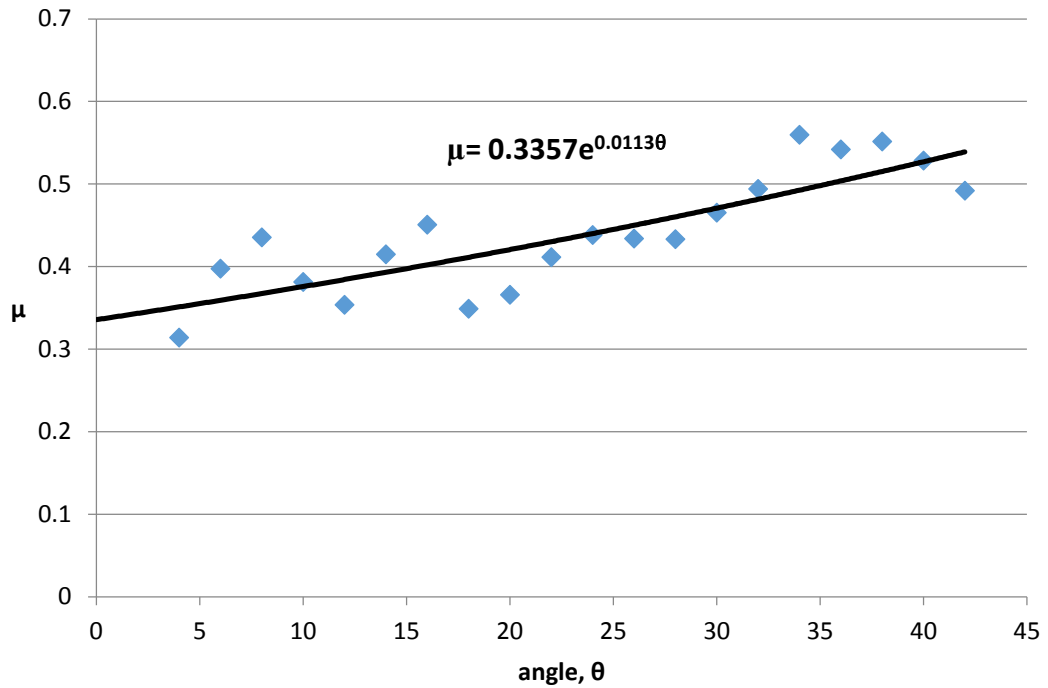


Figure 6.11: COF values using Eq. 4.42 for Test 2

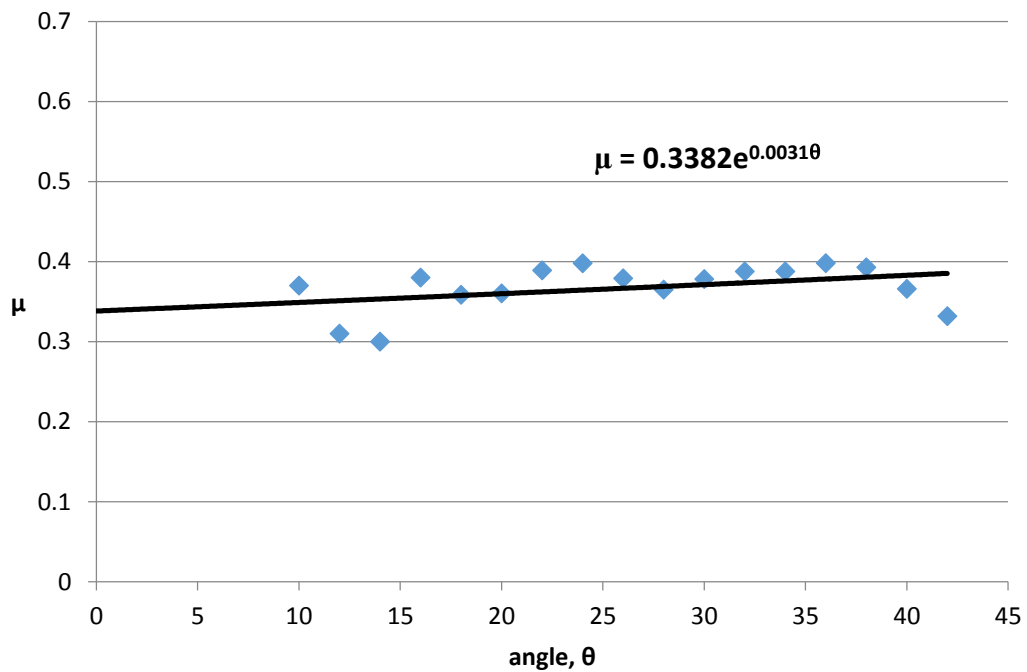


Figure 6.12: COF values using new derived equation Eq. 4.72 for Test 2.

Table 6.12 Stretch forming Test 3.

Material	Temperature	Lubrication	Bulge depth
EN 10346/HX380LAD+Z	Room	Dry	14,73-17,11 mm

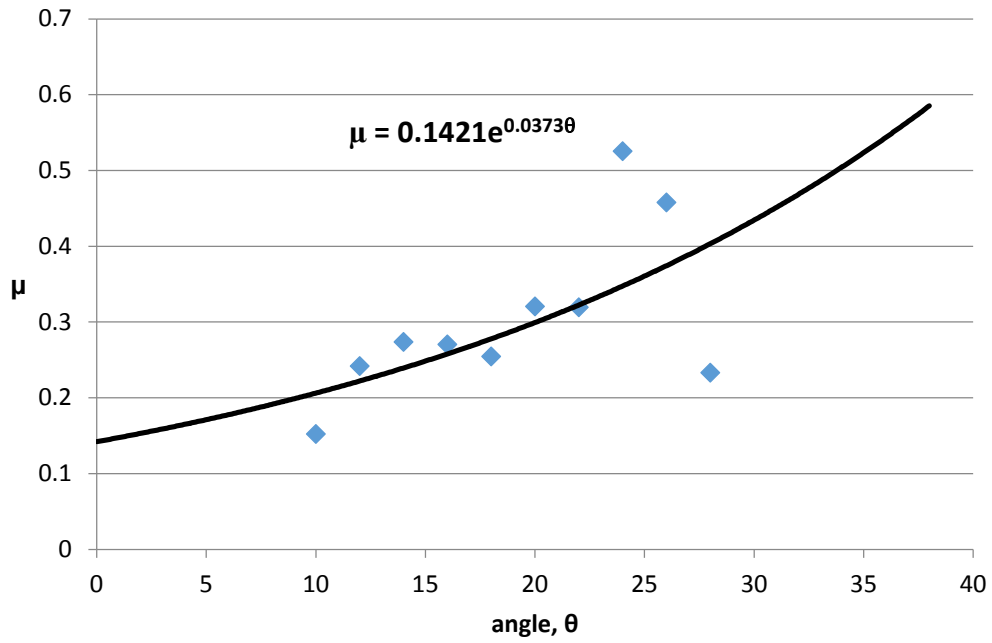


Figure 6.13: COF values using Eq. 4.42 for Test 3.

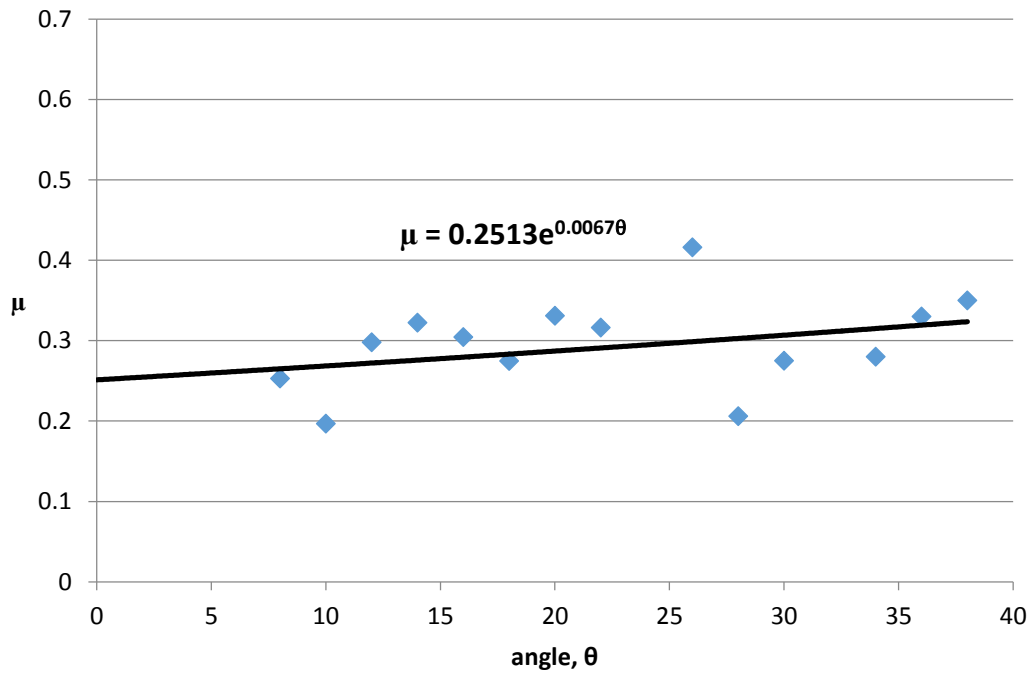


Figure 6.14: COF values using new derived equation Eq. 4.72 for Test 3.

Table 6.13 Stretch forming Test 4.

Material	Temperature	Lubrication	Bulge depth
EN 10346/HX380LAD+Z	Room	Dry	19,47-21,85 mm

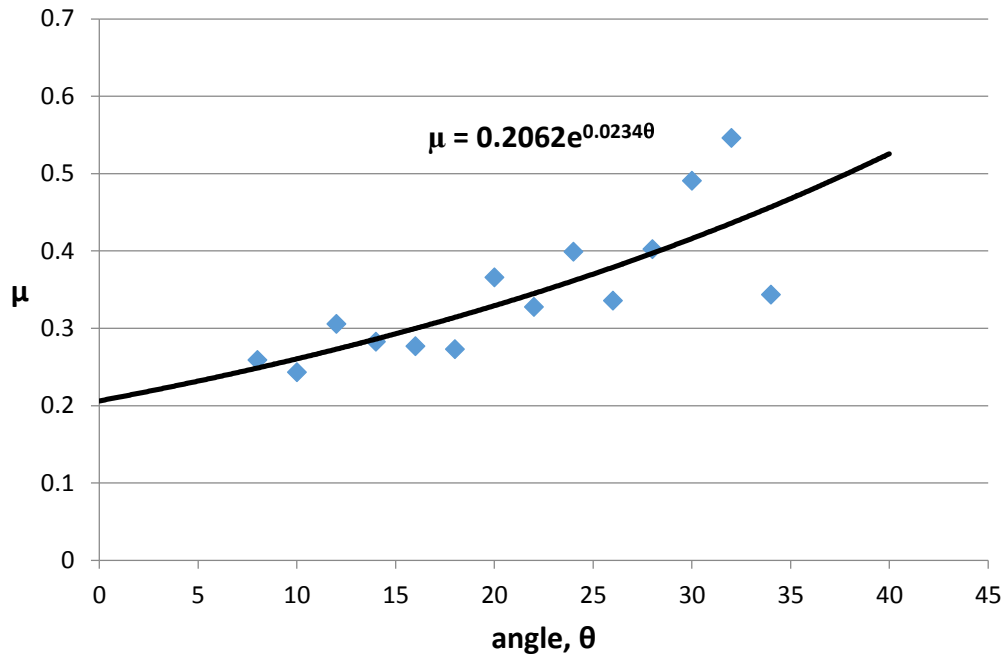


Figure 6.15: COF values using Eq. 4.42 for Test 4.

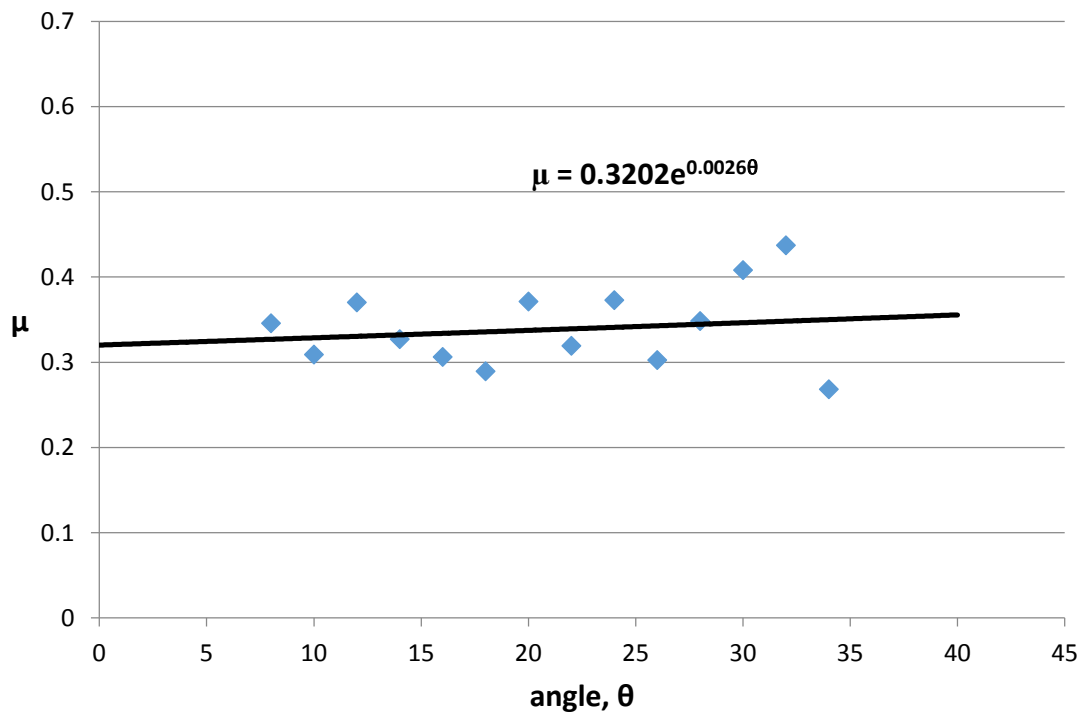


Figure 6.16: COF values using new derived equation Eq. 4.72 for Test 4.

Table 6.14 Stretch forming Test 5.

Material	Temperature	Lubrication	Bulge depth
EN 10346/HX220BD+Z	Room	Dry	18,25-20,64 mm

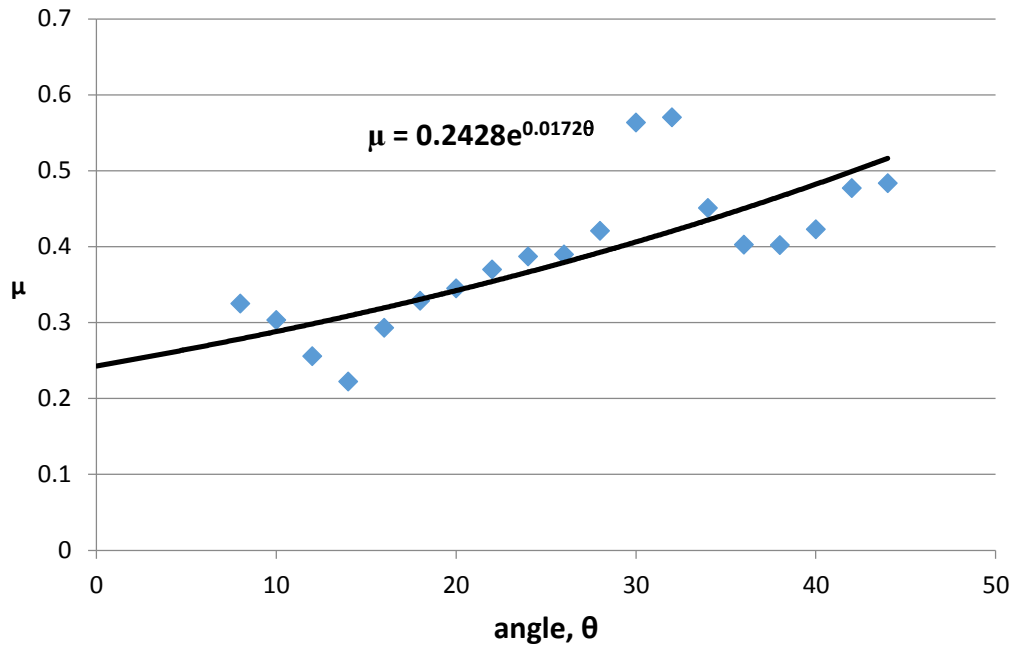


Figure 6.17: COF values using Eq. 4.42 for Test 5.

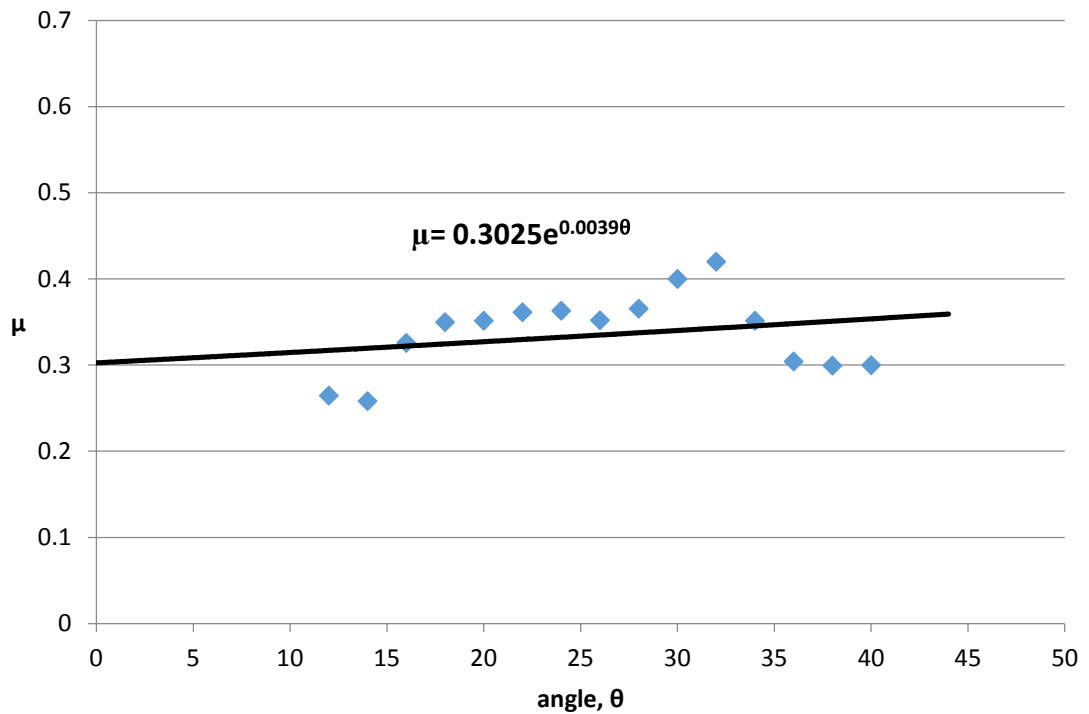


Figure 6.18: COF values using new derived equation Eq. 4.72 for Test 5.

Table 6.15 Stretch forming Test 6.

Material	Temperature	Lubrication	Bulge depth
EN 10346/HX220BD+Z	Room	Dry	23,03-25,44 mm

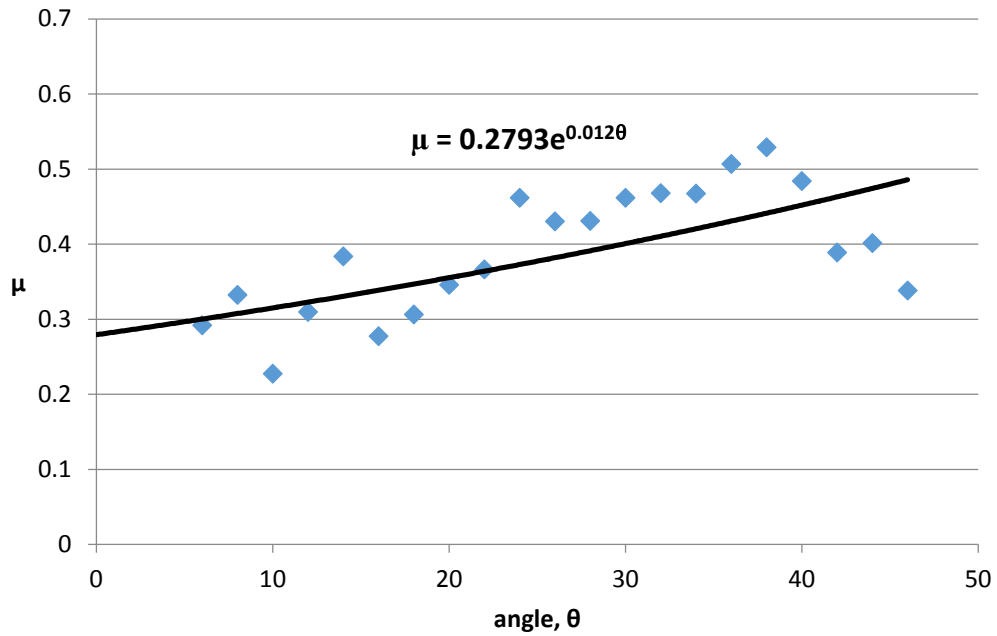


Figure 6.19: COF values using Eq. 4.42 for Test 6.

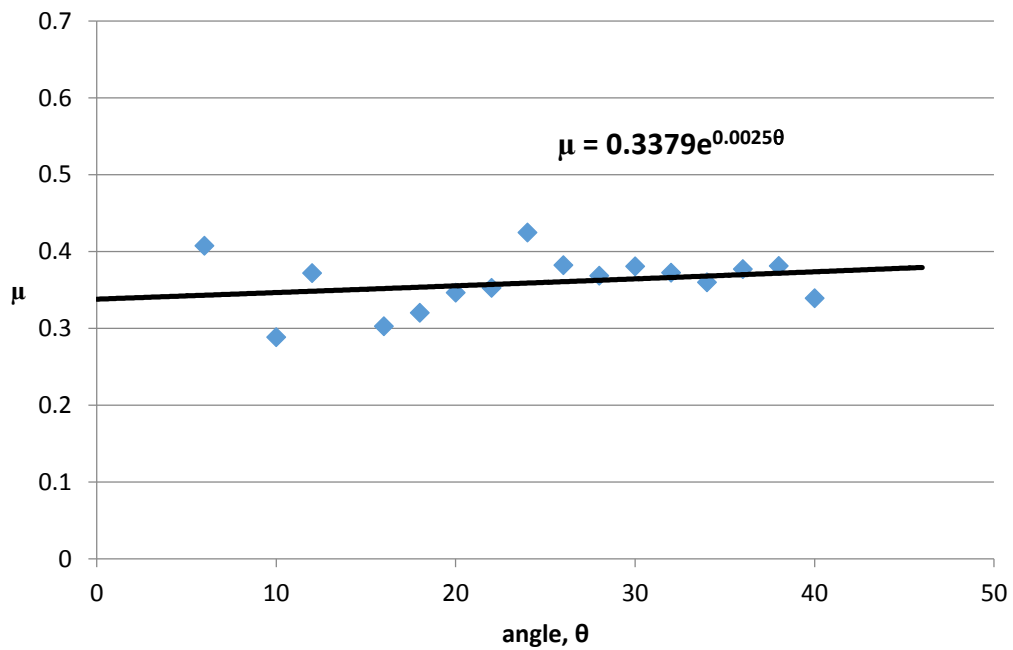


Figure 6.20: COF values using new derived equation Eq. 4.72 for Test 6.

Table 6.16 Stretch forming Test 7.

Material	Temperature	Lubrication	Bulge depth
EN 10346/DX54D+Z	Room	Graphite	22,59-23,76 mm

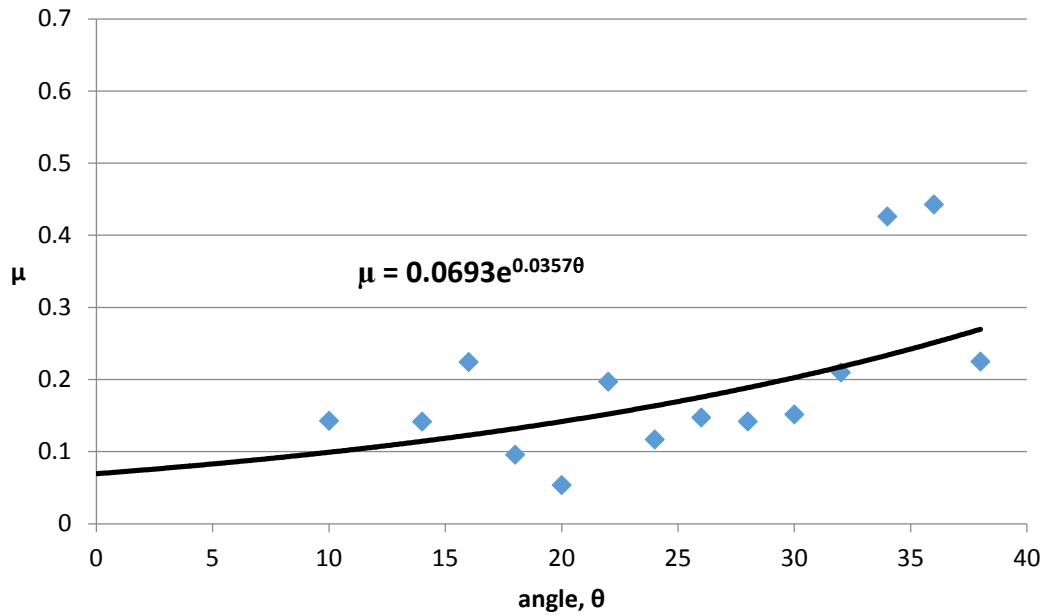


Figure 6.21: COF values using Eq. 4.42 for Test 7.

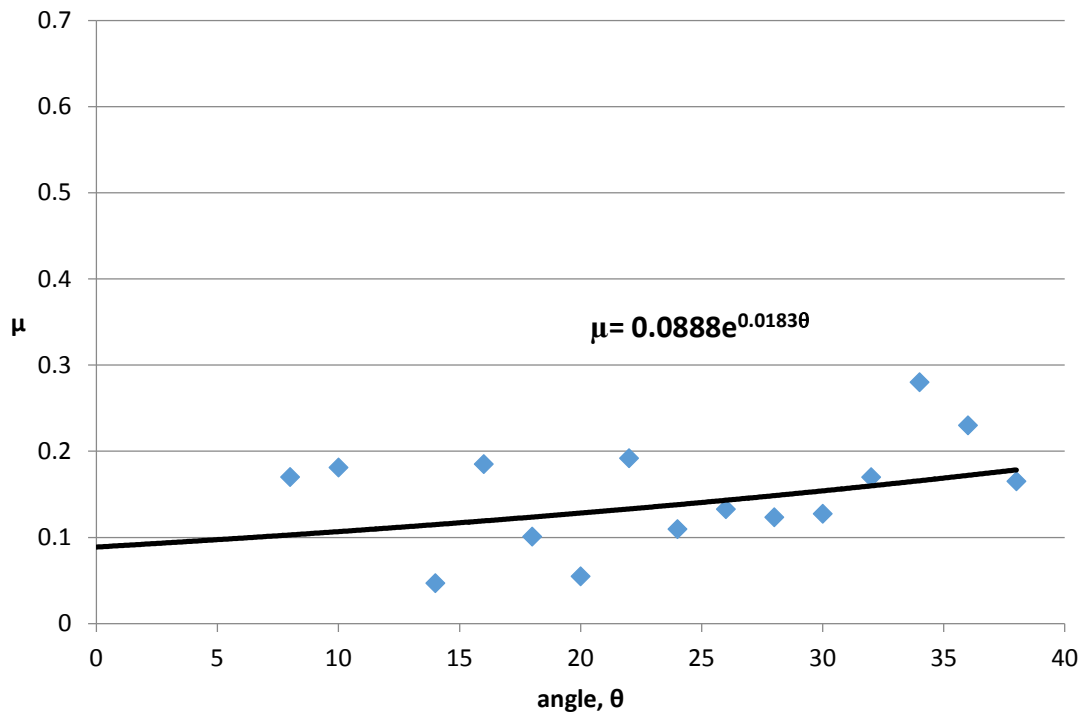


Figure 6.22: COF values using new derived equation Eq. 4.72 for Test 7.

Table 6.17 Stretch forming Test 8.

Material	Temperature	Lubrication	Bulge depth
EN 10346/HX380LAD+Z	Room	Graphite	12,81-14,62 mm

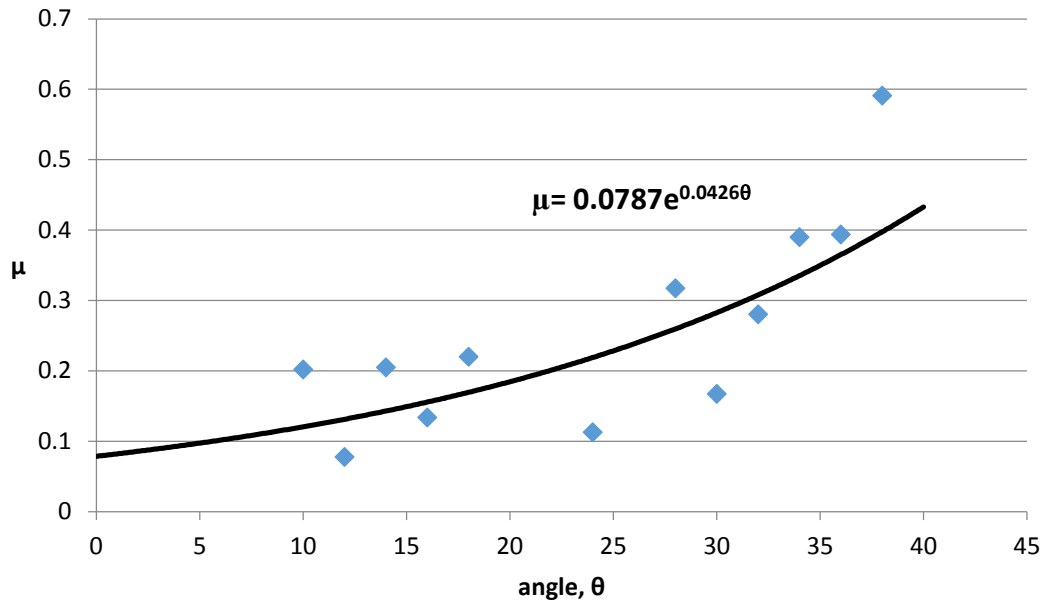


Figure 6.23: COF values using Eq. 4.42 for Test 8.

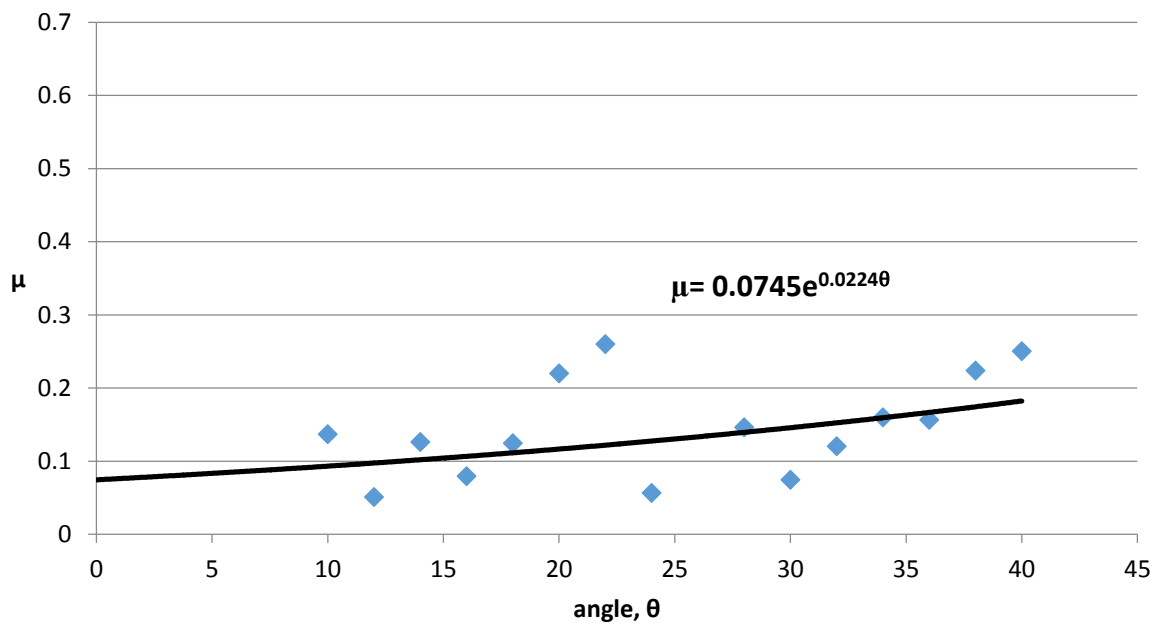


Figure 6.24: COF values using new derived equation Eq. 4.72 for Test 8.

Table 6.18 Stretch forming Test 9.

Material	Temperature	Lubrication	Bulge depth
EN 10346/HX380LAD+Z	Room	Graphite	16,34-17,94 mm

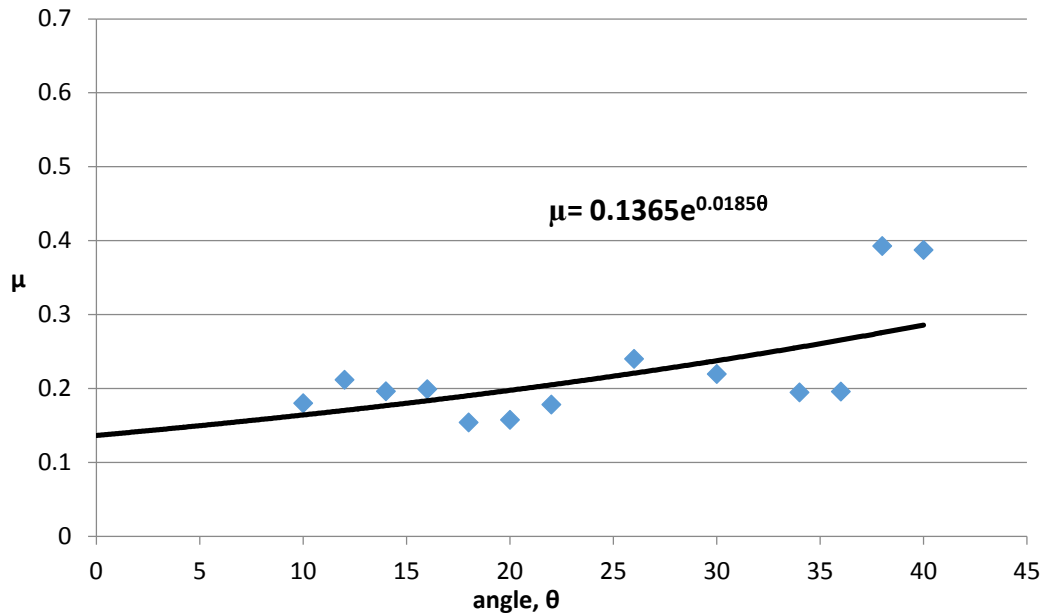


Figure 6.25: COF values using Eq. 4.42 for Test 9.

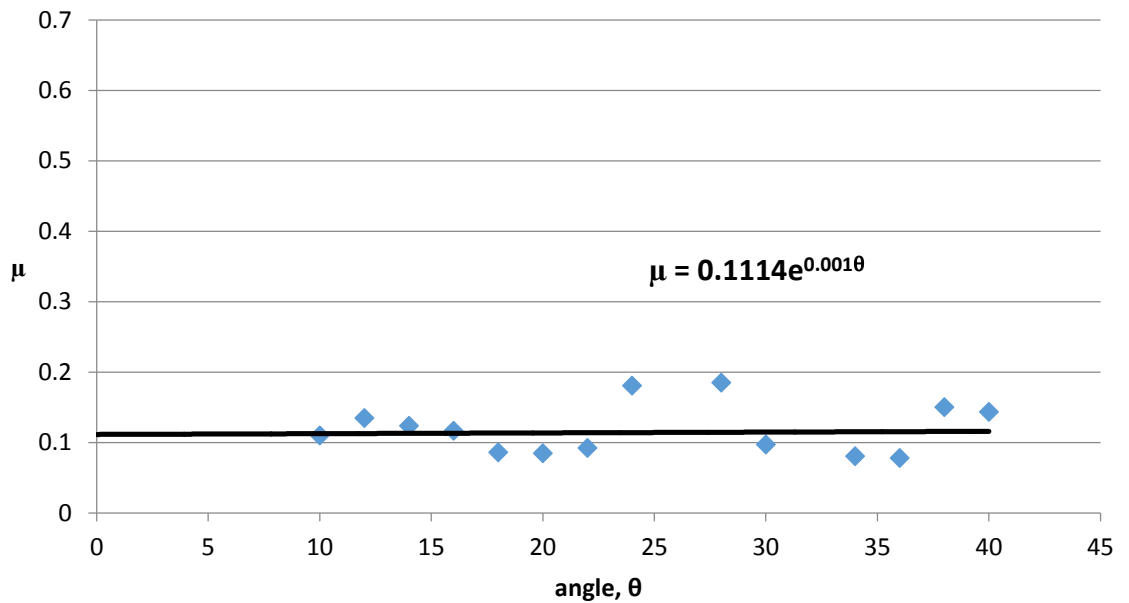


Figure 6.26: COF values using new derived equation Eq. 4.72 for Test 9.

Table 6.19: COF results for the stretch forming tests.

Test	Material Grade	Lubricant	Bulge depths h (mm)	COF obtained from Eq. 4.42	COF obtained from new derived Eq. 4.72	Maximum interfacial pressure (MPa)
1	EN 10346/ DX54D+Z	Dry	21,50- 19,08	0,19	0,29	21,64
2	EN 10346/ DX54D+Z	Dry	29,96- 25,13	0,33	0,33	17,67
3	EN 10346/ HX380LAD+Z	Dry	17,11- 14,73	0,14	0,25	25,45
4	EN 10346/ HX380LAD+Z	Dry	21,85- 19,47	0,20	0,32	21,87
5	EN 10346/ HX220BD+Z	Dry	20,64- 18,25	0,24	0,30	22,37
6	EN 10346/ HX220BD+Z	Dry	25,44- 23,03	0,27	0,33	19,42
7	EN 10346/ DX54D+Z	Paraffin	23,76- 22,59	0,06	0,08	21,01
8	EN 10346/ HX380LAD+Z	Paraffin	14,62- 12,81	0,07	0,07	29,01
9	EN 10346/ HX380LAD+Z	Paraffin	17,94- 16,34	0,13	0,11	25,77

6.3 RESULTS OBTAINED FROM OTHER SOURCES

Coefficient of friction values obtained from previous studies can be seen in Table 6.20. Room temperature and high temperature results can be seen to compare the test results with the previous studies.

Table 6.20: Results Obtained From Other Sources

Type of test	Lubricant	Material	COF	Source
Strip Drawing	HBO 947/11 Mineral oil	AI99.5	0,15-0,32	[33]
Bending Tension	Oil	DP 600	0,14-0,16	[38]
Strip drawing	Mineral oil	A1100	0,2-0,23	[21]
Draw bead	Stamping oil	DP 600	0,12-0,16	[20]
Strip tension	Dry	AA 1050	0,29	[27]
Draw bead	Oil	AKDQ steel	0,08-0,17	[25]
Flat drawing	Dry	SPHC steel	0,45 (600 ⁰ C) 0,44 (700 ⁰ C) 0,48 (800 ⁰ C)	[11]
Hot stamping	Waterbase Lubricant	SPHC steel	0,12 (600 ⁰ C) 0,14 (700 ⁰ C) 0,13 (800 ⁰ C)	[11]

6.4 DISCUSSION OF RESULTS

Coefficient of friction in deep drawing operations are investigated for two contact regions, radial drawing zone and stretch forming zones. Previous studies as shown in Table 6.20, were performed using simulative test conditions such as strip drawing and bending under tension. However, this study was performed in a real deep drawing/stretch forming process.

Results obtained for the stretch forming tests as shown in Table 6.19 for dry conditions indicate a slight increase in coefficient of friction as a function of the bulge depth. It is seen that the use of paraffin as a lubricant is very effective and reduces the coefficient of friction drastically. If the strain data can be obtained at the higher temperatures, the method allows the calculation of coefficient of friction at such temperatures.

In the radial drawing region, for dry and graphite lubricated conditions at room temperatures, coefficient of friction slightly decreases as deformation progresses. This is a result of the flattening of the peaks during the process. Similar, but less pronounced behavior is also observed at 300 °C. There is also a reduction in coefficient of friction at 300 °C under dry conditions. Graphite lubrication significantly lowers the coefficient of friction both in cold and hot conditions.

Coefficients of friction obtained in radial drawing zone and stretch forming zone regions fall in the same ranges. The values for the coefficient of friction found in the literature fall in similar ranges with bigger variations as shown in Table 6.20. Since they are obtained in other simulative tests, such variations can be expected.

Results obtained from deep drawing and stretch forming tests can be used in finite element simulations to validate the efficiency of the results. Punch load curves and strain distributions can be used to compare the simulations and the test results.

CHAPTER 7

CONCLUSION AND SUGGESTIONS FOR FUTURE WORK

Two methods are developed to evaluate coefficient of friction in radial drawing and stretch forming regions. It is found that for the stretch forming processes new developed equation gives more accurate results to obtain coefficient of friction. According to the experimental results, maximum and minimum values for the coefficient of friction closed together with the new equation. To calculate the coefficient of friction at the pole where $\theta = 0$, values of the coefficient of friction are extrapolated. Contraction of data range allows to reach more precise coefficient of friction values for the pole region.

It is concluded that for the stretch forming operations;

- Interfacial pressure decreases with the increase of bulge depths. Coefficient of friction values at different bulge depths were discussed in Table 6.19. While the bulge depths ranges are 19,08-21,50 to 25,13-29,96 mm for the test 1 and test 2, coefficient of friction values increased from 0,294 to 0,338. Other tests results validates this observation.
- Coefficient of friction values decrease with the increasing interfacial pressure. For the same material with paraffin lubricated condition at test 8 and 9 maximum interfacial pressures are 29,01 and 25,77 MPa. From these tests results coefficient of friction values are increase from 0,074 to 0,111. Except test 5 and 6 all other test results validate this conclusion.
- Results obtained in dry and lubricated conditions agree with those found in the literature. It is seen that paraffin lubrication in stretch forming and graphite in radial drawing are very effective.

From the deep drawing tests following conclusions are obtained;

- It is seen that using graphite lubrication in radial drawing are very effective to decrease coefficient of friction both room and high temperature conditions.
- Coefficient of friction values decreases with the increasing embrance angle α . When embrance angle has risen from 15° to 40° , calculated coefficient of friction values are decreased from 0,381 to 0,245 for test 1. All other tests results in Table 6.9 validates the conclusion.
- New derived equation is dependent on interfacial pressure. Taking the pressure into account increased the accuracy of the results.
- Increasing blank holder load increases the coefficient of friction values both room and high temperature conditions. When blank holder force ranges has risen from 14900-22350 N to 22350-29800 N, average coefficient of friction values increased from 0,308 to 0,331.
- At the non-lubricated dry condition coefficient of friction values decreased with the increase of the temperature. From Table 6.9 it can be seen that average coefficient of frictions has decreased from 0,308 to 0,216 and 0,331 to 0,316. However, for the graphite lubricated condition, it is concluded that the coefficient of friction increased with the increase of temperature from room temperature to 300°C . From Table 6.9 average coefficient of friction values for the lubricated condition increased 0,092 to 0,147 and 0,113 to 0,165. This increase can be explained by the bad lubrication performance at high temperatures.

Methods for calculating the coefficient of friction used in this study can be used to evaluate the lubrication performance for the future studies. On the other hand deep drawing and stretch forming tests can be performed at different temperature ranges to investigate the effect of temperature on coefficient of friction.

New derived coefficient of friction equation for stretch forming zone is very long and contains many parameters. A computer program can be developed to decrease the long calculation time. Thus will cause to increase the efficiency and accuracy of the results. In this study coefficient of friction values are shown depend on angle. However, as a future study result can be shown related to several variables by using surface response method.

As it is concluded that this study aims to obtain coefficient of friction values for the FE simulations. The obtained results can be validated by using the proper FE simulation softwares. Strain distributions and the punch load curves comparisons will be effective to compare the test and simulation results.

REFERENCES

1. Altan T., Tekkaya A. E., 2012, "Sheet Metal Forming Processes and Applications", ASM International, Materials Park Ohio.
2. Kaftanoğlu B., 1973, "Determination of coefficient of friction under conditions of deep-drawing and stretch forming", *Wear*, Vol 25/2, 177-178.
3. Kaftanoglu B, Alexander JM., 1961, "An Investigation of the Erichsen Test." *J Inst Met* 90:457–470
4. Totten G. E., 2006, "Handbook of lubrication and Tribology." Volume I, Application and Maintenance, Second edition, 2006.
5. Altan T., Tekkaya A. E., 2012, "Sheet Metal Forming Processes and Applications", ASM International, Materials Park Ohio,.
6. T. Altan, A. E. Tekkaya, 2012, "Sheet Metal Forming Fundamentals", Asm International, No 05340G.
7. E. Orowan, 1943, "The Calculation of Toll Pressure in Hot and Cold Flat Rolling", *Proceedings of Institutional Engineers Symposium*, Vol 67, 140-150.
8. Wanheim, Bay and Peterson, 1974, "A Theoretically Determined Model for Friction in Metal Working Processes", *Wear*, Vol 28, 251-258.
9. F. P Bowden and D. Tabor, 1967, "Friction and Lubrication", Methuen and Co. Ltd,.
10. Subramonnan S., Kardes N., Demiralp Y., and Altan T., 2009, "Evaluation of Stamping Lubricants to Improve Stamping Quality." CPF report no:CPF 2.5/09/03, The Ohio State University.
11. Subramonnan S, Kardes N, Demiralp Y, Jurich M, Altan T., 2011, "Evaluation of Stamping Lubricants in Forming Galvannealed Steels for Industrial Application", *Journal of Manufacturing Science and Engineering*, 133/6:061001-9.

12. Yanagida A, Azushima A., 2009, "Evaluation of coefficients of friction in hot stamping by hot flat drawing test", *Annals of the CIRP*, 58/1:247-250.
13. Bech J, Bay N, Eriksen M., 1998, "A Study of Mechanisms of Liquid Lubrication in Metal Forming", *Annals of the CIRP*, 47/1:221-226.
14. Olsson D. D, Bay N, Andreasen J. L, 2004, "Prediction of limits of lubrication in strip reduction testing.", *Annals of the CIRP*, 53/1:231-234.
15. B. Meng & M. W. Fu & M. Wan, 2014, " Drawability and frictional behavior of pure molybdenum sheet in deep-drawing process at elevated temperature", *Int J Adv Manuf Technol*, 78:1005–1014.
16. M. Dilmec, M. Arap, 2016, "Effect of geometrical and process parameters on coefficient of friction in deep drawing process at the flange and the radius regions", *Int J Adv Manuf Technol* 86:747–759.
17. Schmoeckel D, Prier M, Staeves J., 1997, "Topography Deformation of Sheet Metal during the Forming Process and Its Influence on Friction", *Annals of the CIRP*, 46/1:175-178.
18. Berglund J, Brown CA, Rosén BG, Bay N., 2010, "Milled die steel surface roughness correlation with steel sheet friction", *Annals of the CIRP*, 59/1:577-580.
19. Jeon J, Bramley AN, 2007, "A friction model for microforming". *Int J Adv Manuf Technol* 33:125–129.8
20. Darendeliler H, Akkök M, Yücesoy C. A, 2002, "Effect of variable friction coefficient on sheet metal drawing." *Tribology International* 35 97-104.
21. Figueredo L, Ramalho A, Oliveira M.C, Menezes L.F., 2011, "Experimental study of friction in sheet metal forming." *Wear*, Vol 271, 1651-1657.
22. Azushima A, Kudo H., 1995, "Direct observation of contact behaviour to interpret the pressure dependence of the coefficient of friction in sheet metal forming." *Annals of the CIRP*, 44/1 209-212.
23. Azushima A, Sakuramoto M, 2006, "Effects of plastic strain on surface roughness and coefficient of friction in tension bending test." *Annals of the CIRP*, 55/1.
24. Ahmetoglu M, Broek T. R, Kinzel G, Altan T, 1995, "Control of blank holder force to eliminate wrinkling and fracture in deep drawing rectangular parts." *Annals of the CIRP*, 44/1, 247-250.

25. Osakada K, Wang C. C, Mori K, 1995, "Controlled FEM simulation for determining history of blank holding force in deep drawing." *Annals of the CIRP* Vol. 44/1, 243-246.
26. Weinmann K. J, Kernosky K. S, 1996, "Friction studies in sheet metal forming based on a unique die shoulder force transducer." *Annals of the CIRP*, 45/1, 269-272.
27. Kong Y, Sun Y, Wang X, Wagoner R. H, 1993, "Development of a new friction test device in sheet metal forming.", *Advanced Technology of Plasticity*, 835-838.
28. Fratini L, Casto L. S, Valvo E. L, 2006, "A technical note on an experimental device to measure friction coefficient in sheet metal forming." *Journal of Materials Processing Technology*, 172, 16-21.
29. Karadogan C, Hatipoglu H. A, 2014, "Direct evaluation of coulomb friction coefficient from sheet strip stretch test on a cylinder surface." *Advanced Materials Research Vols.*, 966-967, 242-248.
30. Hol J, Cid Alfaro M. V, Rooij M.B, Meinders T, 2011, "Advanced friction modelling for sheet metal forming." *Wear*, Vol 04/004.
31. Cho H, Ngalle G, Altan T, 2003, "Simultaneous determination of flow stress and interface friction between by finite element based inverse analysis technique.", *Annals of the CIRP*, 52/1:221-224.
32. Makinouchi A, Teodosiu C, Nakagawa T., 1998, "Advance in FEM Simulation and its Related Technologies in Sheet Metal Forming", *Annals of the CIRP*, 47/2:641-649.
33. F. Klocke, D. Trauth, A. Shirobokov, P. Mattfeld, 2015, "FE-analysis and in situ visualization of pressure-, slip-rate- and temperature-dependent coefficients of friction for advanced sheet metal forming: development of a novel coupled user subroutine for shell and continuum discretization", *Int J Adv Manuf Technol* 81:397–410.
34. Vollertsen F, Hu Z., 2006, "Tribological Size Effects in Sheet Metal Forming Measured by a Strip Drawing Test", *Annals of the CIRP*, 55/1:291-294.
35. www.erdemir.com.tr/Sites/1/upload/files/Urun_katalog-EN-146.PDF, Erdemir Product Catalogue website.
36. Gürbüz, İ., 2014, "Enhanced Characterization and Die Design for Sheet Metal Forming in Automotive Industry", Master Thesis, Atılım University.

37. Prete, Del, A., Papad, G., Spagnollo, A., 2001, "Computer Aided Engineering for Warm Bulging Test Tooling Design", ICTP Proc. 10th Int. Conf. Techn., 805.
38. Kayhan, E., 2015, "The Development Of A Method To Improve The Limit Drawing Ratio Of Blanks Using Preferential Heating", PhD. Thesis Atılım University.



APPENDICES

APPENDIX A

STRAIN DISTRIBUTION AND PRESSURE DISTRIBUTION GRAPHS FOR STRETCH FORMING

TEST 1:

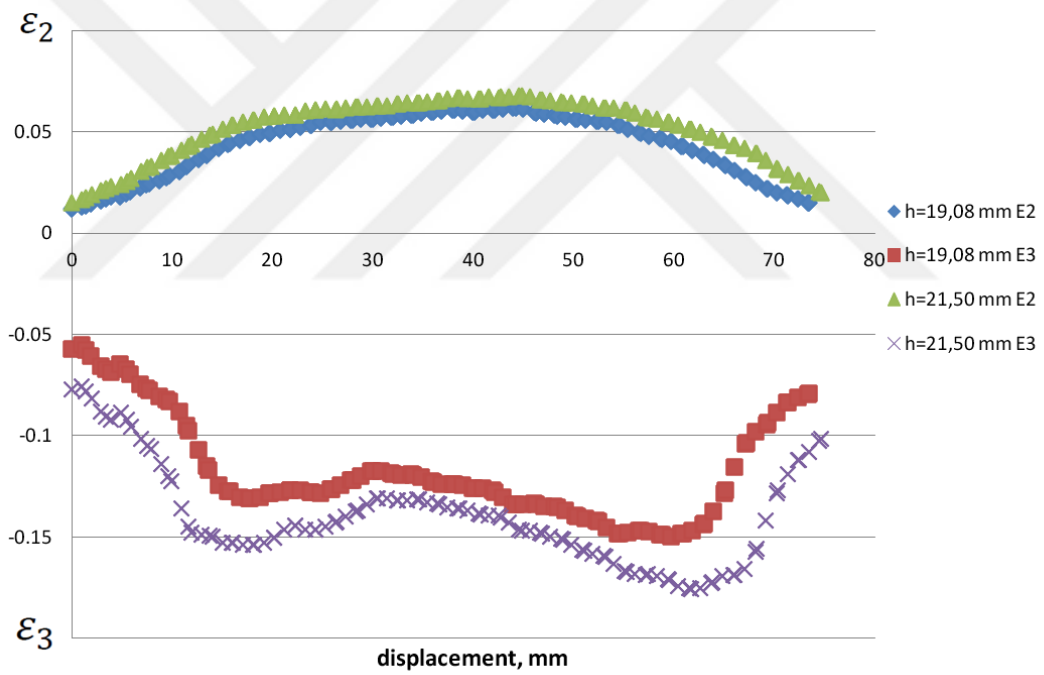


Figure A.1: Test 1 Strain distributions-displacement

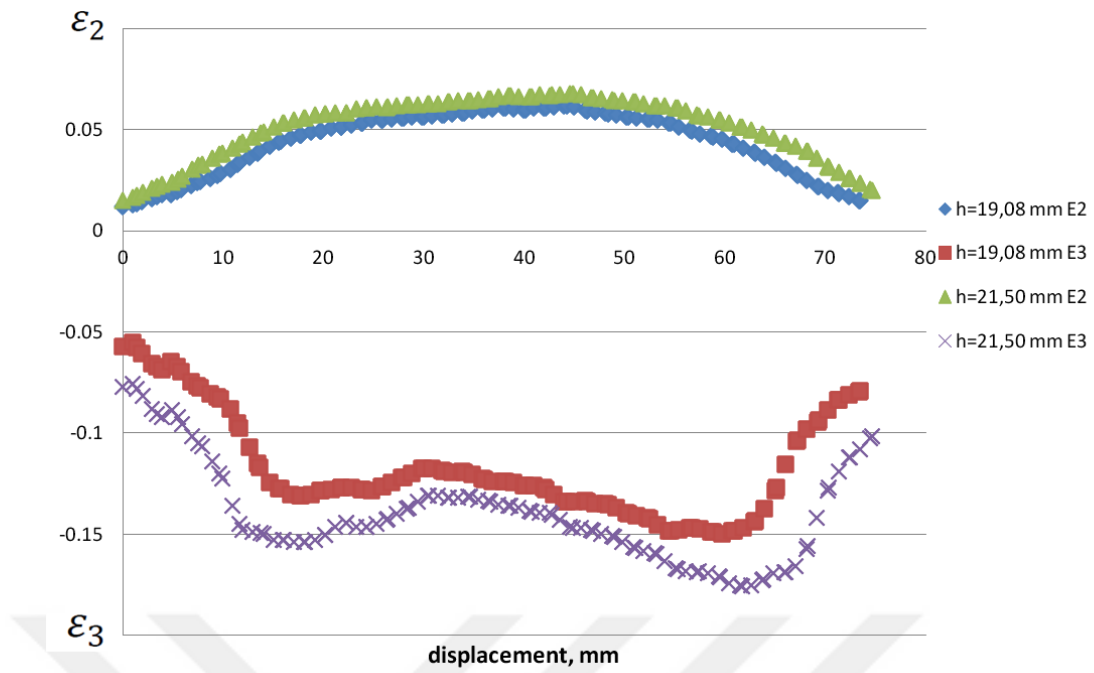


Figure A.2: Test 1 Strain distributions-angle, θ

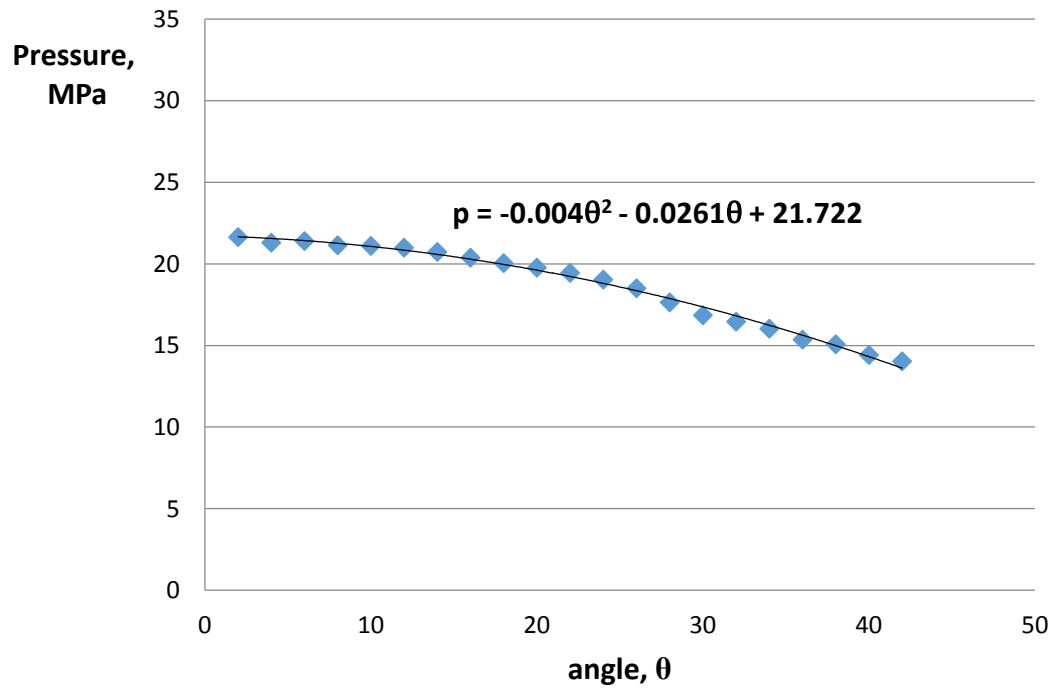


Figure A.3: Test 1 Pressure distributions

TEST 2:

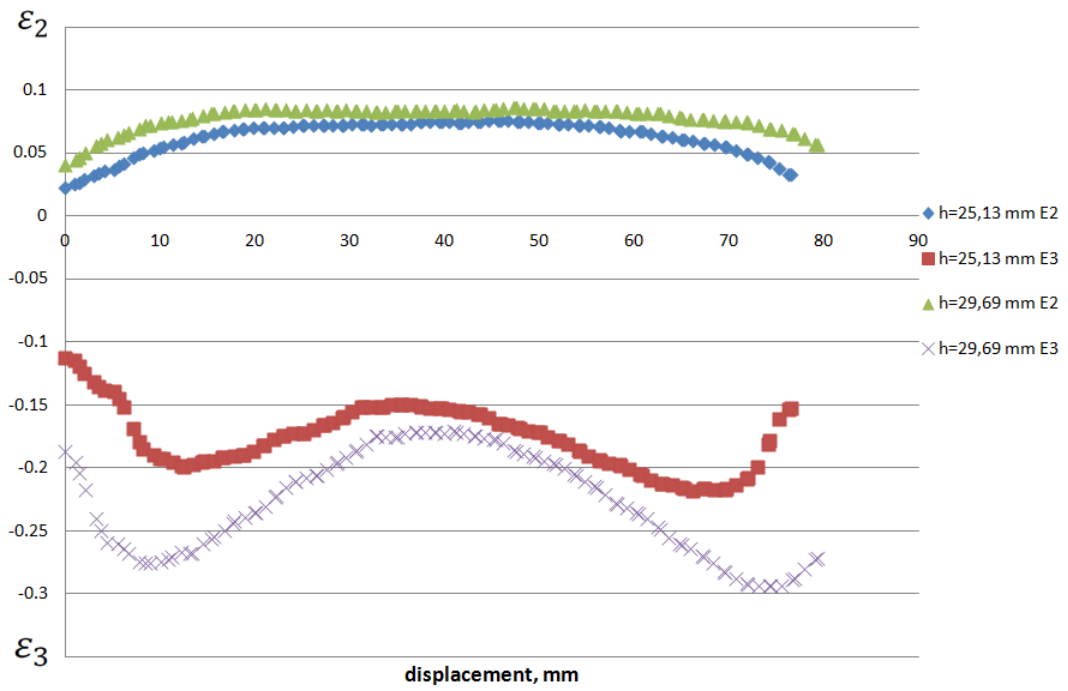


Figure A.4: Test 2 Strain distributions-displacement

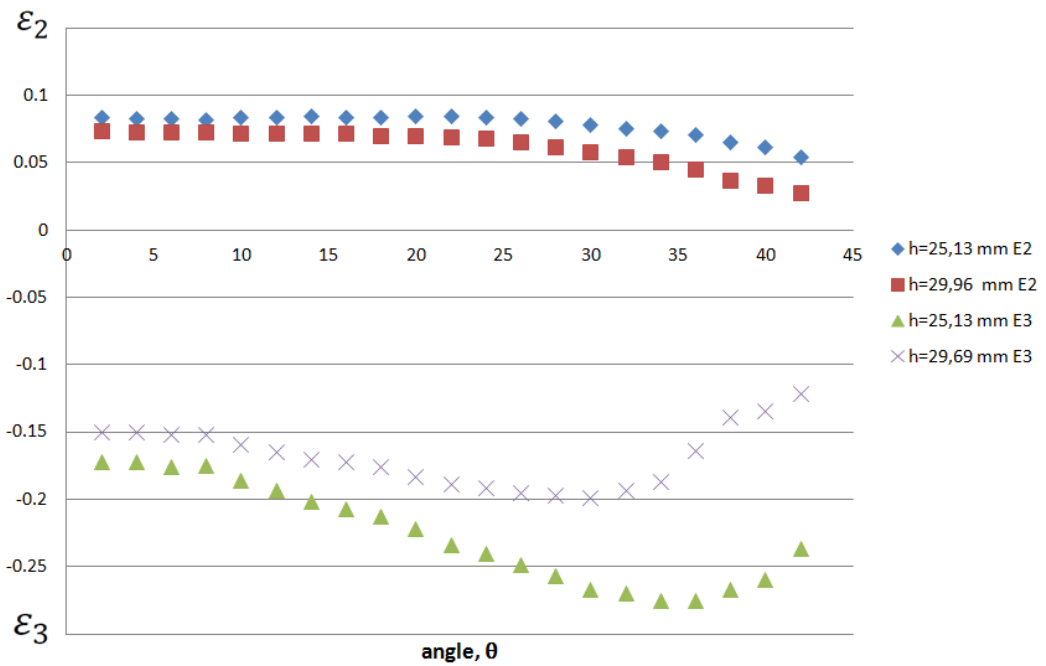


Figure A.5: Test 1 Strain distributions-angle, θ

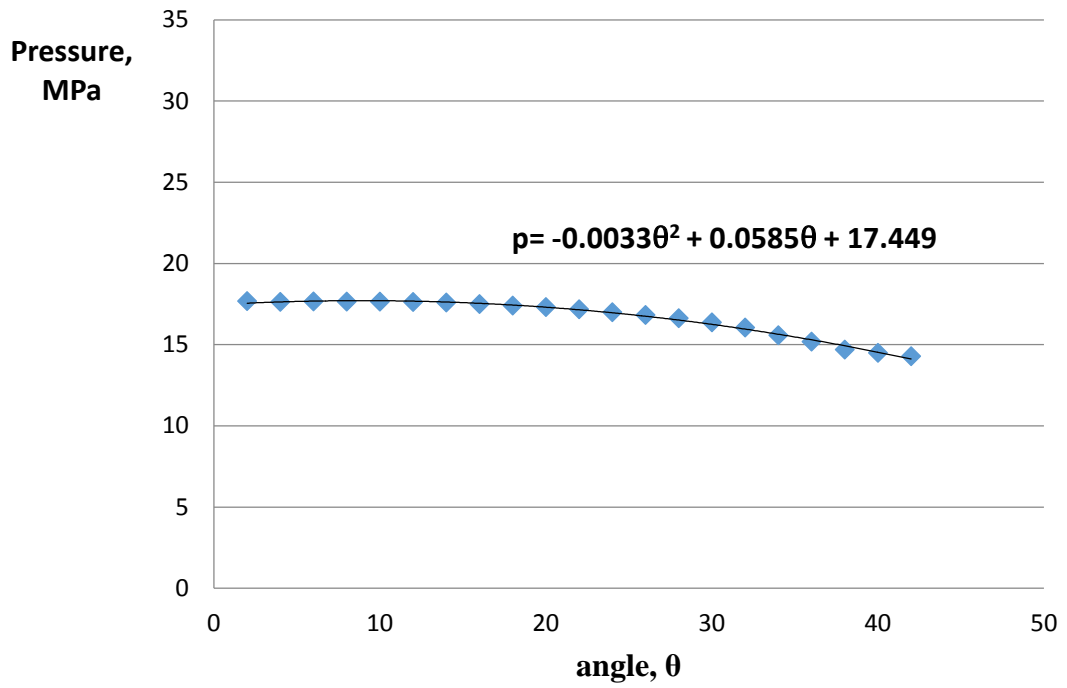


Figure A.6: Test 2 Pressure distributions

TEST 3:

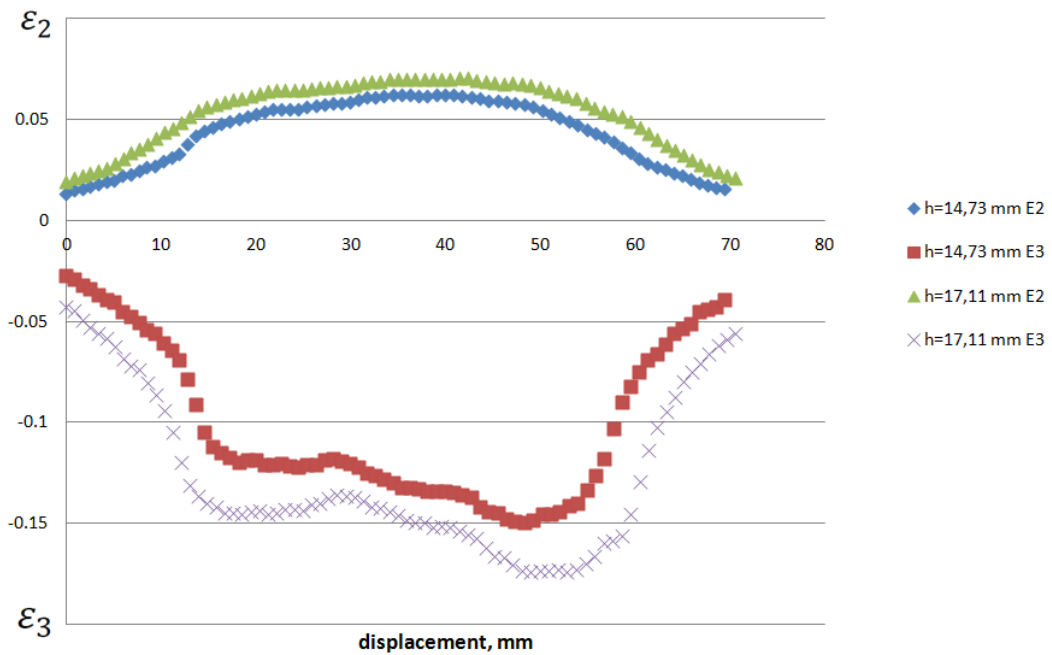


Figure A.7: Test 3 Strain distributions-displacement

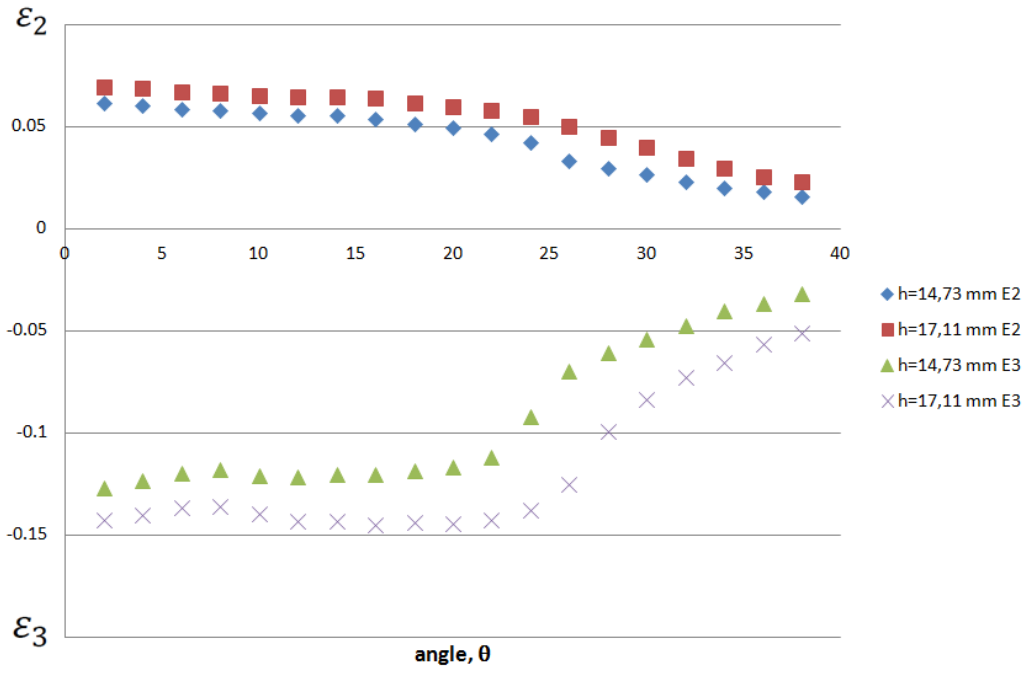


Figure A.8: Test 3 Strain distributions-angle, θ

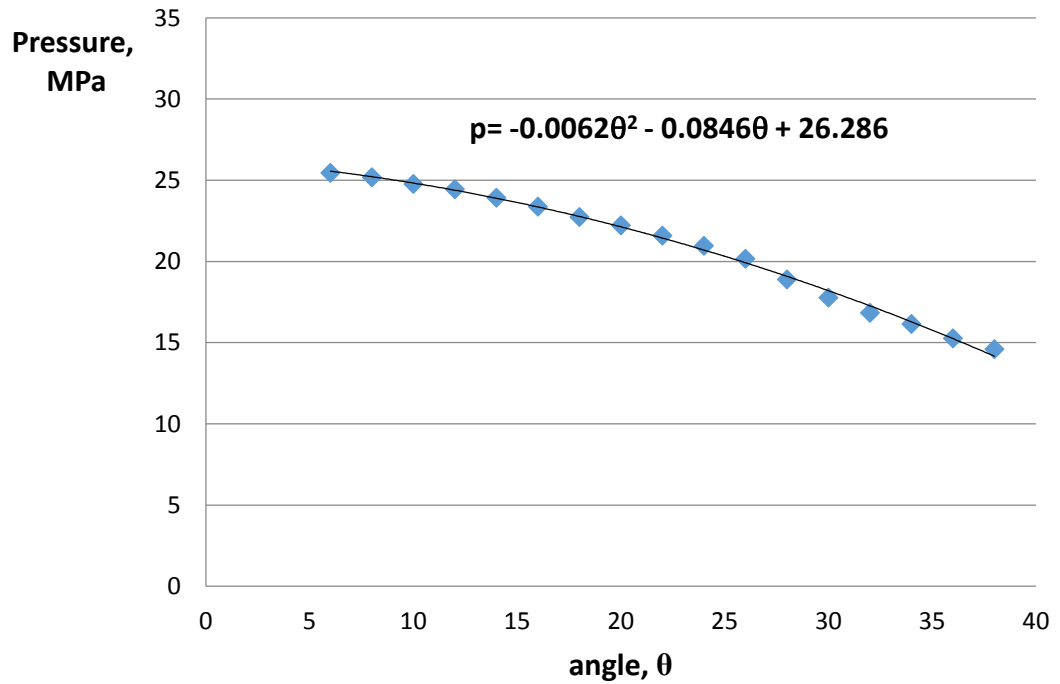


Figure A.9: Test 3 Pressure distributions

TEST 4:

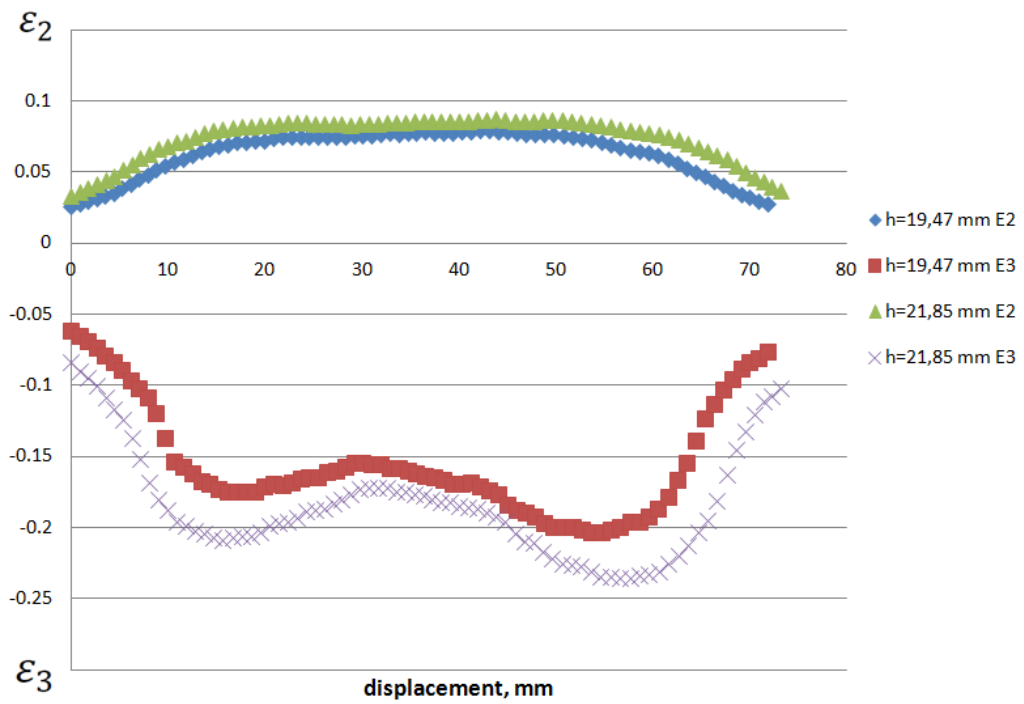


Figure A.10: Test 4 Strain distributions-displacement

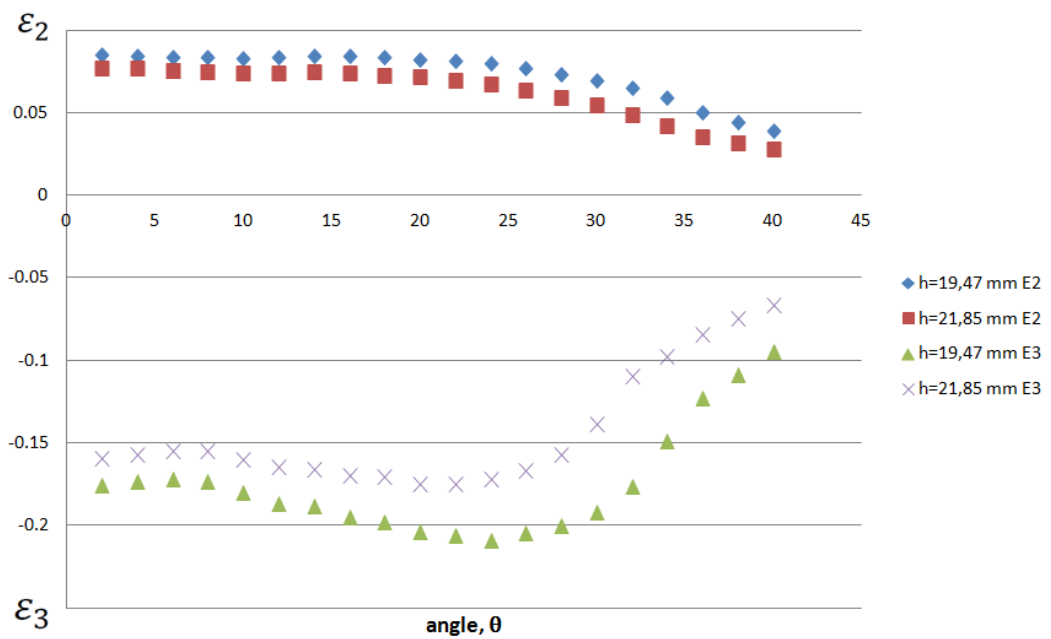


Figure A.11: Test 4 Strain distributions-angle, θ

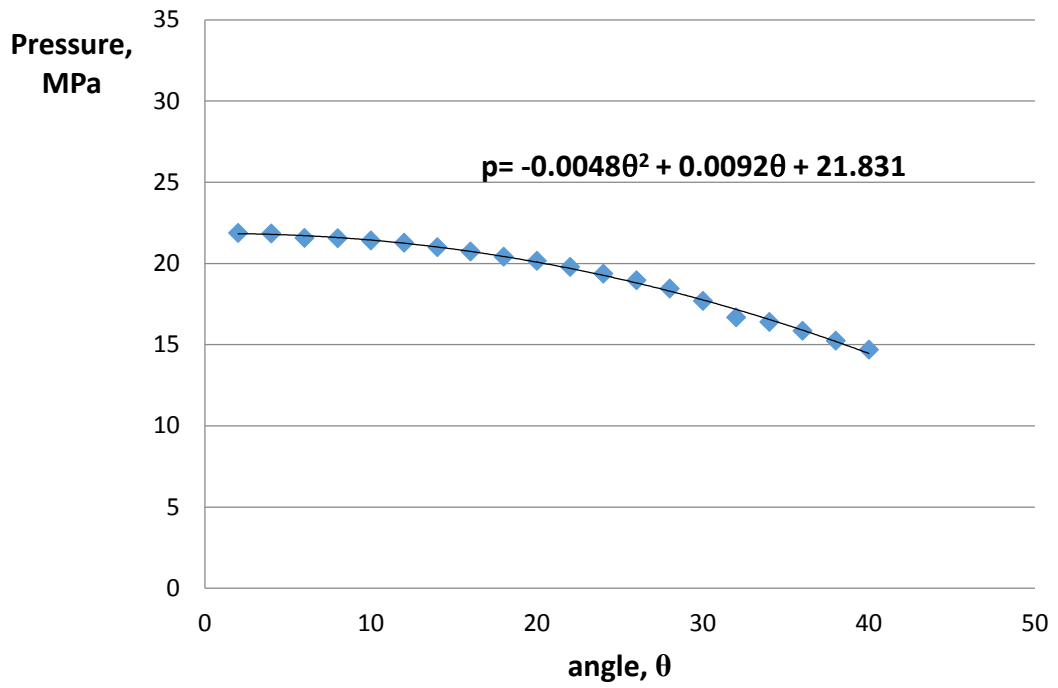


Figure A.12: Test 4 Pressure distributions

TEST 5:

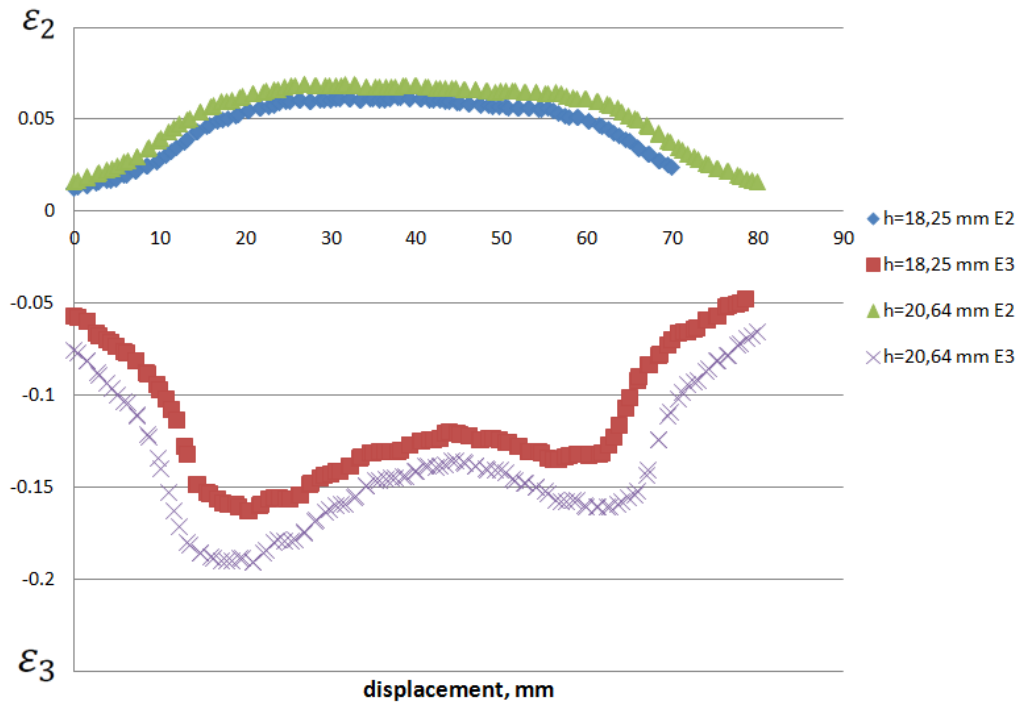


Figure A.13: Test 5 Strain distributions-displacement

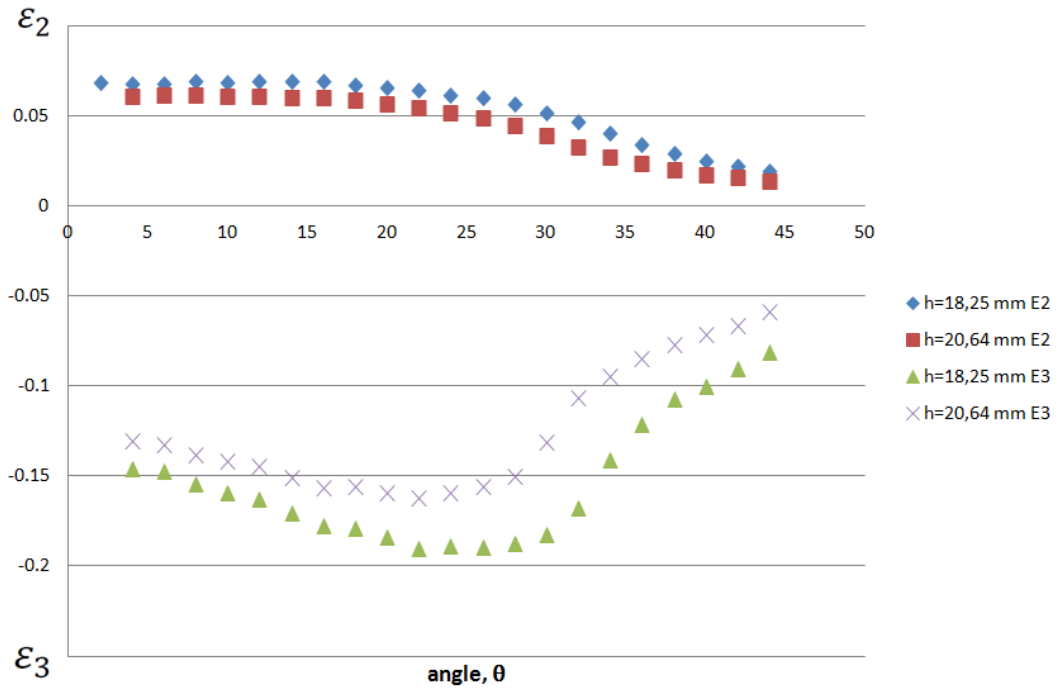


Figure A.14: Test 5 Strain distributions-angle, θ

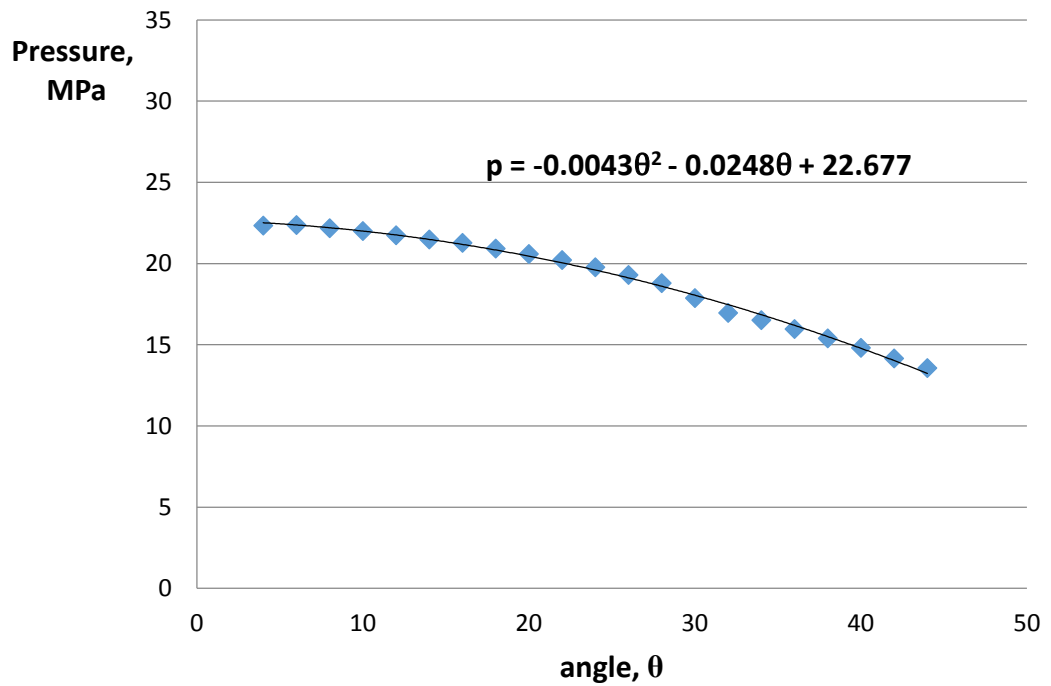


Figure A.15: Test 5 Pressure distributions

TEST 6:

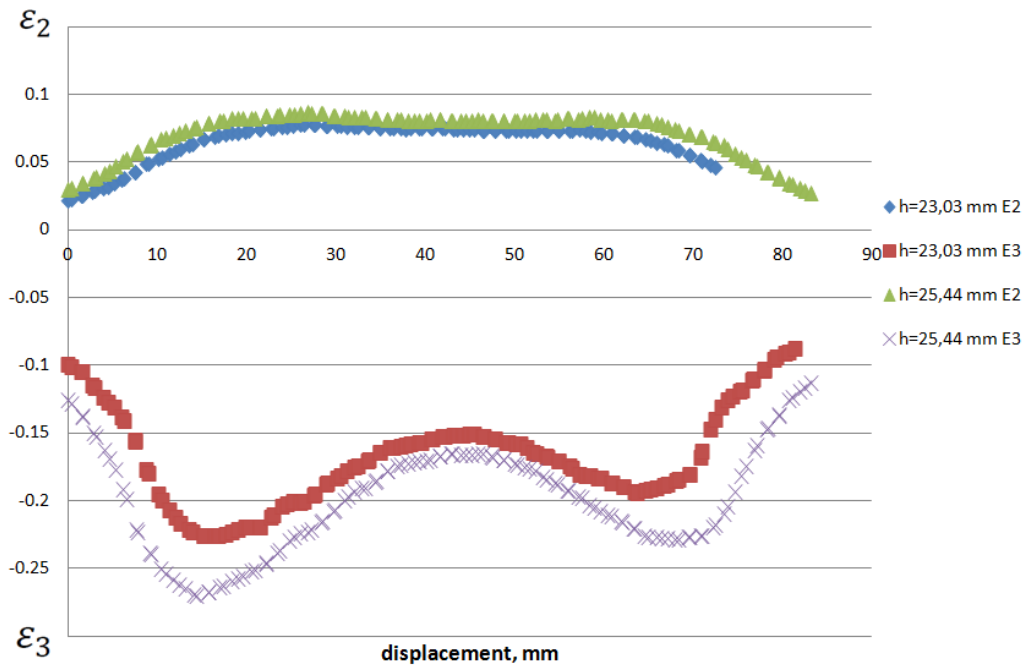


Figure A.16: Test 6 Strain distributions-displacement

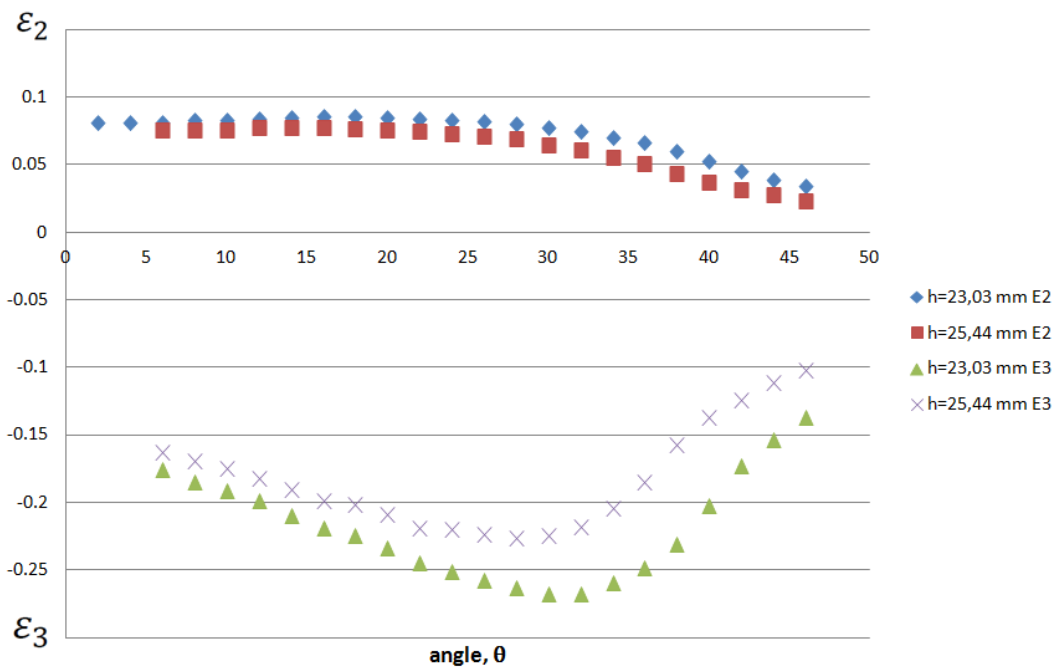


Figure A.17: Test 6 Strain distributions-angle, θ

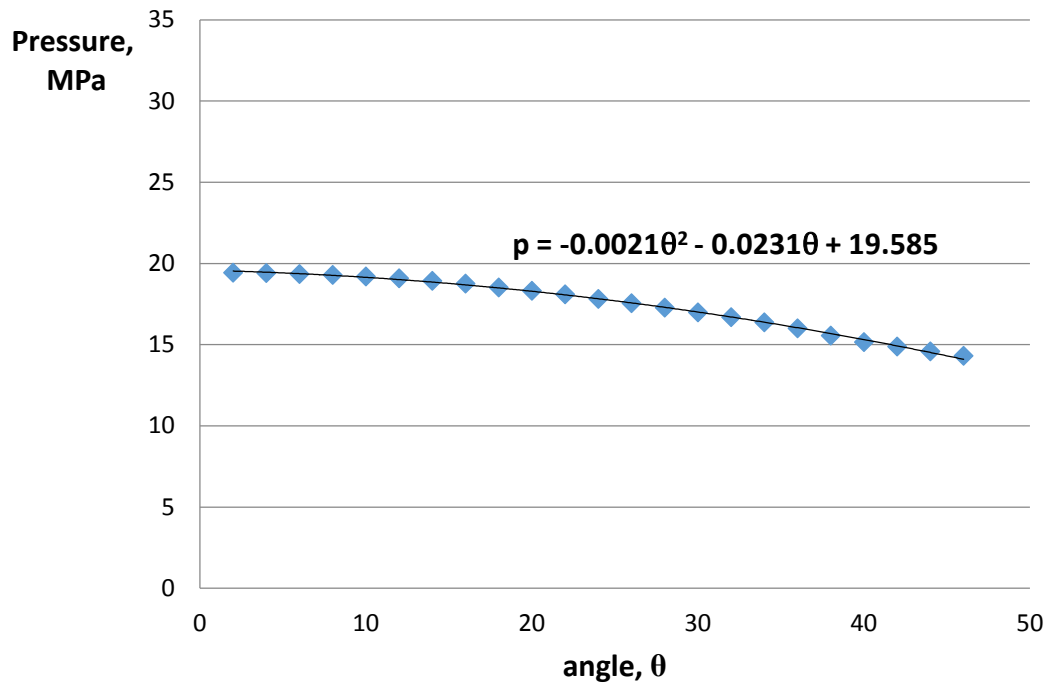


Figure A.18: Test 6 Pressure distributions

TEST 7:

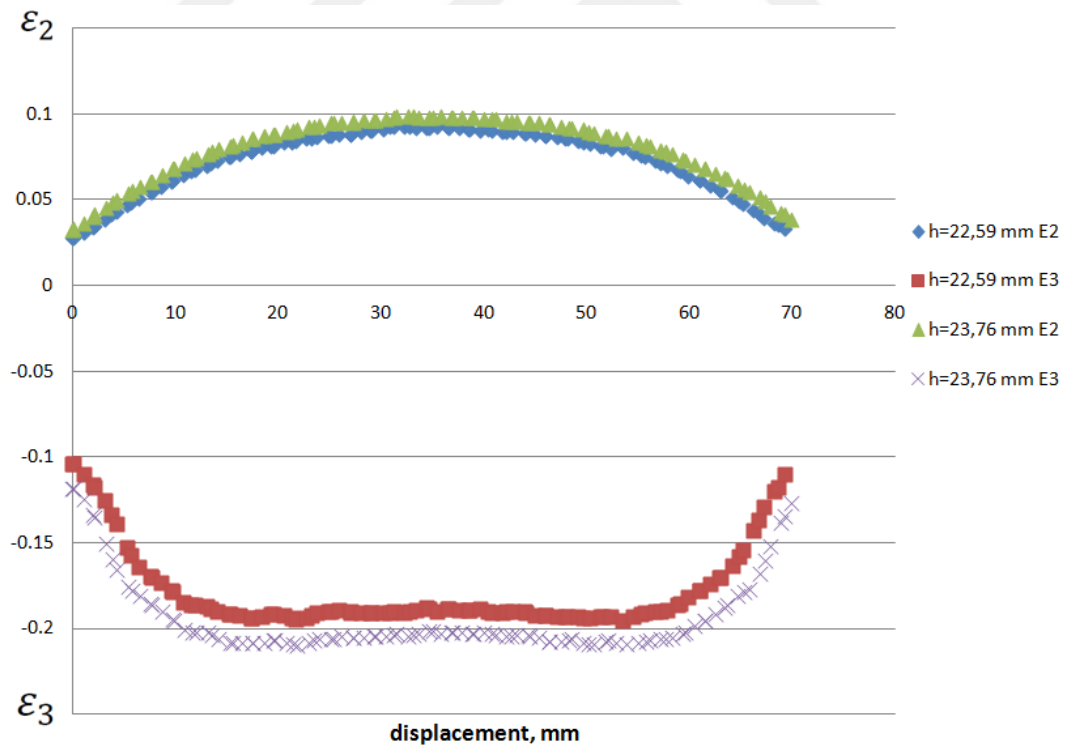


Figure A.19: Test 7 Strain distributions-displacement

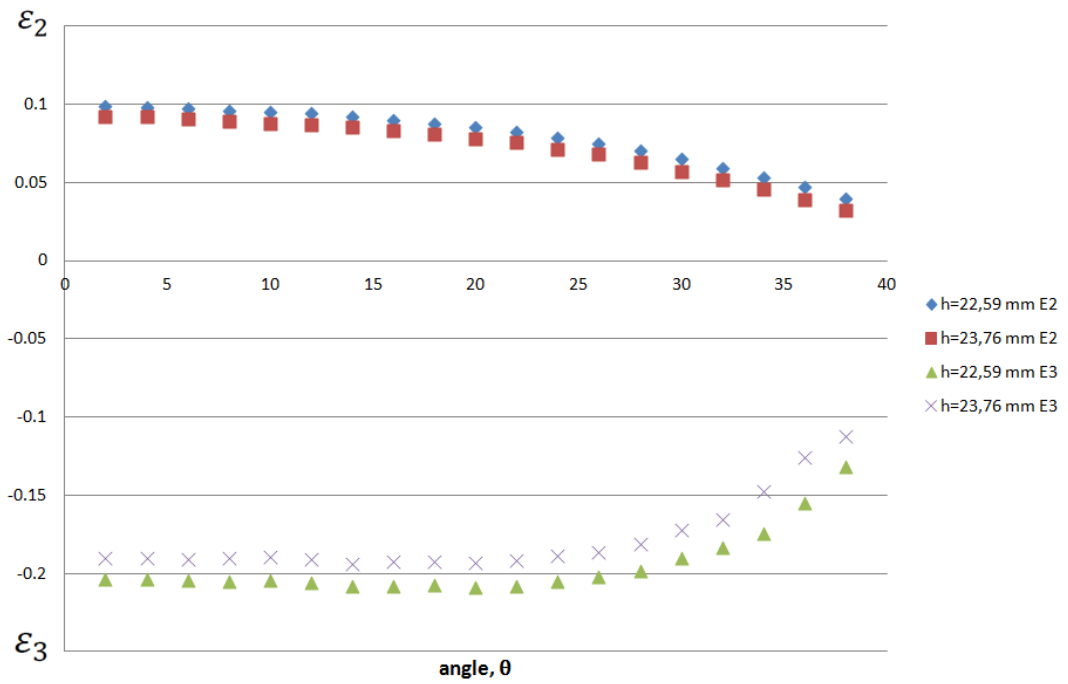


Figure A.20: Test 7 Strain distributions-angle, θ

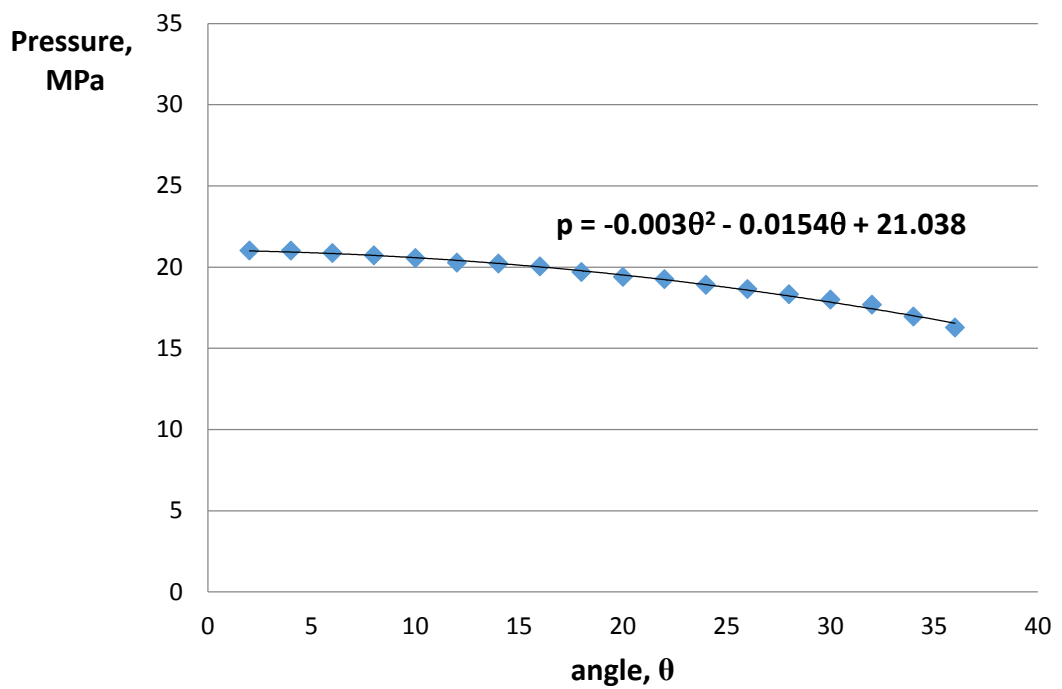


Figure A.21: Test 7 Pressure distributions

TEST 8:

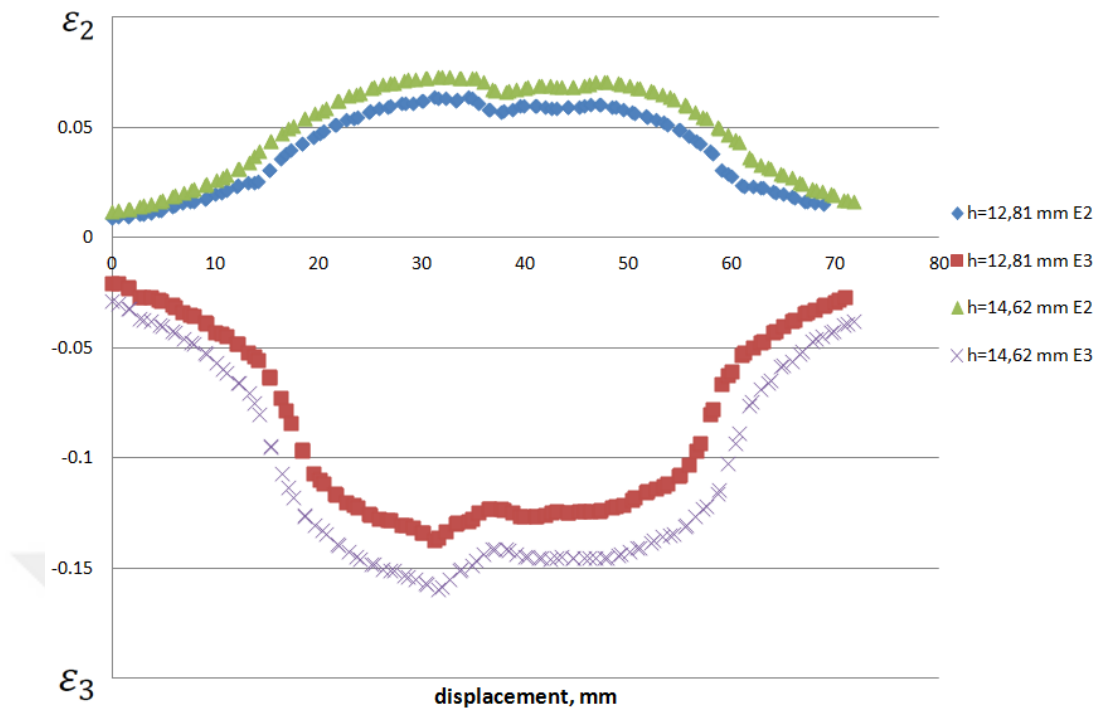


Figure A.22: Test 8 Strain distributions-displacement

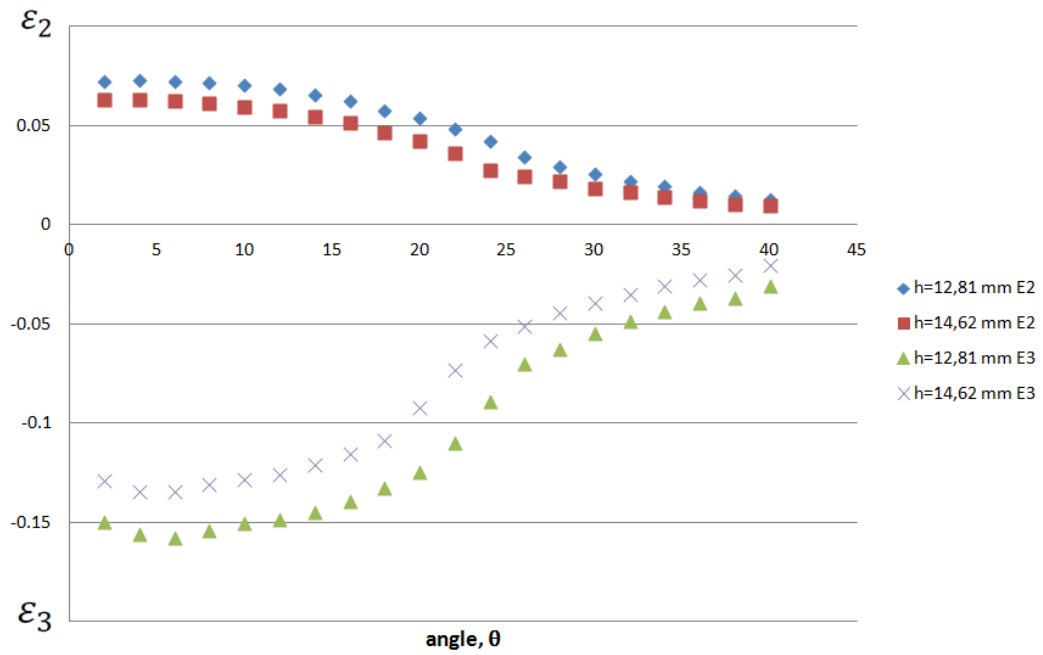


Figure A.23: Test 8 Strain distributions-angle, θ

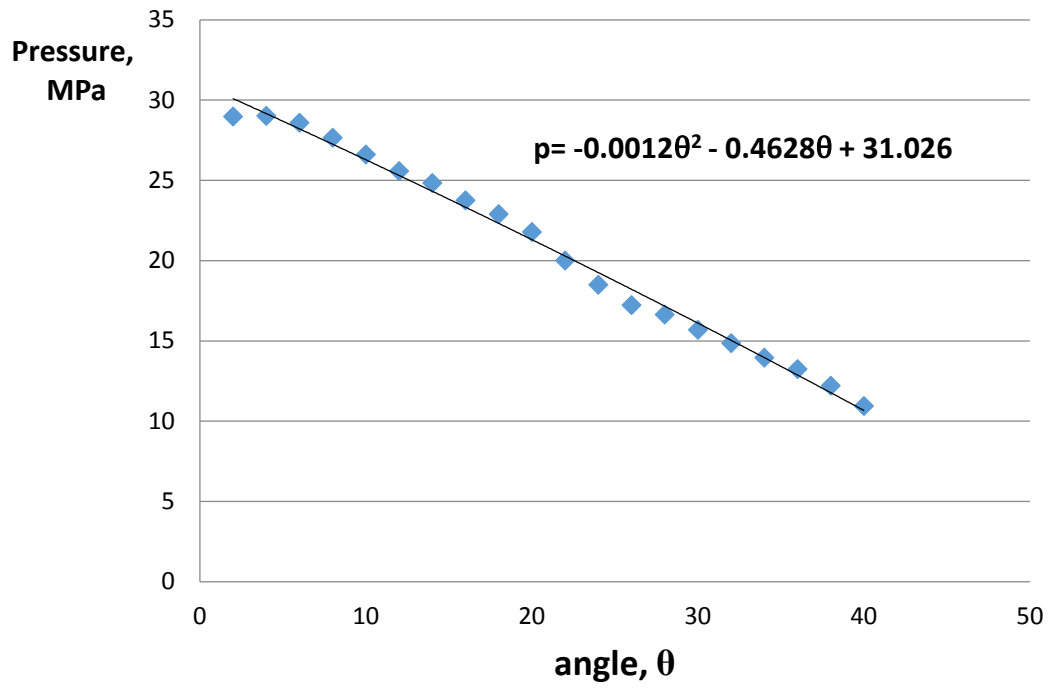


Figure A.24: Test 8 Pressure distributions

TEST 9:

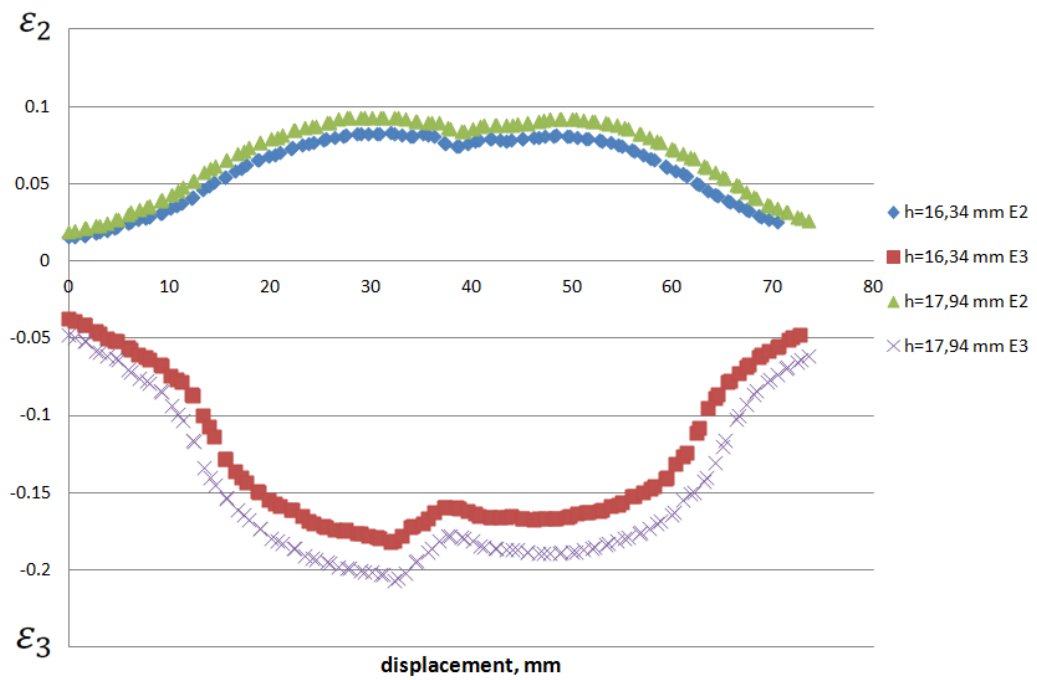


Figure A.25: Test 9 Strain distributions-displacement

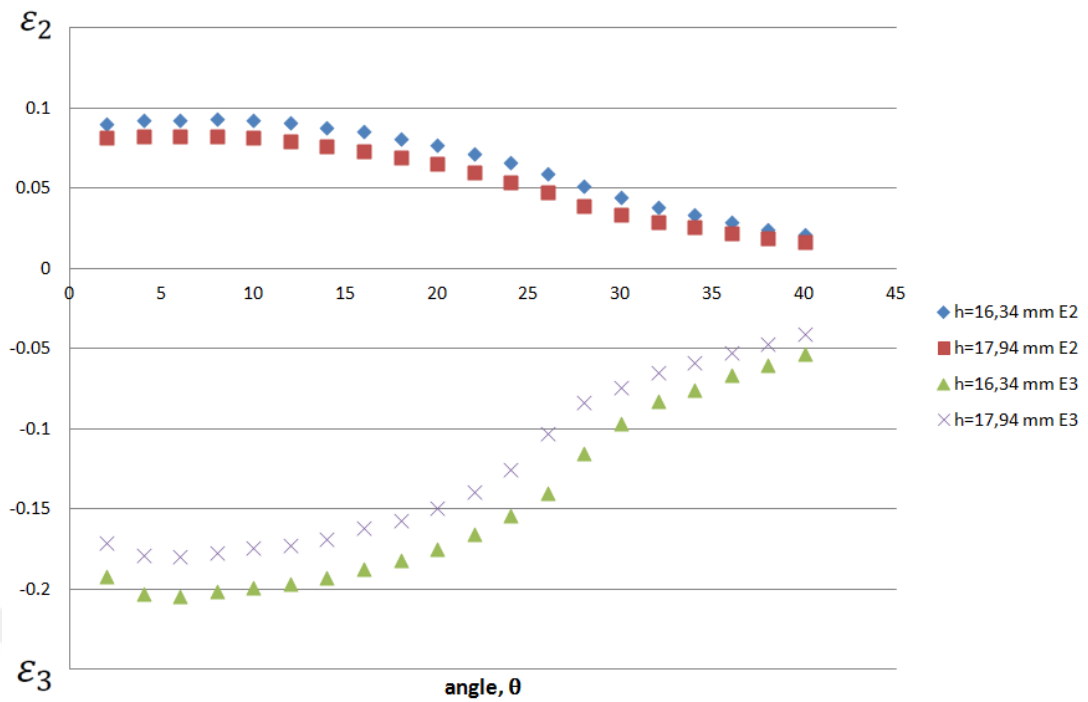


Figure A.26: Test 9 Strain distributions-angle, θ

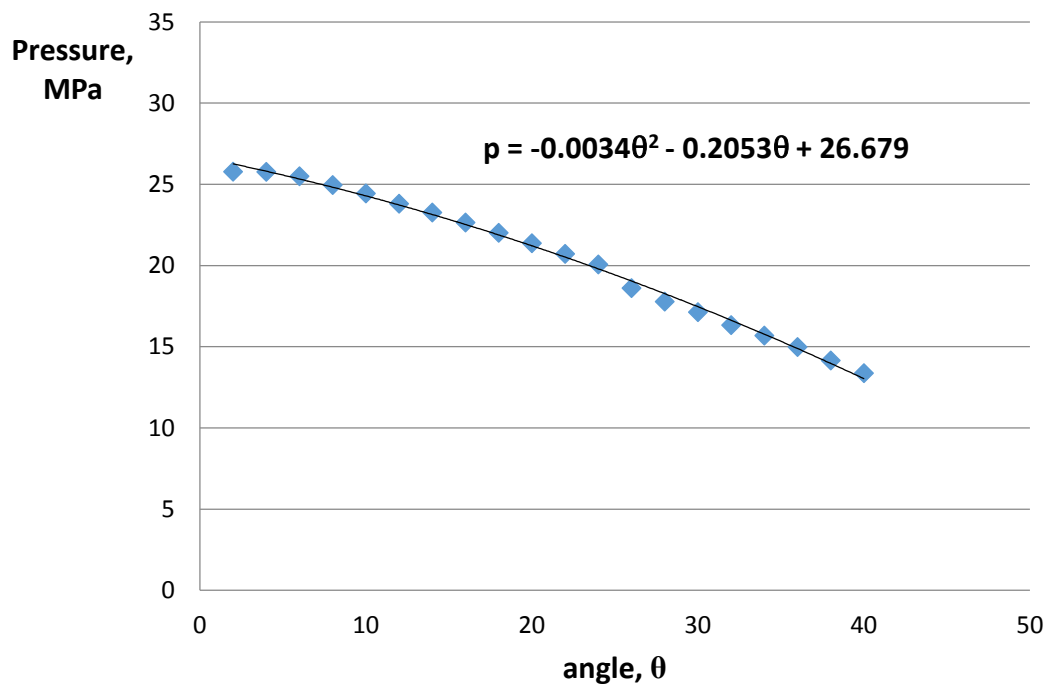


Figure A.27: Test 9 Pressure distributions

APPENDIX B

SURFACE ROUGHNESS MEASUREMENTS

Deep drawing die:

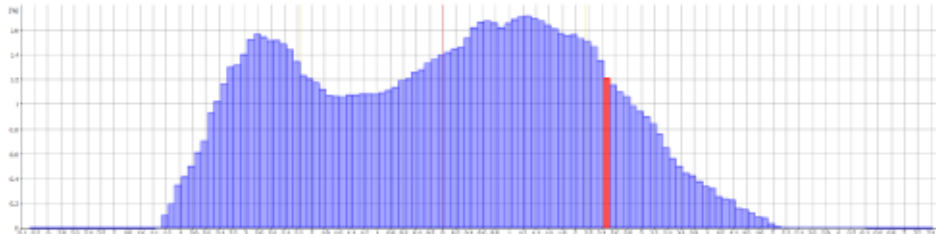
Alicona Imaging GmbH
Dr.-Auner Strasse 21a
A-8074 Raaba/Graz

Measurement Report

Surface Texture Measurement

Surface Texture of Primary Dataset

Sac-Rough-50x-Large



Histogram Histogram Settings

Number of Classes: 137
Minimum Value: -6.27 μm
Maximum Value: 7.43 μm
Class Width: 0.10 μm

Statistics

Name	Value	[u]
Elements	8683832	
Classes	137	
Mean Value	0.00	μm
Standard Deviation	2.16	μm

Selected Class

Name	Value	[u]
Class Index	88	
Percentage	1.2135	%
Lower Border	2.43	μm
Upper Border	2.53	μm

Parameters

Name	Value	[u]	Description
Sa	1.84	μm	Average height of selected area
Sq	2.16	μm	Root-Mean-Square height of selected area

Measurement performed by Alicona InfiniteFocus, 07.01.2016 14:10:37

1

Alicona Imaging GmbH
Dr.-Auner Strasse 21a
A-8074 Raaba/Graz

Name	Value	[u]	Description
Sp	7.36	µm	Maximum peak height of selected area
Sv	6.27	µm	Maximum valley depth of selected area
Sz	13.63	µm	Maximum height of selected area
S10z	11.50	µm	Ten point height of selected area
Ssk	-0.023275		Skewness of selected area
Sku	1.9931		Kurtosis of selected area
Sdq	0.26785		Root mean square gradient
Sdr	3.2291	%	Developed interfacial area ratio
FLTt	13.63	µm	Flatness using least squares reference plane

Measurement Report

Surface Texture Measurement

Surface Texture of Primary Dataset

Die-FR



Histogram Histogram Settings

Number of Classes: 100
 Minimum Value: -4.09µm
 Maximum Value: 0.91µm
 Class Width: 0.05µm

Statistics

Name	Value	[u]
Elements	9897726	
Classes	100	
Mean Value	0.00	µm
Standard Deviation	0.49	µm

Parameters

Name	Value	[u]	Description
Sa	0.29	µm	Average height of selected area
Sq	0.49	µm	Root-Mean-Square height of selected area
Sp	0.88	µm	Maximum peak height of selected area
Sv	4.09	µm	Maximum valley depth of selected area
Sz	4.97	µm	Maximum height of selected area
S10z	4.80	µm	Ten point height of selected area
Ssk	-3.812		Skewness of selected area
Sku	23.865		Kurtosis of selected area
Sdq	0.047274		Root mean square gradient

Measurement performed by Alicona InfiniteFocus, 07.01.2016 14:34:00

1

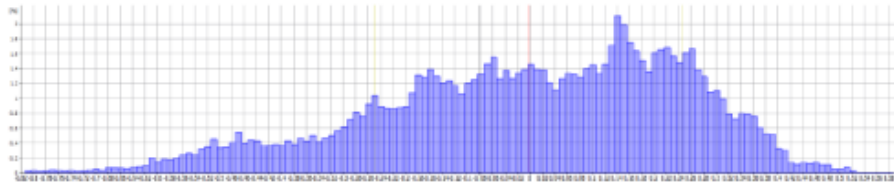
Name	Value	[u]	Description
Sdr	0.11142	%	Developed interfacial area ratio
FLTt	4.97	µm	Flatness using least squares reference plane

Measurement Report

ProfileRoughnessMeasurement

Parameters of Roughness Profile

__temp_20160107_141545895



Histogram Histogram Settings

Number of Classes: 140
 Minimum Value: $-0.81\mu\text{m}$
 Maximum Value: $0.59\mu\text{m}$
 Class Width: $0.01\mu\text{m}$

Statistics

Name	Value	[u]
Elements	52430	
Classes	140	
Mean Value	0.00	μm
Standard Deviation	0.25	μm

Parameters

Name	Value	[u]	Description
Ra	0.20	μm	Average roughness of profile
Rq	0.25	μm	Root-Mean-Square roughness of profile
Rt	1.39	μm	Maximum peak to valley height of roughness profile
Rz	1.19	μm	Mean peak to valley height of roughness profile
Rmax	1.39	μm	Maximum peak to valley height of roughness profile within a sampling length
Rp	0.58	μm	Maximum peak height of roughness profile
Rv	0.81	μm	Maximum valley height of roughness profile
Rc	0.70	μm	Mean height of profile irregularities of roughness profile
Rsm	91.86	μm	Mean spacing of profile irregularities of roughness profile
Rsk	-0.53278		Skewness of roughness profile
Rku	2.725		Kurtosis of roughness profile
Rdq	0.037313		Root-Mean-Square slope of roughness profile

Measurement performed by Alicona InfiniteFocus, 07.01.2016 14:17:48

1

Name	Value	[u]	Description
Rt/Rz	1.1698		Extreme Scratch/Peak value of roughness profile, ($\rho=1$), higher values represent larger scratches/peaks
l	8.51024	mm	Profile Length
Lc	800.00	μm	LambdaC: cut off wavelength

Sheet material:

Alicona Imaging GmbH
 Dr.-Auner Strasse 21a
 A-8074 Raaba/Graz

Measurement Report

Profile Measurement

Advanced Parameters of Roughness Profile

$L_c = 800.00\mu\text{m}$

__temp_20160107_134312350

Mean of Profile Parameters

Name	Value	[u]	Description
mean Ra	1.82	μm	Average roughness of profile
mean Rq	2.06	μm	Root-Mean-Square roughness of profile
mean Rt	8.11	μm	Maximum peak to valley height of roughness profile
mean Rz	7.39	μm	Mean peak to valley height of roughness profile
mean Rmax	8.08	μm	Maximum peak to valley height of roughness profile within a sampling length
mean Rp	3.95	μm	Maximum peak height of roughness profile
mean Rv	4.16	μm	Maximum valley height of roughness profile
mean Rc	5.12	μm	Mean height of profile irregularities of roughness profile
mean Rsm	110.81	μm	Mean spacing of profile irregularities of roughness profile
mean Rsk	-0.28811		Skewness of roughness profile
mean Rku	1.8049		Kurtosis of roughness profile
mean Rdq	0.1772		Root-Mean-Square slope of roughness profile
mean Rt/Rz	1.0962		Extreme Scratch/Peak value of roughness profile, (≥ 1), higher values represent larger scratches/peaks
Lc	800.00	μm	LambdaC: cut off wavelength

Standard Deviation of Profile Parameters

Name	Value	[u]	Description
sigma Ra	0.00	μm	Average roughness of profile
sigma Rq	0.00	μm	Root-Mean-Square roughness of profile
sigma Rt	0.02	μm	Maximum peak to valley height of roughness profile
sigma Rz	0.00	μm	Mean peak to valley height of roughness profile
sigma Rmax	0.01	μm	Maximum peak to valley height of roughness profile within a sampling length
sigma Rp	0.02	μm	Maximum peak height of roughness profile
sigma Rv	0.00	μm	Maximum valley height of roughness profile
sigma Rc	0.01	μm	Mean height of profile irregularities of roughness profile
sigma Rsm	0.67	μm	Mean spacing of profile irregularities of roughness profile
sigma Rsk	0.0024782		Skewness of roughness profile
sigma Rku	0.0047503		Kurtosis of roughness profile
sigma Rdq	78.107e-6		Root-Mean-Square slope of roughness profile
sigma Rt/Rz	0.0029178		Extreme Scratch/Peak value of roughness profile, (≥ 1), higher values represent larger scratches/peaks
Lc	800.00	μm	LambdaC: cut off wavelength

Alicona Imaging GmbH
Dr.-Auner Strasse 21a
A-8074 Raaba/Graz

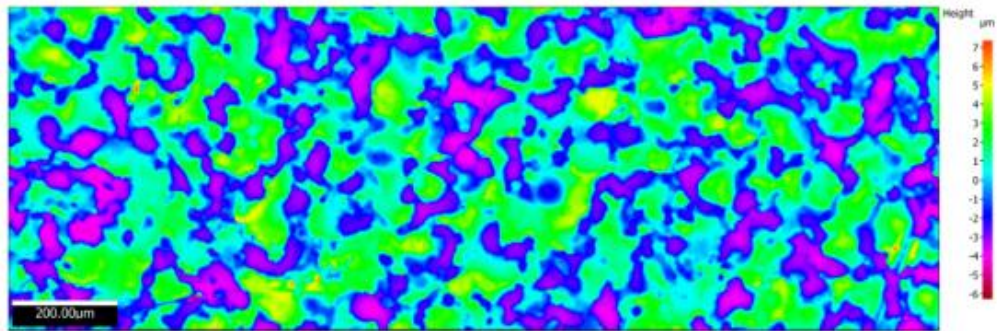
Measurement Report

Surface Texture Measurement

Original Dataset

Sac-Rough-50x-Large

Metric size: 1.76318mm x 611.39µm
Size: 5018 x 1740 points
2016-01-07T14:06:26



Alicona Imaging GmbH
Dr.-Auner Strasse 21a
A-8074 Raaba/Graz

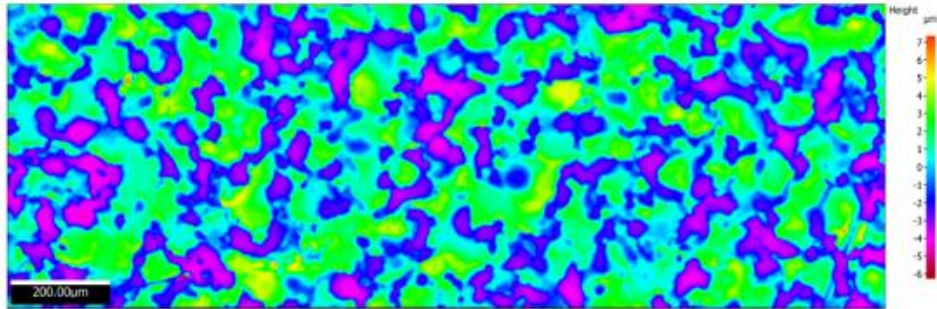
Measurement Report

Surface Texture Measurement

Original Dataset

Sac-Rough-50x-Large

Metric size: 1.76318mm x 611.39 μ m
Size: 5018 x 1740 points
2016-01-07T14:06:35



APPENDIX C

LUBRICANT PROPERTIES



TECHNICAL DATA SHEET

702



GAPHENE 702

GRAPHITE-BASED DRY LUBRICANT

DOES NOT ATTRACT DUST

DEFINITION

Micronized graphite-based dry lubricant in aerosol form for easy application, formulated to treat surfaces that require a lower coefficient of friction.

ADVANTAGES

Chemically inert; does not decompose in high temperatures; conducts electricity well (coating for interior and exterior cathode tubes).
Can be used in presence of oxygen, at very low temperatures without oxygen after evaporation of solvents.
Forms a perfectly uniform, dry film.
Lowers the coefficient of friction, protects parts against contact corrosion and prevents premature wear, diminishing the risk of damage due to partial or complete wrenching.
Demonstrates greater effectiveness than some other solid-based coatings with various additives, since Graphene GB does not catalyse decomposition.
Recommended especially for stainless steel assemblies.
Dry lubrication of metals and plastics.
Bonds exceptionally well to all surfaces.
Conducts electricity well.

Unlike traditional oils and greases, dry grease does not attract dust.

APPLICATION FIELDS

Workshops for mounting, repair, etc.
Industries related to the nuclear industry.
Treatment of metal and plastic parts to protect against friction.
Lubrication in dusty environments (flour, sand, cement, fibreglass, etc.)
Lubricate in temperatures as low as -70°C; aspect and consistency do not change according to circumstances.
Mould releasing, especially with tin.

Manufacturing site and registered office - 1/2 -
Parc Industriel de la Plaine de l'Ain
5, allée des Cèdres - 01150 Saint-Vulbas - France
Tel. +33 (0)4 74 40 20 20 - Fax +33 (0)4 74 40 20 21
www.orapi.com

TDS 702 / Index 1 – 13/09/2010

ORAPI® cannot know about every application for which the products are used nor their conditions of use. ORAPI® cannot be held responsible for the suitability of the products for a given use or a specific purpose. The information contained here can on no account be a substitute for the preliminary tests which are essential and which must be carried out in order to check the suitability of the product to each specific case.



TECHNICAL DATA SHEET

TECHNICAL CHARACTERISTICS

Aspect	Rapid-drying liquid
Colour	Black
Operating temperature	-70°C to +900°C
Coefficient of friction	< 0.05
Graphite granularity	5 microns
% graphite in dry film	> 80%

INSTRUCTIONS FOR USE

Shake aerosol well before every use.

PACKAGING

405 ml aerosol	Ref. 4702 A2	x 12 (non-flammable version)
650 ml aerosol	Ref. 4702 A4	x 12

PMUC:

650 ml aerosol	Ref. 6702 A4	x 12
----------------	--------------	------

Bulk versions available in 1 L bottles 717 - A20N and 716 – A20.

AUTHORISATIONS



-  19-227
- Complies with **MIL L 26548**.

Manufacturing site and registered office - 2/2 -
Parc Industriel de la Plaine de l'Ain
5, allée des Cèdres - 01150 Saint-Vulbas - France
Tel. +33 (0)4 74 40 20 20 - Fax +33 (0)4 74 40 20 21
www.orapi.com

TDS 702 / Index 1 – 13/09/2010

ORAPI® cannot know about every application for which the products are used nor their conditions of use. ORAPI® cannot be held responsible for the suitability of the products for a given use or a specific purpose. The information contained here can on no account be a substitute for the preliminary tests which are essential and which must be carried out in order to check the suitability of the product to each specific case.